ISSN 1422 - 1381

MeteoSchweiz

Veröffentlichungen

Nr. 64

Martin Bolliger

On the characteristics of heavy precipitation systems observed by Meteosat-6 during the MAP-SOP

August 2002

Bestellungen an:

Bundesamt für Meteorologie und Klimatologie (MeteoSchweiz)
Office fédéral de météorologie et de climatologie (MétéoSuisse)
Ufficio federale di meteorologia e climatologia (MeteoSvizzera)
Uffizi federal per meteorologia e climatologia (MeteoSvizra)
Federal Office of Meteorology and Climatology (MeteoSwiss)

MeteoSchweiz
Krähbühlstrasse 58
Postfach 514
CH-8044 Zürich

Telefon +41 1 256 91 11
Telefax +41 1 256 92 78
info@meteoschweiz.ch
www.meteoschweiz.ch

ISSN 1422 - 1381

MeteoSchweiz

Nr. 64

Martin Bolliger

On the characteristics of heavy precipitation systems observed by Meteosat-6 during the MAP-SOP

Veröffentlichungen

August 2002

Bestellungen an:

Bundesamt für Meteorologie und Klimatologie (MeteoSchweiz)
Office fédéral de météorologie et de climatologie (MétéoSuisse)
Ufficio federale di meteorologia e climatologia (MeteoSvizzera)
Uffizi federal per meteorologia e climatologia (MeteoSvizra)
Federal Office of Meteorology and Climatology (MeteoSwiss)

MeteoSchweiz
Krähbühlstrasse 58
Postfach 514
CH-8044 Zürich

Telefon +41 1 256 91 11
Telefax +41 1 256 92 78
info@meteoschweiz.ch
www.meteoschweiz.ch

The scientist does not study nature because it is useful; he studies it because he delights in it, and he delights in it because it is beautiful. If nature were not beautiful, it would not be worth knowing, and if nature were not worth knowing, life would not be worth living. - Jules Henri Poincaré (1854-1912)

CONTENTS

LIST OF FIGURES

LIST OF TABLES

ABSTRACT

During the field phase of the Mesoscale Alpine Programme (MAP) in autumn 1999 the standby satellite Meteosat-6 performed rapid scans of a region centred over the Alpine area. The present study focuses on the investigation of heavy precipitation systems on the southern side of the Alps (Ticino) and analyses their characteristics on the synoptic and meso-β scale.

The rapid scan dataset is used to tackle the following items:

1. What are the key ingredients to heavy precipitation systems in terms of the synoptic and mesoscale flow setting?
2. Is it possible to separate convective from stratiform cloud regions?
3. What is the quantitative contribution of convection to the overall precipitation event?
4. What type of life cycles do these precipitation systems undergo?

An ensemble of past and MAP-SOP cases show common characteristics with respect to the synoptic and mesoscale flow setting leading to strong precipitation on the southern side of the Alps. With the help of long-term radiosounding data from Milano the conceptual model from Kappenberger and Kerkmann (1997) of a heavy precipitation event on the southern side of the Alps can be confirmed.

The analysis of satellite imagery concentrates on investigations of non-calibrated data from the infrared and water vapor channel and on normalized data from the visible channel. It is assumed, that temporal and spatial characteristics of cloud top structures allow inferences from cloudiness associated with convective or stratiform precipitation. The temporal information is derived from the calculation of cooling- and warming rates of each pixel over a ten-minutes period. This information is supplemented by the calculation of the spatial variance within 3 x 3 pixel arrays.

Since clouds observed by satellites move with respect to the earth's surface seemingly strong cooling effects mainly at the leading edge of the clouds result from the calculation of the temporal evolution. These signals prevent an unambiguous identification of cooling areas attributable to convective activity. The implementation of a tracking algorithm reduces these unwanted effects and enhances signals due to cloud development since the earth-relative motion of the cloud is minimized. The tracking algorithm relies on the pattern recognition technique (Schmetz and Nuret, 1987) and is regarded as a methodological prerequisite for the extraction of signals evoked by cloud evolution. In the context of the implementation of the tracking algorithm some sensitivity studies are carried out, illustrating the advantage of tracking cloud features in a complex terrain like the Alps with imagery of high temporal resolution. The results of these studies show, that the quality of the tracking is dependent on the temporal resolution of the images, the search box, the target window size and the target pattern persistence.

Data from satellite provide information on cloud top structure, the radar data offer insight into dynamical properties within a precipitating cloud. For the verification of the satellite-based results, data from the operational Mt. Lema C-band radar is exploited. The region of interest is centred over the Lago Maggiore (Ticino). Polar data from the radar is interpolated on the pixel grid of the Meteosat image. The interpolated radar data is then classified by a convective-stratiform algorithm and compared to the analysed rapid scan imagery.

The satellite- and radar-based approaches do not produce matching classifications. It is assumed, that the limited intensity and limited extent of the embedded convective activity do not permit a recognition of temporal and spatial characteristics in satellite imagery. The lack of such characteristics does not allow the identification of typical cloudiness associated with stratiform precipitation. In contrast, cloud structures evoked by deep convective systems (Mesoscale Convective Systems) are well recognizable by their distinct cloud patterns.

Furthermore, the limited potential use of brightness temperature/count thresholds as discriminator between convective and stratiform cloud regions is demonstrated. Convection is not restricted to cold cloud areas, whereas cold clouds are not necessarily accompanied by convection. A fixed brightness temperature or count threshold is not a sufficient criterion for the separation of convective from non-convective cloud areas.

An automated classification scheme based on empirical thresholds is proposed for a quantitative use of the satellite-derived information. The classes of the classification scheme represent different magnitudes of cloud development as seen by satellite and allow the localization of areas with strong cloud development. The results demonstrate, that the preferred area of cloud development is localized over the northern Po Valley ahead of the Alpine barrier in a precipitation-free atmosphere. Investigations from radar data provide evidence, that in most cases the generation of precipitation and the convective activity is concentrated in the areas along the southern foothills of the Alps. It is remarkable that the occurrence of convection is strongly tied to orography.

It is one of the major findings of this study, that in several cases being classified as stratiform by radar, strong cloud development is observed in satellite imagery. In some cases, the strong cloud development is underlined by radiosounding data from Milano, showing an unstably stratified atmosphere. The classical scheme of stratiform cloudiness with a smooth cloud top and weak evolution is only partly encountered. The analyses of satellite data do not confirm the classical schemes of cloudiness associated with convective and stratiform precipitation as derived from radar and do not allow a systematic separation between the two. The fact that strong cloud development occurs together with stratiform precipitation accentuates the complementary character of the information derived from satellite and radar data. It must be assumed that significant vertical motion within the atmosphere occurs also in an atmosphere characterized as "stratiform" by radar. Since the areas of strong cloud development occur mainly in a precipitation-free atmosphere it remains open, to what extent the development is related to convection.

Rapid scan data supplement information from existing meteorological datasets and are well-suited to observe the different stages in the life cycle of strong convective phenomena. This implies an immediate availability of rapid scan data for an operational exploitation.

ZUSAMMENFASSUNG

Während der Feldphase des meteorologischen Grossprojekts Mesoscale Alpine Programme (MAP) im Herbst 1999, lieferte der standby Satellit Meteosat-6 zeitlich hochaufgelöste Bilder (rapid scans) des Alpenraums. Die vorliegende Studie befasst sich mit Starkniederschlägen auf der Alpensüdseite (Tessin) und analysiert deren Charakteristika auf der synoptischen und meso-β Skala mit Hilfe der rapid scan Daten.

Folgende zentrale Fragestellungen werden behandelt.

1. Welches sind die mesoskaligen und synoptischen Rahmenbedingungen für das Auftreten von Starkniederschlagsereignissen auf der Alpensüdseite?
2. Ist es möglich, konvektive und stratiforme Wolkenregionen zu unterscheiden?
3. Kann der konvektive Beitrag eines Niederschlagsereignisses quantifiziert werden?
4. Welche Art von Lebenszyklus durchlaufen diese Starkniederschlagsereignisse?

Die Auswertung von Fallstudien vor und während der Feldphase von MAP zeigen, dass die synoptischen und mesoskaligen Rahmenbedingungen für das Auftreten von Starkniederschlagsereignissen auf der Alpensüdseite sehr ähnlich sind. Anhand von Auswertungen langer Zeitreihen von Radiosondierungsdaten von Mailand kann das konzeptionelle Modell eines Starkniederschlagsereignisses auf der Alpensüdseite von Kappenberger und Kerkmann (1997) bestätigt werden.

Die Satellitenbildanalyse konzentriert sich auf die Auswertungen der nicht-kalibrierten Daten von Infrarot und Wasserdampf und auf normalisierte Daten des sichtbaren Kanals. Es wird angenommen, dass zeitliche und räumliche Charakteristika von Wolkenoberflächen Rückschlüsse über konvektive und stratiforme Niederschlagsregionen erlauben. Informationen über die zeitliche Entwicklung einzelner Pixel liefert die Berechnung der Abkühlungs- oder Erwärmungsraten über eine zehnminütige Periode. Informationen über die räumliche Struktur liefert die Berechnung der Pixelvariabilität innerhalb von 3 x 3 grossen Pixelfeldern.

Da die Eigenbewegung der Wolkensysteme insbesondere an den Wolkenrändern hohe scheinbare Abkühlungsraten hervorruft, können konvektiv aktive Zonen nicht eindeutig identifiziert werden. Diese scheinbaren Abkühlungssignale stören die eindeutige Identifikation von potentiell konvektiven Regionen. Mit der Einführung eines Tracking Algorithmus werden die unerwünschten Entwicklungssignale der Wolkenregionen reduziert und die Erkennung von potentiell konvektiven Regionen erleichtert. Der Tracking Algorithmus basiert auf dem Mustererkennungsverfahren (Schmetz and Nuret, 1987) und gilt als methodische Voraussetzung für die Erfassung der Intensität der Wolkenentwicklung. Im Zusammenhang mit der Einführung des Tracking Algorithmus werden einige Sensitivitätsstudien durchgeführt welche zeigen, dass die hohe zeitliche Auflösung der rapid scans vorteilhaft für das Verfolgen von Wolkenmustern in einem komplexen Terrain wie den Alpen ist. Die Resultate der Sensitivitätsstudien zeigen die Abhängigkeit der Qualität des Trackings von der zeitlichen Auflösung der Bilder, der Grösse der Suchregion, der Grösse des zu suchenden Wolkenmusters sowie der Persistenz der Wolkentextur.

Die Daten von Meteosat-6 liefern Strukturinformationen von den Wolkenoberflächen, jedoch keine Informationen über dynamische Prozesse innerhalb der Wolken wie ein Radar. Deshalb werden Radardaten vom operationellen C-Band Doppler-Radar der MeteoSchweiz vom Monte Lema zur Verifikation der satellitengestützten Resultate beigezogen. In einem Gebiet zentriert über dem Lago Maggiore (Tessin) werden die polaren Radardaten räumlich auf die Maschenweite von Meteosat Gitterzellen interpoliert. Die interpolierten Radardaten werden anschliessend mit einem konvektiv-stratiform Algorithmus klassifiziert und direkt mit den Resultaten der analysierten rapid scan Bilder verglichen.

Die Anwendung der satelliten- und radargestützten Methoden zeigen keine übereinstimmenden Klassifikationsresultate. Es wird angenommen, dass die schwache Ausprägung der eingelagerten konvektiven Aktivität keine charakteristischen räumlichen und zeitlichen Merkmale in Satellitenbildern hervorruft. Das Fehlen solcher Erkennungsmerkmale erlaubt auch keine Identifikation typischer Bewölkung, welche zusammen mit stratiformem Niederschlag auftritt. Im Gegensatz dazu sind die Wolkenstrukturen mit hochreichender Konvektion (Mesoscale Convective Systems) anhand der auffälligen Wolkenformen einfach zu identifizieren.

Die vorliegende Studie demonstriert weiter die beschränkte Anwendbarkeit von Temperatur/count-Schwellenwerten als Kriterium für die Unterscheidung von konvektiven und stratiformen Wolkenregionen. Es zeigt sich, dass Konvektion auch in warmen Wolkenregionen auftritt und dass kalte Wolkenoberflächen nicht zwingend mit konvektiver Aktivität auftreten. Ein fixer Temperatur- oder count-Schwellenwert ist nicht ein hinreichendes Kriterium für die Unterscheidung zwischen konvektiven und nicht-konvektiven Wolkenregionen.

Ein automatisches Klassifikationsschema basierend auf empirischen Schwellenwerten wird verwendet, um die Informationen aus den Satellitenbildern zu quantifizieren. Die Klassen des Klassifikationsschemas repräsentieren unterschiedliche Intensitäten der Wolkenentwicklung und erlauben die Lokalisierung von Regionen mit starker Wolkenentwicklung abgeleitet aus Satellitenbildern. Die Resultate zeigen, dass sich die Gebiete starker Entwicklung auf die nördliche Poebene konzentrieren, vor der alpinen Orographie in einer niederschlagsfreien Atmosphäre. Die Auswertungen von Radardaten zeigen, dass sich in den meisten Fällen die Niederschlagsbildung und die konvektive Aktivität auf die südlichen Voralpengebiete konzentrieren. Insbesondere ist das Auftreten von Konvektion stark an die alpine Orographie gebunden.

Eine wichtige Erkenntnis der vorliegende Studie ist die Tatsache, dass bei mehreren Niederschlagsereignissen, welche mit Hilfe von Radardaten als stratiform charakterisiert werden, starke Wolkenentwicklung festgestellt werden kann. In einigen Fällen wird die starke Wolkenentwicklung durch eine labile atmosphärische Schichtung begünstigt, was Radiosondierungsdaten von Milano bestätigen. Die klassische Bewölkung mit stratiformem Niederschlag, gekennzeichnet durch eine schwache Wolkenentwicklung und schwach texturierte Wolkenoberfläche, ist nur teilweise anzutreffen. Die Satellitendaten bestätigen nicht das klassische Gedankenmodell von typischer Bewölkung, welche mit konvektivem und stratiformem Niederschlag auftritt und erlauben keine Trennung zwischen diesen beiden Wolkentypen. Die Feststellung, dass in stratiformen Niederschlagsgebieten starke Wolkenentwicklung möglich ist, verdeutlicht die Komplementarität der aus Satelliten- und Radardaten gewonnenen Informationen. Es ist davon auszugehen, dass starke vertikale Umwälzungen während den Niederschlagsereignissen mit stratiformem Niederschlag auftreten. Da die Regionen mit starker Wolkenentwicklung hauptsächlich in niederschlagsfreier Atmosphäre auftreten, bleibt es offen, ob und in welchem Mass die festgestellte Entwicklung durch Konvektion hervorgerufen wird.

Rapid scan Daten ergänzen Informationen von bestehenden meteorologischen Messnetzen und sind gut geeignet, die Lebenszyklen von stark konvektiven Ereignissen zu erfassen. Eine solche operationelle Anwendung von rapid scans setzt eine rasche Verfügbarkeit der Daten voraus.

1 Introduction

The impacts of heavy precipitation events have always been a big threat to human life. Flooding, violent runoff, raise of lake levels and soil movement related to heavy precipitation events often produce tremendous damages and loss of life. In recent years, an increasing frequency of extreme precipitation events (Bader and Kunz, 2000) resulted in devastating floods causing enormous damages to lives and goods of the local population (e. g. Brig: 23 September 1993, Piemonte: 4-6 November 1994; southern tip of the Ticino: 14 September 1995, Gondo: 16 October 2000).

Accurate forecasts with respect to timing, location and quantity of precipitation can help to avoid damage by taking adequate safety measures in the affected regions. Meteorological forecasts, possibly in combination with hydrological run-off and lake-rise predictions, can substantially extend the alert time which is a decisive factor for initiating protective measures. For this purpose, the recognition and understanding of relevant processes related to precipitation systems are essential. Meteorological processes like advection of moisture and temperature or the generation of convection contribute on different time and space scales to the severity of precipitation events and their consequences.

If we consider a possible result of a precipitation event like flooding as a picture of a puzzle (Figure 1-1) and if we regard the pieces of this puzzle as meteorological processes contributing to the overall precipitation event, the puzzle gets more complete the more pieces we put together. Thus, by knowing the processes which are relevant to heavy precipitation systems the understanding of extreme events increases. However, the relations between the various components which lead to heavy precipitation are complex and non-linear, and not every heavy precipitation event causes severe damage. Usually strong precipitation events are only made public, when damages occur (Grebner, 1996). Today and in future, the qualitative knowledge of relevant meteorological processes of a heavy precipitation event will help to quantify their effects as contribution to the overall event.

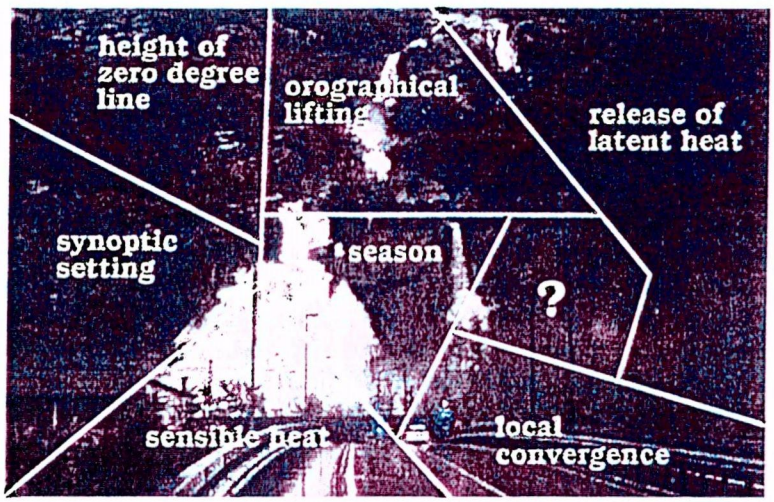

FIGURE 1-1. Waterfall near Lodrino (Ticino) - pictured as a puzzle - due to heavy precipitation as observed on 26.09.99. Heavy precipitation results from different meteorological processes (e. g. sensible and latent heat) and given natural conditions (e. g. season, orography). These processes and conditions - represented by pieces of the puzzle - may interact with each other resulting in devastating precipitation events. Up till now, not all meteorological processes of heavy precipitation events are sufficiently understood (questionmark).

From a meteorological point of view, there are different foci for the analysis of heavy precipitation events. Data from observing systems like conventional and automatic

measuring sites, radar and satellite may be exploited or numerical model studies may be carried out. In order to improve the understanding of processes related to heavy precipitation events, the specific advantages and disadvantages of the different observing systems and models must be evaluated. Meteorological field experiments like the Mesoscale Alpine Programme (MAP) from 1999 provide high density datasets of many meteorological observing and measuring systems. Investigations of these datasets will lead to a better understanding of meteorological processes. The present study focuses on the use of satellite data of high temporal resolution with the aim to retrieve additional meteorological information on heavy precipitation events which occurred during the field phase of MAP on the southern side of the Alps.

1.1 Precipitation in the Alps

The arc of the Alps is approximately 800 km long and 200 km wide with an average height of 2500 metres above sea level and acts as a climatic barrier producing several different climate regions (Bader and Kunz, 2000). By blocking the trans-European airflow from various directions, the Alps exert a profound influence on Europe's weather and elicit practically all known orographic phenomena of the atmosphere (Houze et al., 1998).

In this study we focus on the climatic region south of the Alps which provides an ideal natural laboratory for the investigation of orographic precipitation mechanisms. Climatological investigations show that the southern flank of the Alps is a preferred region for heavy precipitation events (Fliri 1984, Spinedi 1992, Spinedi et al. 1995, Kappenberger and Kerkmann 1997, Frei and Schär 1998, Grebner and Roesch 1998).

Frei and Schär (1998) assembled an Alpine-scale daily precipitation data-base with about 6000 stations and describe the spatial and seasonal distribution of the Alpine precipitation. The precipitation fields were analysed on a regular-longitude grid (resolution: 25 km) by spatial averaging of the irregularly distributed precipitation observations. They found that - apart from the preferred precipitation regions - the most prominent Alpine effects include the enhancement of precipitation along the Alpine foothills, and the shielding of the inneralpine valleys. In their investigations of cross sections across the Alps they found no precipitation-height relationship on the Alpine scale. According to them, much of the topographic signal is associated with slope and shielding rather than effects of height.

There exist geographical spots exhibiting large precipitation amounts and above-average frequencies of storm occurrence: the area of Lago Maggiore, the Friuli-Slovenian border, furthermore the south-east flank of the Massif Central (Cevennes) in the Rhone Valley and the Veneto region in Italy (Frei and Schär, 1998). It is interesting to see that these maxima are tied to specific orographic features like the alternately concave and convex configurations of the Alps in their south slopes. This lends support to the fact that the orographic modification of the precipitation producing systems is a major factor determining location, intensity and frequency of heavy rain storms.

In the Lago Maggiore region, Camedo is the location where the highest precipitation amounts were registered in Switzerland within 24 hours (414 mm, 10.09.1983, Spinedi, 1992). Climatological precipitation maps and precipitation maps of single events exhibit in many cases a clearly identifiable center of precipitation maximum in the Camedo region in the Centovalli (Spinedi 1992, Spinedi et al. 1995, Kappenberger and Kerkmann 1997, Grebner and Roesch 1998, Frei and Schär 1998). Figure 1-2 illustrates the preferred areas of precipitation of selected years with precipitation maxima located in the Ticino. Investigations at MeteoSwiss of heavy precipitation on the southern side of the Alps have been documented in Spinedi (1992, 1995, 1998) and Courvoisier (1975, 1981, 1998). Often, the precipitation falling in the Lago Maggiore region is geographically not only restricted to the southern side of the Alps. Considerable precipitation amounts may be registered on the northern side of the

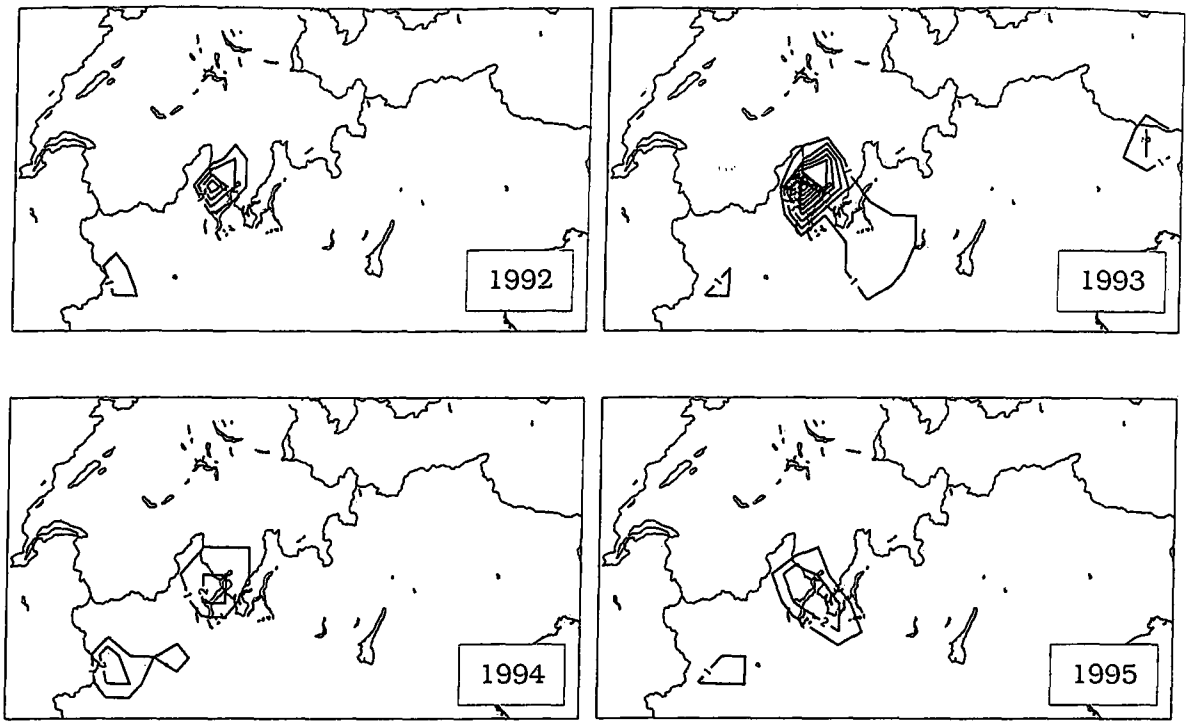

FIGURE 1-2. Number of precipitation events with precipitation ≥ 100 mm/24 h in selected years, based on the dataset of the Frei and Schär precipitation climatology (1998). The thick black lines depict the grid points exceeding the threshold ≥ 100 mm/24 h over a period of one year. Note that precipitation greater than 20 mm/24 h can be regarded as heavy since the grid point analysis represents area mean conditions (Frei and Schär, 1998).

Alps, preferably in the region between Sedrun or Hinterrhein up to St. Gallen or even up to the Lake of Constance (Grebner, 1993).

Investigations of the occurrence of heavy precipitation on the south side of the Alps reveal, that there is a clear maximum in autumn (Figure 1-3, p. 14). As shown in this figure, a secondary frequency maximum of heavy precipitation is observed in spring. Note the sharp decrease in frequency of heavy precipitation by mid-November. Courvoisier (1998) suggests that the frequency maximum in autumn is due to the strong vertical temperature gradients causing instability and due to the high temperature of the Mediterranean Sea, which serves as moisture source. In spring, the moisture supply from the Mediterranean Sea is weaker because of the cooler water temperatures resulting in a less pronounced secondary frequency maximum. From a climatological point of view, the Lago Maggiore target area is - especially in autumn - best suited to study all aspects related to heavy orographic precipitation (Bougeault et al., 1998). Within Figure 1-3 the daily precipitation sums of the MAP cases during the field phase (cf. section 1.2, p. 15) are colored black, concentrated mainly in the period from mid-September to the beginning of October.

In the last years, many studies have been carried out in order to study the influence of global climate variability and change on the European Alps (i. e. Wanner et al. 1997, 2000 and 2001). Special attention was given to the analysis of the variability of large scale synoptic pressure distributions like the North Atlantic Oscillation (NAO). The NAO describes a large scale meridional oscillation in atmospheric mass between the north Atlantic regions of the subtropical anticyclone near the Azores and the subpolar low pressure system near Iceland (Wanner et al., 2001). The state of the NAO is represented by the North Atlantic Oscillation Index (NAOI) and uses a standardized air pressure difference between the high pressure area

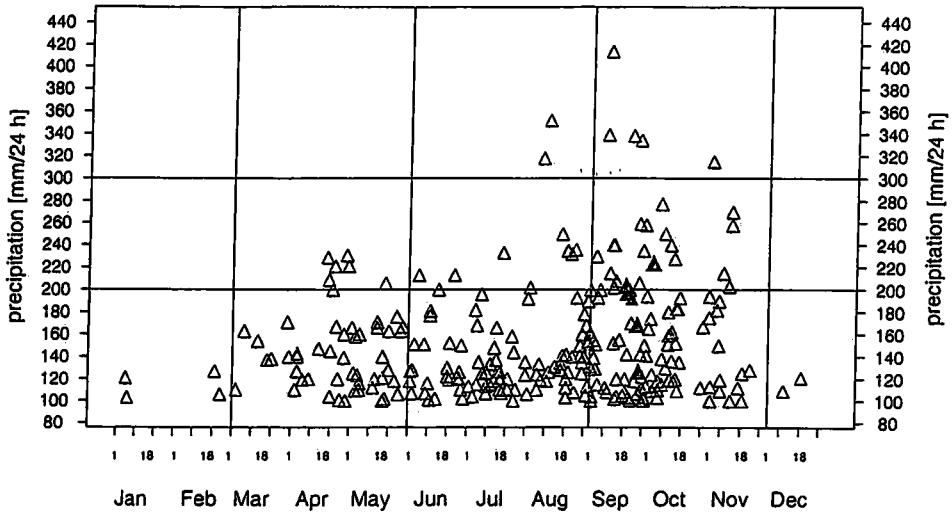

FIGURE 1-3. Number of days with maximum precipitation rate (≥ 100 mm/24 h]) at measurements sites in the Ticino from 1961-2001. The preferred period for the occurrence of heavy precipitation events is autumn, a secondary maximum is observed in spring. Events related to the MAP field phase (cf. section 1.2, p. 15) are depicted with black color. The number of analysed measurements sites vary in time between 25 and 30 stations (data: courtesy of F. Spinedi).

located over the Azores and the Iceland low and is an indicator for the strength of the westerlies over the eastern north Atlantic and western Europe (Wanner et al., 2001). The NAOI is positive with strong westerlies and negative with weak westerlies. Wanner et al. (1997) found that in northern Europe the climate trends have been characterized by dominant westerly winds, i. e. by a positive NAOI since the late 1970s. The positive and negative phases of the NAO are accompanied by different spatial patterns of precipitation: In the positive phase, precipitation activity is high over Scotland and southwestern Norway, in the negative phase, high amounts of precipitation are observed in the Mediterranean area and the Black Sea (Wanner et al., 2001). For central Europe, Schmutz (2000) found only a weak linkage between the Alpine precipitation and the NAO in the twentieth century and underlined the results of Wibig (1999). An explanation of this weak linkage may be the location of the Alps. Wanner et al. (1997) pointed out, that the Alps are positioned in a transitional region between Mediterranean and north Atlantic climates and are not in the center of important mean pressure systems. As a consequence of that, the linkage between the steering pressure centers and the precipitation patterns in the Alps may be ambiguous.

From precipitation data in the Ticino Courvoisier (1998) derived a significant increase of days with precipitation rates of ≥ 100 and 150 mm/24 h in the Sopraceneri and Misox region during the period 1976-1995. Precipitation measuring sites in the Sottoceneri region (i. e. south of Locarno) show no significant climatological trend towards an increase of strong precipitation. Frei and Schär (2001) investigated the frequency of intense precipitation in Switzerland using a statistical trend analysis and found increasing trends for autumn and winter seasons.

The following Figure 1-4 shows the total annual sum of observations at 15 stations in the Ticino with precipitation exceeding 100 mm/24 h and 150 mm/24 h from 1961-2001. The sum of observations is subjected to a large year-to-year variability, with a minimum of events occurring between 1969 and 1975, followed by a period of increased frequency from 1976-1984. In 1993 a clear maximum of days with precipitation exceeding 100 mm/24 h is well depicted, what is underlined by Figure 1-2 (upper right panel). The figure confirms the tendency towards a frequency increase of observations of days with heavy precipitation starting in 1976.

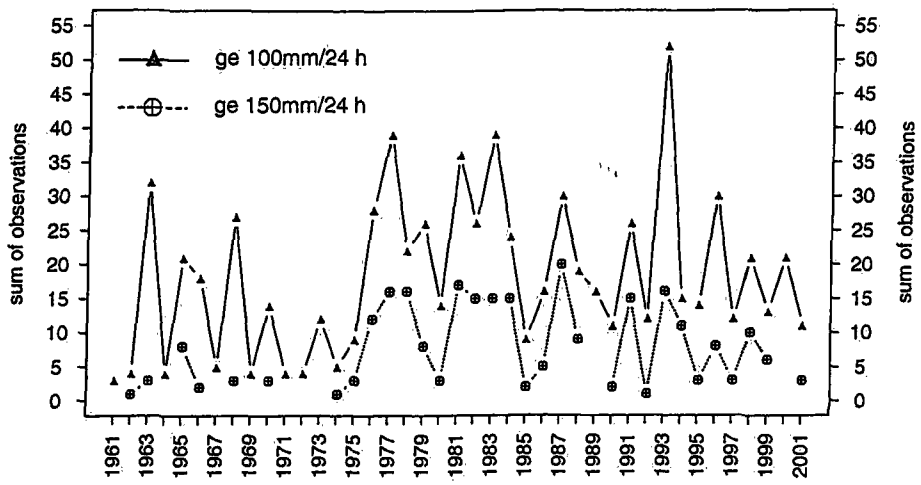

FIGURE 1-4. Sum of observations of heavy precipitation in the Ticino at 15 stations from 1961-2001. During this period the total number of observations exceeding the precipitation threshold 100 mm/24 h is 748, those exceeding the threshold 150 mm/24 h is 264 (data: courtesy of F. Spinedi).

In summary, especially in autumn the southern side of the Alps provides excellent conditions for a meteorological research experiment like the Mesoscale Alpine Programme aiming to gain data on processes related to heavy precipitation.

1.2 The Mesoscale Alpine Programme (MAP)

The present study is strongly embedded within the Mesoscale Alpine Programme (MAP), an international meteorological programme devoted to the research of atmospheric and hydrological processes over mountainous terrain. The notion *mesoscale* characterizes flow systems, that possess space scales of 2 to 2000km and time scales between 2 hours and 2 days (Binder and Schär, 1996). MAP aims towards expanding the knowledge of weather and climate over complex topography, and thereby to improve current forecasting capabilities (www.map.ethz.ch).

An overview of the complete list of the scientific objectives for MAP is given in the MAP Design Proposal (Binder and Schär, 1996), a complete list of detailed scientific questions can be found in the MAP Science Plan (Bougeault et al., 1998). The present study is related to the so-called "Wet-MAP", which aims to investigate orographic precipitation and flooding. The so-called "Dry-MAP" is related to dry dynamics of flow over mountains like gravity wave breaking or Foehn. The primary objectives of the "Wet-MAP" are:

1a. To improve the understanding of orographically influenced precipitation events and related flooding episodes involving deep convection, frontal precipitation and runoff.

1b. To improve the numerical prediction of moist processes over and in the vicinity of complex topography, including interactions with land-surface processes.

After a five years planning phase the MAP field phase, called Special Observing Period (SOP) took place from 7 September to 15 November 1999 in the Alpine region. The SOP field activities were concentrated in three target areas (Figure 1-5): The Lago Maggiore target area (LMTA) was the main focus of the "Wet-MAP" part, while the Rhine Valley and the Brenner target areas were the focus of the "Dry-MAP". All target areas were equipped with additional

instruments for the SOP and ground-based observation campaigns were supported by airborne missions over the target areas (Bougeault et al., 1998). A full description of the instrumental and operational set-up of the experiment is given in the MAP Implementation Plan (Binder et al., 1999).

During the SOP, the field activities were coordinated by three centers, the MAP Operations Center (MOC) at Innsbruck Airport (Austria), the MAP Project Operations Center (POC) at Milano-Linate airport (Italy) and the MAP Coordination and Operations Center (COC) in Bad Ragaz, Switzerland (Bougeault et al., 2001).

The MOC was the main center of decision and defined the start and end of an Intensive Observations Period (IOP) and the flight missions. During the IOPs, extra measurements (e. g. enhanced operational radiosounding) and coordinated research activity took place (Binder et al., 1999). In the POC, radar data from the southern side of the Alps were used to construct a real-time composite of precipitation areas and provided fore- and nowcasting support for aircraft missions and other research activities. The COC coordinated the radiosounding activities of the Swiss Army in the Rhine Valley. The MAP Data Center (MDC) located at Zurich (Switzerland) stored and makes available all data gathered during the MAP field phase (Bougeault et al., 2001).

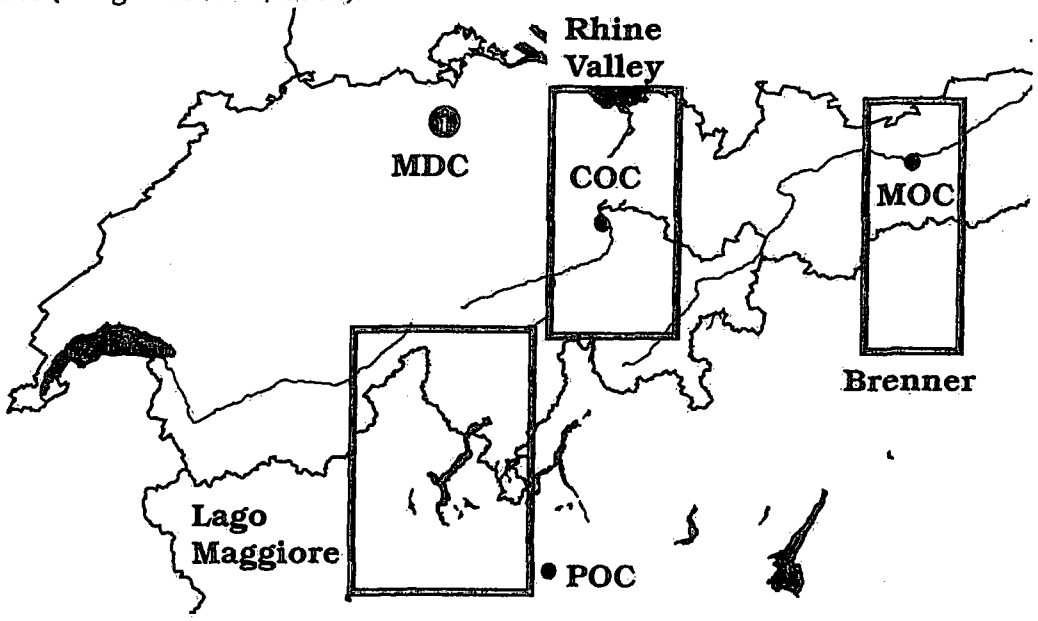

FIGURE 1-5. Target areas of the MAP and related operation centers: Innsbruck (MAP Operations Center, MOC), Bad Ragaz (Coordination and Operations Center, COC) and Milano (Project Operations Center, POC). Zurich hosted the MAP Data Center (MDC).

The SOP experienced excellent weather conditions and, in total, 17 IOPs were carried out. MAP was probably the largest field experiment ever conducted in Europe and the largest meteorological field programme over the Alps since ALPEX (1982) (Bougeault et al., 2001). MAP is endorsed by EUMETNET and WWRP.

1.3 Objective of the present work

For the duration of the MAP-SOP, EUMETSAT, the European organisation for the exploitation of meteorological satellites, has agreed to provide rapid scan data of the stand-by spacecraft Meteosat-6. In this special imaging mode the radiometer scanned a reduced latitude range, centred over the Alps, in a 5-minute interval. Each rapid scan covered the latitude range of approximately 40°- 52° N in the infrared, water vapor and visible channel. These rapid scans were very successful and smooth (Bougeault et al., 2001). In the meantime EUMETSAT is offering an operational rapid scanning service (www.eumetsat.de). During the SOP, several heavy precipitation events were observed by Meteosat-6 rapid scans on the southern side of the Alps. The satellite data from these events are explored in order to characterize the precipitation events by analysing information from cloud top structures in the LMTA.

A characterization of heavy precipitation events is of crucial interest for practical forecasting purposes in the Alpine region. Looking at the southern side of the Alps, practitioners' experience says that convection plays always a role in producing heavy precipitation, but there is no *quantitative indication* of the contribution *of convective activity*. The scale may reach from "pure" convective systems like Mesoscale Convective Systems (MCS) over the Po Valley undergoing a "standard" life cycle while moving towards the Alps, through every weighted combination of advective (large- or meso-scale ascent and/or orographic lifting) and convective processes. While deep convection was rarely observed during the MAP-SOP most events are characterized by a mixture of convective activity and orographic lifting embedded in stratiform precipitation (cf. chapter 2). In the present study, satellite information shall be exploited aiming to separate between convective and stratiform cloud areas. The separation would allow a quantitative estimation of the relative contributions of stratiform and convective activity to an overall precipitation event. In addition, some conceptual ideas concerning the appearance of cloudiness associated with heavy precipitation events shall be developed. *Conceptual models* attempt to condense the complexity of individual weather systems to the essential components and processes helping to describe the different stages of *life cycles* of the observed precipitation systems. The attribution of different life cycles to a precipitation system could be used successfully for nowcasting and shortrange forecasting purposes.

In summary, the present study contributes to the overall objectives of "Wet-MAP" by addressing the following specific questions using rapid-scan data from Meteosat-6 in the LMTA:

1. What are the key ingredients to those heavy precipitation events in terms of the synoptic and mesoscale flow setting
2. Is it possible to differ between convective and stratiform cloud regions?
3. What is the quantitative contribution of convection to an overall precipitation event?
4. What type of life cycles do these precipitation systems undergo?

The first question is tackled by analysing the MAP-SOP events and an ensemble of past cases with heavy precipitation intending to provide a limited background concerning the synoptic and mesoscale flow setting. Literature studies are carried out trying to summarize the main meteorological ingredients accompanied by heavy precipitation events and the broader context they develop in.

For the investigations related to the identification of convective and stratiform cloudiness and their life cycles satellite-based methods are developed aiming at an exploitation of satellite data in the mesoscale. In order to verify the satellite-derived results, weather radar data from the Monte Lema radar is analysed. The Monte Lema radar, located near Lugano in the Ticino, is the operational weather radar from MeteoSwiss and provides volume scans

every 5 minutes. Due to the 6-fold increase in satellite observation frequency the same sampling cycles as the Monte Lema radar is established, therefore a comparison between radar and satellite data with high temporal resolution (i. e. 5-minute interval) is possible.

The present study is based on satellite and radar investigations and may be regarded as *a complementary study* to the variety of investigations based on the different observing systems. The combined use of satellite- and radar-based information provides a synthesized view of precipitation events which occurred during the MAP-SOP pinpointing the event-specific characteristics. The study should further demonstrate the potential of rapid scanning but also the current limitation of using geostationary satellite images as a supplemental source of meteorological information in complex terrain like the Alps. The results are expected to be of relevance for nowcasting and short-term forecasting purposes using satellite data in an operational manner.

1.4 Outline

After these introductory remarks in chapter 2 some synoptic aspects of heavy precipitation events are explained and the key ingredients for the generation of heavy precipitation events in the LMTA will be illuminated.

Chapter 3 gives a general introduction of the characteristics of the satellite and radar data used in the present study, including an overview on the presently available software for identification of convection in geostationary satellite images.

In chapter 4 the established satellite-based methods are presented comprising the analysis of pixel variability and temporal evolution of cloud structures. The chapter concludes with the description of the first results from the application of the introduced satellite-based methods and the consequences thereof for the study. The results revealed that the implementation of a cloud tracking algorithm is necessary for a quantification of cloud development.

For the comparison between satellite and radar data, the region of interest is defined in Chapter 5. Further, the convective-stratiform classification algorithm established for radar data is explained.

Chapter 6 describes the pattern correlation coefficient (PCC) tracking algorithm and its implementation within the framework of the present study. Moreover, results from sensitivity studies are presented demonstrating the gain in information by the enhanced temporal resolution of the rapid scans. At the end of the chapter, the major findings of the tracking algorithm are presented and conclusions are drawn.

In chapter 7 a short summary of the investigated events is given with a description of the specific characteristics.

The main conclusions are drawn in chapter 8 where a quantification of the satellite-based signals is described and the characteristics of the investigated heavy precipitation events in consideration of the main challenges of this study are pointed out. The fundamental properties of the satellite data are explored and related to radar data for verification.

In the last chapter, chapter 9, the overall conclusions of the study are discussed concluding with some final remarks.

2 Synoptic aspects

Climatological studies reveal, that the southern side of the Alps, especially the region of Ticino, is a favoured spot for the occurrence of heavy precipitation (cf. Figure 1-2). As pointed out in the introduction, several meteorological processes interacting with the Alpine orography are required to produce a heavy precipitation event. For climatological studies, Courvoisier (1998) regarded a precipitation event as heavy if the rainfall amount was $\geq$ 100 mm/24 h over an area of $\geq$ 500 km^2 on the southern side of the Alps. In this chapter the meteorological phenomena considered as key ingredients for heavy precipitation events are elucidated, with respect to the LMTA.

According to Grebner (1997) the generation of precipitation requires humidity and lifting processes producing two kinds of precipitation: convective and advective precipitation. Table 2-1 shows that the intensities and the daily sums of the two kinds of precipitation are different on the north side and on the south side of the Alps, respectively.

TABLE 2-1. Characterization of precipitation events: (N) = northalpine and (S) = southalpine (after Grebner, 1997)

characterization of lifting	lifting process	characterization of precipitation	(extreme) intensities	daily sums	horizontal extension
convective	vertical displacement	shower	100 mm/h	100 mm/d	local (20 km)
advective	slanted gliding	continuous	15 mm/h (N) 40 mm/h (S)	250 mm/d (N) 400 mm/d (S)	large region (200 km)

The intensities and the daily sums of precipitation on the south side of the Alps are remarkably higher than on the north side. These differences in rain intensities and daily sums may be explained - especially in autumn - by high temperatures of the Mediterranean sea. The Mediterranean provides latent and sensible heat which may be transported with the large scale airflow towards the southern Alps. Therefore, the south side of the Alps possesses a quasi-permanent source of moist, high equivalent-potential temperature air from the warm Mediterranean Sea. Investigations on single heavy precipitation events are frequent, the literature is consequently manifold. Examples give Spinedi (1992), Grebner (1994, 1997), Buzzi et al. (1995), Spinedi et al. (1995), Jansa et al. (1995), and Massacand et al. (1998).

There are many different facets of heavy precipitation events on the southern side of the Alps. Some meteorological ingredients for the occurrence of heavy precipitation are presented in this chapter.

2.1 Some ingredients for heavy precipitation events

Within the framework of MAP several cases of heavy precipitation on the southern side of the Alps have been, and are, studied in detail. Many of these investigations use numerical prediction models as principal tool to elucidate the main influencing factors leading to the mechanisms working during such events (e. g. Binder and Rossa 1995, Benoit et al. 1996, Benoit et al. 1997, Buzzi et al. 1998, Schneidereit and Schär 2000, Rotunno and Ferretti 2001, Smull et al. 2001, Arena et al. 2001, Buzzi and Davolio 2001, and Gheusi and Stein 2001).

Investigations from the pre-SOP precipitation events (Vaison-La-Romaine, Brig, Piemonte, Ticino) show, that the heavy precipitation events were related to the occurrence of large scale frontal systems like a deep trough with an associated cold front. About 40 % of the annual precipitation received by central Europe is related to the passage of cold fronts (Hoinka, 1985). In the upper-level, a trough extending from the British Isles to the southwestern Mediterranean steers the large scale advection. Figure 2-1 is based on a ten years

climatology of heavy precipitation events as dedicated from the measuring sites in Ticino. Figures 2-1 a) - c) summarize the large scale pressure distribution at different pressure levels and the position of maximum cyclonic curvature of the trough associated with heavy precipitation in the LMTA. The threshold for the definition as strong precipitation is 100 mm/24 h at least at one of the investigated 25 stations. Figures 2-1 a) and b) show a pressure "dipole", with low pressure from the central Europe to the west and high pressure to the east over continental regions. This pressure "dipole" leads to a south/southwesterly airflow towards the Alps. The positions of the associated trough axis in Figure 2-1 c) show either a southwest-northeast or a northwest-southeast orientation.

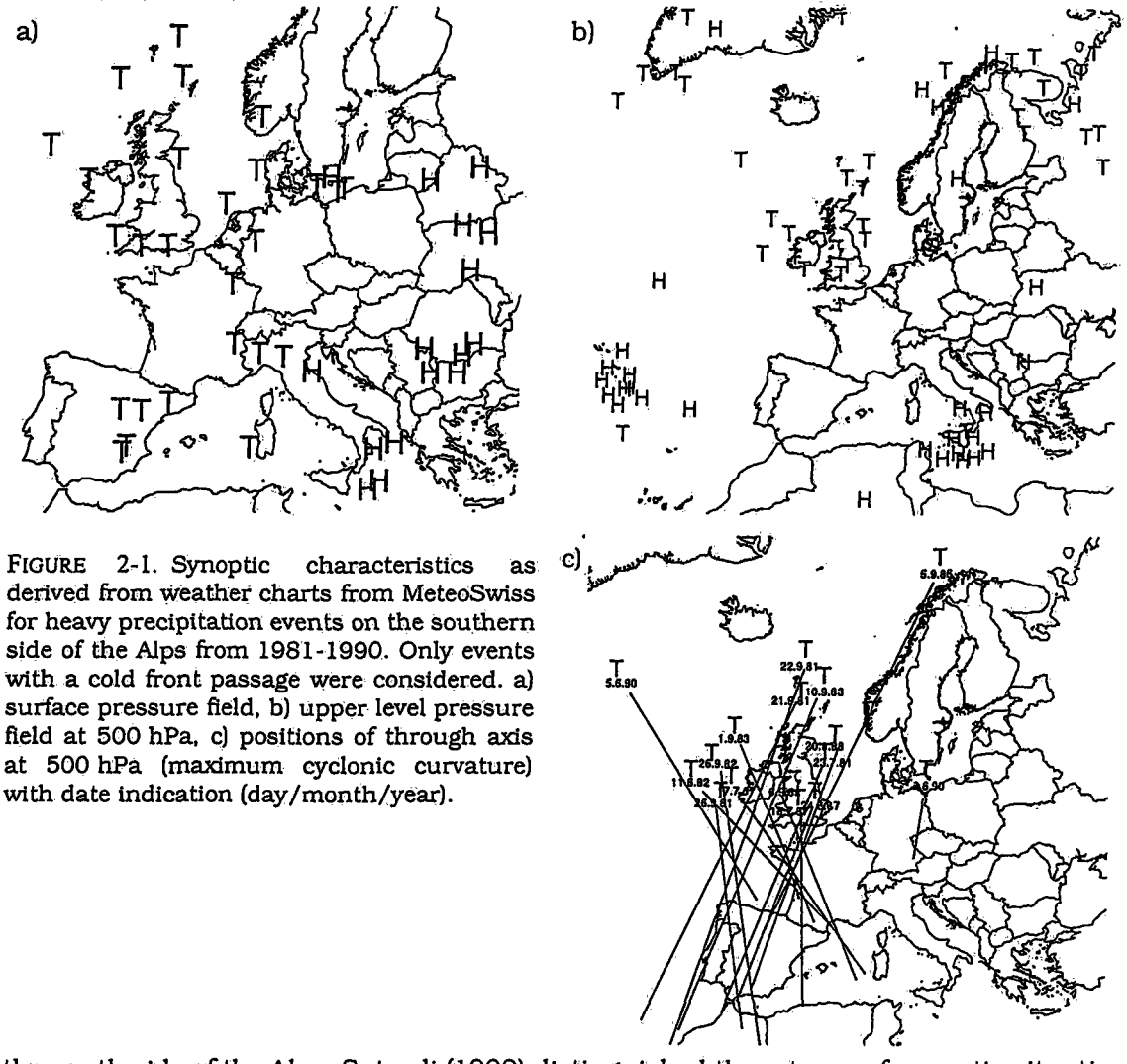

FIGURE 2-1. Synoptic characteristics as derived from weather charts from MeteoSwiss for heavy precipitation events on the southern side of the Alps from 1981-1990. Only events with a cold front passage were considered. a) surface pressure field, b) upper level pressure field at 500 hPa, c) positions of through axis at 500 hPa (maximum cyclonic curvature) with date indication (day/month/year).

For the south side of the Alps, Spinedi (1992) distinguished three types of synoptic situations leading to important precipitation events:

1. Blocked airflow: ahead of an upper level through, continuous and abundant precipitation occurs leading to important total precipitation amounts but only moderate precipitation rates. The whole region of southern Switzerland is affected by this precipitation type.
2. Situations with Atlantic cold fronts crossing the Alps, with prefrontal advection of warm-humid subtropical air and thunderstorm activity near or ahead of the front. This type causes the greatest disasters like flooding and violent run-off.
3. Situations with local thunderstorm activity causing high precipitation rates within short periods (~ 30 mm/10 minutes) but with effects limited to a small region. They occur during summer.

The last type is restricted to the summer time, the other ones occur over the whole year. However the effects of type one and two are strongest during spring, summer and autumn. Cacciamani et al. (1995) investigated thunderstorm activity in the Po Valley and found, that during thundery days the most frequent upper-level weather type is the trough situation while during non-thundery days upper level ridges and surface high pressure fields appeared to be predominant. They further recognized that in the presence of frontal structures widespread thunderstorm conditions are likely.

In fact, situations with cold fronts (situation two) can be regarded as final phase of a "Stau"[1] situation since with the passage of a cold front, the winds turn to northerly directions and end the moisture supply from the south and therefore the "Stau" effect. The positions of the surface low pressure centers are depicted in Figure 2-1 a). Often, the formation of a stationary cut-off cyclone can be observed over the Gulf of Genoa. The position of the low pressure center and the associated cold front determine the advection of airmasses. Jansa et al. (1995, 1996) have compiled a climatology of the positions of low-pressure centers in the Mediterranean Sea which clearly shows that a local maximum exists over the Gulf of Genoa. Many of these depressions drive warm and moist air masses from the Mediterranean Sea towards the Alps contributing to the precipitation maxima seen in the high-resolution precipitation climatology.

A major aspect of the amount of precipitation within a geographical area is the propagation velocity of the whole large-scale driven precipitation system. Slowly moving or stationary systems - interacting with orography - lead to severe local precipitation events with the occurrence of floods. A slow propagation of precipitation systems is favoured by the strong and extensive high pressure area in eastern Europe which blocks the large scale motion (cf. Figures 2-1 a) and b)).

According to Buzzi et al. (1995) a strong and moist pre-frontal low-level jet is probably the most significant dynamical feature associated with the occurrence of heavy precipitation. They found that in the Piemonte flood the highest precipitation rates were observed in the pronounced confluence zone between the post-frontal southwesterly flow and the pre-frontal southeasterly flow at 850 hPa located more to the east, where the pre-frontal jet was having the characteristics of a warm conveyor belt.

Also numerical studies reveal that the prefrontal low-level jet is an important ingredient for heavy precipitation events since it provides the pertinent moisture flux, determines the nature of the atmospheric flow response and the orographic lifting leading to the triggering of convective and/or stratiform precipitation (Schneidereit and Schär, 2000). A general description of low-level jet structure ahead of midlatitude cold fronts is given in Browning (1973).

2.1.1 Upper-level forcing

Numerical modelling studies show that specific upper-tropospheric structures, expressed in terms of positive potential vorticity (PV) anomalies, over the east Atlantic and western Europe have a high correlation with heavy precipitation events on the southern side of the Alps (Massacand et al., 1998). According to Morgenstern (1998), orography, moisture advection from the Mediterranean and a tropopause-level PV anomaly constitute the dynamical elements essential to the formation of MCSs. In his idealized numerical experiments he found tower-like mid-tropospheric PV anomalies occurring with severe convection. The upper-tropospheric PV anomalies associated with the deep short-wave trough may help trigger ascent on the forward flank of the anomalies and generate or enhance convection produced by orographically induced upward motion (Massacand et al., 1998). There are also indications that the fine structure of these pre-cursors has an impact on the development of

[1] blocked airflow

the mesoscale circulations and determines therefore, at least to some extent, time and location of heavy precipitation (Quadri et al., 2000).

PV generated in the boundary layer may interact with PV structures at upper-levels. Rossa (1995) found that the diabatically induced low-level potential vorticity anomalies are coupled with positive upper-level anomalies during frontal wave development. When positive PV is advected over a baroclinic zone, a destabilization of the atmosphere occurs. A synthesis of the Piemonte flood as an example (4-6 November 1994), covering aspects of the upper-level precursor structure derived from numerical model output, low-level mesoscale circulation patterns and radar observations is given in Binder and Rossa (1995).

2.1.2 Conceptual model

A conceptual model describes essential features of a meteorological phenomenon and identifies the principal processes taking place allowing a description of the phenomena's life cycle in terms of appearance, size, intensity, and accompanying weather (Zwatz-Meise, 2000). Bader et al. (1995) define a conceptual model as a schematic representation of the physical and dynamical components of a particular weather system. Browning (1985) presents an overview on conceptual ideas for precipitation producing systems related to cyclones in the mid-latitudes. The following Figure 2-2 presents the conceptual model for heavy precipitation events on the southern side of the Alps as proposed by Kappenberger and Kerkmann (1997). This model describes the "precipitation type two" according to Spinedi (1992) with prefrontal advection of warm-humid air and thunderstorm activity near or ahead of the front. Two jets ahead of the front transport humidity towards the LMTA at different heights, the lower at 1500 m a. s. l. from the Adriatic Sea and the upper from the Ligurian Sea at 3000 m a. s. l. In the prefrontal area the wind veers with height from southeast to southwest, on the backside of the front northwesterly winds predominate.

In this conceptual model, cloudiness is generated near the front north of Milano (i. e. in the LMTA). However, the clouds causing severe precipitation in the LMTA may be generated further south or southwest far from the LMTA. The IOP 2 shows an example, where the clouds producing strong precipitation in the LMTA were generated over the Thyrreanian Sea and were transported towards the Alps.

Near and over the Alps, the clouds experience a modification through orography. Orographic effects on atmospheric flow can produce or modify precipitating clouds through orographic lifting, triggering of convection, indirect effects of flow splitting or blocking, and mountain induced waves (Bougeault et al., 1998). An overview of precipitation mechanisms in interaction with orography is given in Houze (1993). Schaaf et al. (1988) investigated initiation sites for convection in the Rocky Mountains for 633 mountain thunderstorms, tracing back these thunderstorms to their initiation sites by using GOES images. They found that the initiation sites tended to cluster into preferred topographical areas or genesis zones. Also Banta (1990) found that thunderstorms develop in preferred areas of the topography, depending on external factors such a ridgetop winds and moisture distribution.

Schiesser et al. (1995) compared the intensity of MCSs between Oklahoma and Switzerland and concluded, that MCS north of the Alps are weaker due to the mountain barriers which prevent the moisture input from the Mediterranean. In addition, the complex terrain of the Alps and its surroundings suppress a higher degree of MCS organization. With the help of polar orbiting satellites Collier and Lilley (1994) investigated locations of storm initiation and their movements in Europe over a two year period. According to them, storms tend to develop among other locations over the higher Alps in and around Switzerland. Monk (1987) investigated the spatial and temporal distribution of topographically forced convection in polar maritime airstreams with the help of satellite and radar imagery. He found that the bands of cloud and precipitation repeatedly occur in similar air masses relative to the same topographic features. Hand and Sénési (1998) investigated 67 MCS in the western

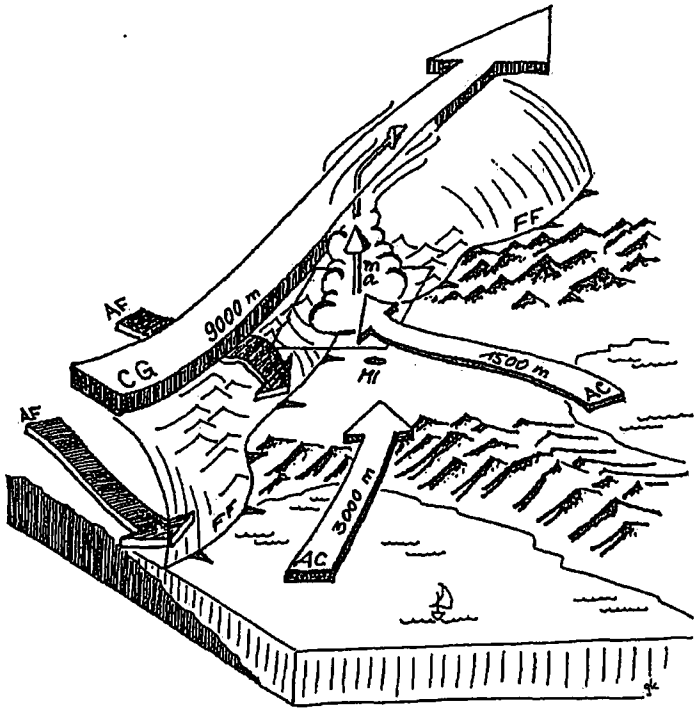

FIGURE 2-2. A conceptual model for the generation of a heavy precipitation event. Low-level jets (AC) at two different heights (1500 m and 3000 m) ahead of an approaching cold front (FF) offer continuous moisture supply. The front (FF) is being retarded/deformed by the orographic obstacle of the Alps, behind the front cold air (AF) is advected. North of Milano (MI) clouds are being generated indicating the area of strong precipitation activity (ma). Above the front a jet (CG) is situated, generated by upper level pressure fields (Figure from Kappenberger and Kerkmann, 1997).

Mediterranean from which 64 % start over land or near the coast where orographic forcing could be important. Further studies of heavy precipitation events related to orographic impact are presented in Frontero et al. (1997), Rossa and Quiby (1997), and Buzzi and Foschini (2000).

Talking about thunderstorms and their interaction with orography, we have to bear in mind that the peculiarity of heavy precipitation on the southern side of the Alps is the fact that it is produced from a combination of flow patterns associated with a synoptic or mesoscale low-pressure system, convection and the orographic modification of both. Especially on the south side of the Alps, convective activity which is triggered or enhanced through the Alpine orography may contribute to large precipitation amounts. To determine, whether triggering effects of orography can be observed in cloud top structures is one challenge of this study.

In order to give a short summary of necessary ingredients for the generation of heavy precipitation events on the southern side of the Alps, the following synoptic and mesoscale features are important:

1. A quasi stationary synoptic situation with a low pressure system over the British Isles and an upper level through extending from the British Isles to the southwestern Mediterranean Sea, 2. a cold front approaching the Alps, associated with prefrontal advection of latent and sensible heat (low level jets in the "warm conveyor belt") ahead of it, 3. the Alps acting as orographic barrier retarding the motion of the cold front and triggering convection, 4. upper level PV anomaly enhancing destabilization of the lower atmosphere, 5. the Mediterranean Sea as moisture source for the generation of precipitation. Spinedi (1992) estimated that considering three factors (location of the center of the low pressure, wind speed and direction over Milano and cyclonic curvature of the geopotential height over the Alps on the 500 hPa

chart) it would be theoretically possible to identify about 80 % of the events of heavy precipitation. Lin et al. (2001) give a similar summary of key ingredients for the production of orographic precipitation in the Alps.

2.1.3 Radiosoundings from Milano: mesoscale flow structure

Boscacci (1999) analysed radiosoundings at Milano (Italy) for days with thunderstorms in the Ticino and found no atmospheric layer structure typical of convective events. The investigations revealed further that instability indices derived from the Milano radiosoundings are useless for forecasting thunderstorm events. According to Zenone (1979) the wind direction and the wind speed up to 3000 m are the most decisive factors contributing to the occurrence of heavy precipitation events on the southern side of the Alps. As depicted in the conceptual model in Figure 2-2, low level winds at different heights ahead of the cold front seem to play a crucial role in the generation of strong precipitation. Therefore a good reason to have a closer look at the mesoscale flow structure in the region, where the low level jets from 1500 m a. s. l. and 3000 m a. s. l. converge. Figure 2-3 shows three plots with the mean wind direction and the mean wind speed at Milano during heavy precipitation in southern Switzerland. A veering of the wind direction with height is clearly visible.

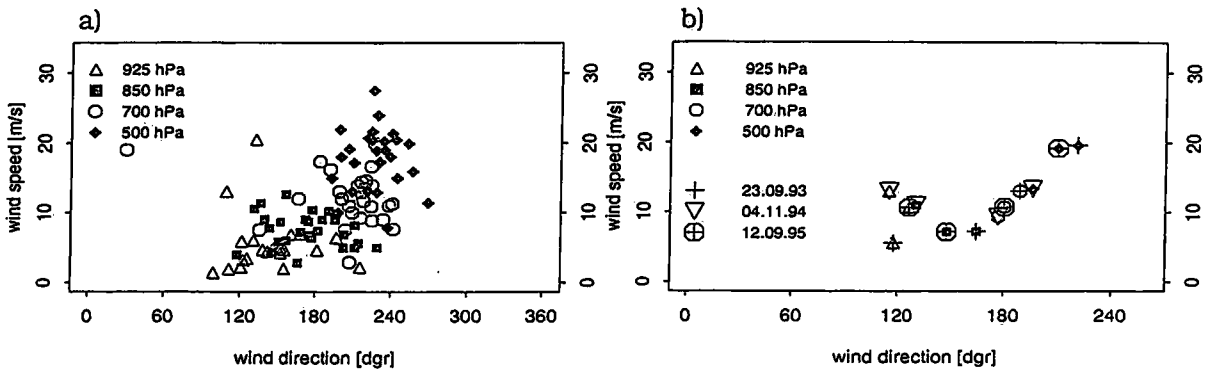

FIGURE 2-3. All figures show mean wind direction (x-axis) and mean wind speed (y-axis) at different pressure levels of days with heavy precipitation in the Ticino from radiosoundings at Milano. The days were associated with cold fronts, corresponding to the "type two" according to Spinedi (1992, see section 2.1). a) shows wind information of a total of 40 days with heavy precipitation in the Ticino from 1961-1998. b) presents wind information of the selected pre-SOP cases: 23.09.93 the Brig case, 04.11.94 the Piemonte case and 12. 09. 95 the Ticino case. c) depicts the selected MAP-SOP cases: 20.09.99 (IOP 2), 25.09. and 26.09.99 (IOP 3). Soundings from 00 UTC+ 24 h were analysed.

Figure 2-3 a) exhibits, that the soundings of each investigated pressure level are characterized by very similar wind properties. Analogue to the long-term radiosounding in Figure 2-3 a) both, the pre-SOP (Figure 2-3 b)) and the SOP (Figure 2-3 c)) cases show similar mean wind direction and speed. All plots show remarkable wind speeds at levels 925 and 800 hPa and a veering of the wind with height.

In summary, the results from the radiosounding investigations from Milano indicate: 1. a veering of the wind with height in the warm conveyor belt ahead of the cold front, confirming the conceptual model of Kappenberger and Kerkmann (1997, see Figure 2-2), 2. that the mean wind direction and the mean wind speed below 500 hPa of the pre-SOP cases are comparable to those of the SOP, 3) that the mean wind direction and wind speed of the selected pre-SOP (Figure 2-3 b)) and SOP cases (Figure 2-3 c)) are in accordance with the long-term radiosounding climatology (Figure 2-3 a)).

2.2 Precipitation events during the MAP-SOP

The statistical evaluation of the MAP Special Observing Period (7 September-15 November 1999) reveals that all investigated meteorological phenomena - including heavy precipitation events - occurred more frequently than expected relative to the average of the last ten years (Bougeault et al., 2001). A total of 25 project days were dedicated to the "Wet-MAP" topic "precipitation" and 17 IOPs were conducted. Figure 2-4 shows a spatial analysis of precipitation during the SOP according to the precipitation climatology of Frei and Schär (1998).

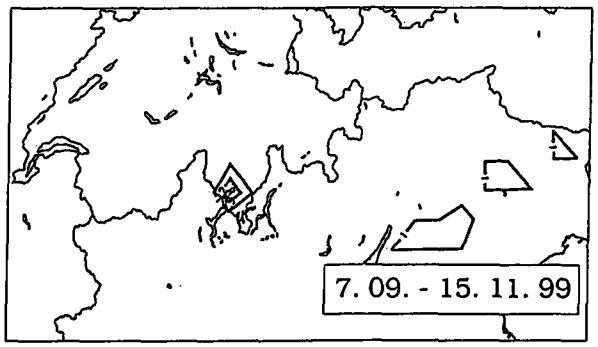

FIGURE 2-4. Number of precipitation events with precipitation ≥ 100 mm/24 h during the MAP-SOP as opposed to the full years in Figure 1-2. The thick black lines depict the grid points exceeding the threshold ≥ 100 mm/24 h. Dataset established by Frei and Häller (2001).

According to Figure 2-4 the preferred region for heavy precipitation during the SOP was the LMTA with some spots of heavy precipitation in the eastern Po Plain. Therefore, during the MAP-SOP no exception concerning the favourite geographical location for heavy precipitation could be found (cf. Figure 1-2, p. 13).

Rotunno (2001) stated that the precipitation over the LMTA had a predominantly stratiform character with the exception of isolated events. In fact, deep convective activity in the LMTA was rare during the SOP. In the evening of the 4 October (IOP 5), a MCS formed in the northeast of LMTA heading southwards but did not strike the Ticino. However, the LMTA experienced heavy precipitation on several occasions with series of perturbations moving over the Alps from east to west. Most of the perturbations were associated with active cold fronts with the classical frontal wind pattern as described in the previous chapter.

In the LMTA several rainstorms with convective activity occurred, especially at the beginning of the SOP. The IOPs 2, 3, and 5 were characterized by moist and potentially unstable air being lifted at the Alpine barrier and the triggered convection resulted in short-term precipitation with accumulations in excess of 200 mm (Steiner et al., 2000a and b). These three IOPs can be regarded as the most important cases where convection occurred in the LMTA. During IOP 2b the LMTA experienced precipitation peaking up to 300 mm/24 h, during the IOP 3 over 400 mm of precipitation was recorded over two days and on the 3 October (IOP 5) 280 mm/24 h were registered causing local flooding.

During the IOPs 6, 7, 8, 9 10, 14 and 15 predominantly stratiform precipitation was registered in the LMTA with lower precipitation amounts within 24 h. However, some of these events caused flooding in other regions (e. g. IOP 9: Ligurian coast, IOP 10: region of Nice, IOP 15: Veneto/Northern Apennines) and do not exclude convective activity. The characterization of the observed convection in the LMTA is described by MAP scientists in terms like "stratiform precipitation with orographical induced convection" or "convective orographically induced precipitation" (MAP Field Catalogue, 2000).

Since MAP does not address deep convection but rather convection which is "embedded" within the airflow approaching the Alps with a limited vertical extension, the kind of encountered convection might be described as "embedded convection in otherwise widespread upslope precipitation". With "embedded" we refer to the fact, that the observed convection was not deep, i. e. the convective activity does not affect the whole troposphere and has a limited vertical extent. The "widespread upslope precipitation" describes the stratiform precipitation area which is subjected to the large-scale ascent of airmasses over the Alps. Since we investigate convection in an Alpine region, the embedded convection can be - to an unknown extent - induced orographically. This is confirmed by Houze et al. (2001) who established a radar-based climatology of heavy precipitation events in autumn 1998 and 1999 in the LMTA. They found bright band echoes at 2-3 km over the Po Valley and embedded convective cells over the southern foothills of the Alps (Figure 2-5). Hence, hereafter we regard the term "embedded convection" as a result of shallow unstable airmass layers which may experience a modification through the underlying orography embedded within a stratiform precipitation area.

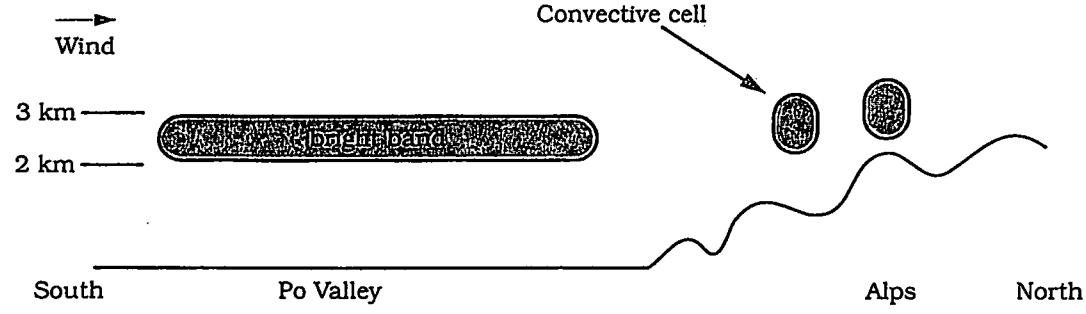

FIGURE 2-5. Conceptual model of convection embedded within a stratiform precipitation area as seen by radar on the southern side of the Alps, in analogy to Houze et al., 2001. The embedded convection is generated aloft the southern slopes of the Alpine barrier.

An overview over the IOP events and operations is given in Bougeault et al. (2001), an overview over the IOPs and available rapid scan imagery can be found in the Appendix A. A description of the IOPs relevant for the present study can be found in chapter 7.

3 Data

This chapter begins with a characterization of the rapid scan dataset[2)] from the SOP, proceeds to methods for the identification of convective regions by geostationary satellites and concludes with an introduction of the radar data characteristics from Monte Lema.

3.1 Meteosat operations during the MAP-SOP

Meteosat satellites are geostationary and fly at an altitude of about 36'000 km over the equator. On board they carry the Meteosat Visible and InfraRed Imager (MVIRI), a high resolution radiometer with three spectral bands: visible, infrared and water vapor (EUMETSAT, 1999). The Meteosat spacecraft are spin-stabilised with a nominal rotation rate of 100 revolutions per minute (rpm) around their main axis, which is aligned nearly parallel to the Earth's north-south axis. The Earth is scanned in the East-West direction using the rotation of the spacecraft and in the South-North direction by stepping the radiometer through a fixed angle every spacecraft revolution (Hanson et al., 2000). With the inclusion of radiometer retrace and stabilisation periods it takes 30 minutes to provide a full scan of the Earth disk. The location of the operational Meteosat is close to 0° longitude and the backup satellite is presently located at 9° West. Imperfections in the orientation of the orbital plane (i. e. satellite inclination) and the uneven shape of the earth cause a drift of the subsatellite point in small oval or figure-eight patterns centred over the equator and requires periodic station-keeping adjustments (Johnson et al., 1994). The first Meteosat satellite was launched in 1977 and provided data for two years, successively followed by new releases. The most recent ones are Meteosat-6 and Meteosat-7, the first one was the operational satellite from February 1997 until June 1998 when the latter took over (EUMETSAT, 1999).

The instantaneous field of view at subsatellite point of Meteosat spacecraft is 5 x 5 km in the infrared and water vapor channel, and 2.5 x 2.5 km in the visible channel (EUMETSAT, 1999). In a geostationary orbit, the field of view of a satellite remains fixed and a constant viewing angle enables the observation of the same geographical area over 24 hours. This allows a sequential observation of meteorological phenomena at high temporal resolution and is regarded as main advantage of this type of satellite. The main disadvantage of many geostationary satellites is the limited spatial resolution as a consequence of the distance to the Earth (Bader et al., 1995) since the radiometer scans away from nadir leading to a decrease in spatial resolution due to the curvature of the earth and the increasing distance to the satellite (Johnson et al., 1994).

Today, all Meteosat spacecraft are operated by EUMETSAT, the European organisation for the exploitation of meteorological satellites. Meteosat-7 is the last mission of the Meteosat Transition Programme (MTP) and will perform half-hourly full-disk scans until the operational start of Meteosat Second Generation (MSG), a new generation of geostationary satellite in mid 2002. For further information on the current and future satellite systems of EUMETSAT see http://www.eumetsat.de. Additional geostationary meteorological satellites are operated by the United States (GOES), Russia (GOMS), China (FY), the Japan Meteorological Agency (GMS) and the Indian Space Research Organization (INSAT).

During the MAP-SOP EUMETSAT provided rapid scan imagery from the standby spacecraft Meteosat-6. A total of 480 hours of rapid scan imaging operations took place, all in 5-minute interval, on request 7 days per week (Hanson et al., 2000). The longest uninterrupted rapid scan period lasted 48 hours from 20.10. 06:00 UTC until 22.10. 06:00 UTC 1999 (Hanson et al., 2000, see Appendix A). During the SOP, EUMETSAT Operations required an order from the MOC in Innsbruck at least 12 hours prior to the requested start time.

[2)] copyright 1999 EUMETSAT

In order to provide images with a high temporal resolution, Meteosat-6 was used in a reduced scanning mode. The rapid scan image data was rectified to the same projection used for the 0° operational mission and the geometric accuracy is comparable to that of the normal full Earth disk image (Hanson et al., 2000). Instead of a complete scan cycle of a full Earth disk which contains 2500 forward lines, only 228 lines were scanned covering a scan area centred over the Alps. After rectification the usable image lines were reduced from 228 to 170 lines and cover a latitude range from approximately 38° N to 49° N before the 30 September (Figure 3-1 a)). The scanning area was moved northwards by 30 lines on the 30 September and the area covered by the rectified image is approximately 40° N to 52° N (Figure 3-1 b)).

The number of pixels per line (i. e. 2500), the spatial resolution and the radiometer stepping rate (once per 0.6 second spacecraft revolution) are identical to the operational scanning mode (Hanson, 1999). The rapid scan procedure comprised hours of continuous operation followed by a few hours of normal scanning procedure for satellite stabilization and calibration of the sensor.

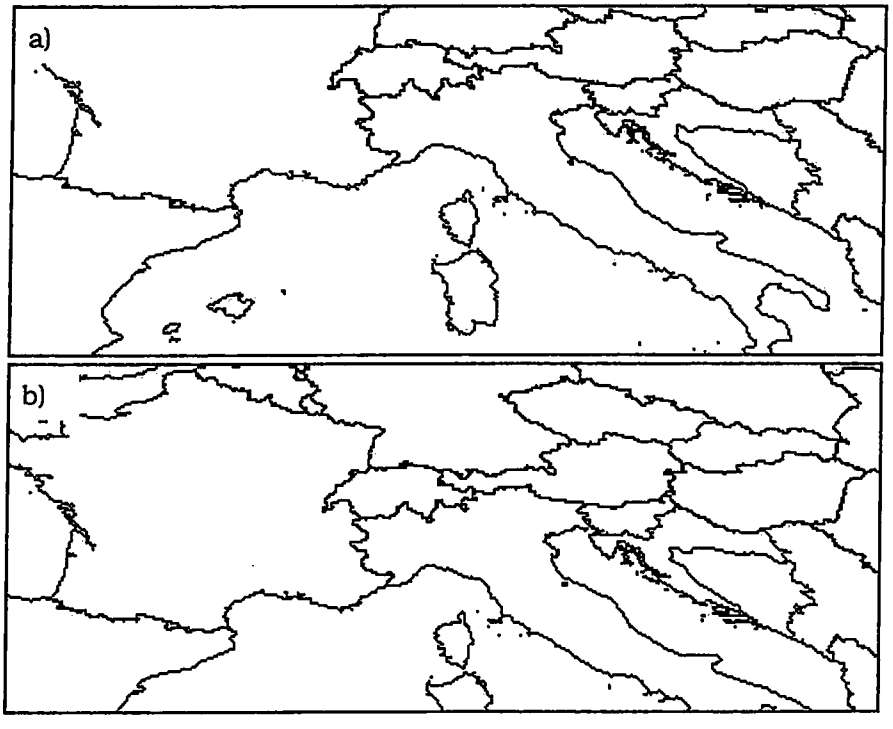

FIGURE 3-1. Rapid scan area over Europe a) *before* and b) *after* 30 September 1999.

During the spacecraft eclipse season (3 September-15 October 1999) it was not possible to scan with Meteosat-6 for a few hours around local midnight and any ongoing rapid scan imaging was interrupted during these times. The file format for image archival was the OpenMTP format which is regularly used for image archival at EUMETSAT's Meteorological Archive and Retrieval Facility (MARF). All rapid scan data are freely available at the MAP Data Center (http://www.map.ethz.ch)

As a direct response to the MAP-SOP EUMETSAT has established in 2000 a rapid scanning service on demand. In September of 2001 EUMETSAT introduced the operational rapid scanning service providing ten-minutes scans covering a latitude range of 15° - 65° N (Image, 2001). In Europe, MAP was the first operational requirement for Meteosat rapid scanning.

Examples of studies using GOES rapid scan imagery can be found in Negri and Adler (1981), Adler et al. (1983, 1985), Purdom (1996), and Vicente et al. (1999).

3.2 Data from the infrared channel

Meteosat infrared (IR) imagery is derived from electro-magnetic emissions by the Earth and its atmosphere at a wavelength between 10.5 and 12.5 μm and provides information on the temperature of the underlying surface or cloud. Since the infrared data is registered in the window region of terrestrial radiation, the modification (i. e. absorption and re-emission) of the emitted radiation through the Earth/atmosphere system is regarded as small (Bader et al., 1995). Data from infrared radiometer allow a continuous observation of cloud evolution over 24 hours with an instantaneous field of view at subsatellite point of 5 x 5 km. For the display of infrared images the grey scale of the data is normally inverted. Therefore, as temperature normally decreases with height, the infrared radiation with lowest intensity is emitted by the highest and coldest clouds and appears white. Regions from the Earth or ocean surface with highest intensity of terrestrial emission appear dark.

Especially in the cold channels (water vapor and infrared) the limited spatial resolution leads to the "beamfilling problem". Clouds smaller than the spatial resolution of channels or, (semi-) transparent and broken cloudiness result in higher temperature than the actual blackbody temperature of the cloud, since these pixels contain information from lower and therefore warmer regions.

3.2.1 Non-calibrated data and radiometer anomaly

The quantitative use of satellite data requires a calibration of the raw data. A calibration attributes to each measured raw radiance (i. e. a count value) a calculated radiance. In a next step, the IR/WV radiance are converted into brightness temperatures using a predefined relationship between radiance (Wm^{-2} sr^{-1}) and brightness temperature (K). In the present study relative differences of counts in space and time were used instead of absolute differences expressed in brightness temperature. Therefore, no calibration was necessary except for the rapid scans[3)] from 04 August 2001. For the images of the MAP-SOP EUMETSAT did not provide any calibration coefficients.

Data from the cold channels were not corrected for the effects of the Meteosat-6 radiometer anomaly. The Meteosat-6 anomaly manifested itself during the Meteosat-6 commissioning as a count variation of the cold channels throughout the taking of an image (personal communication Michael Williams). However, EUMETSAT did not detect the anomaly with 5 minutes scans of the SOP and visual inspection of the image loops did not reveal any count instabilities. In contrast, radiometric instabilities were recognized in Meteosat-6 sequences provided by EUMETSAT's rapid scanning service (personal communication Michael Williams) after the MAP operations from 2001 onwards. For this reason, the cold channels of Meteosat-6 from the most recent event investigated in the present study (04.08.2001) were calibrated.

In summary, for the present study we used non-calibrated Meteosat-6 data and discovered no count anomaly within the analysed datasets.

3.2.2 Cloud displacement/ Parallax correction

Due to viewing-angle geometry and the projection of the satellite image onto a two dimensional plane for display, a cloud displacement occurs (Kidder and Vonder Haar, 1995). The parallax-induced cloud displacement is a function of the viewing angle and the height of

[3)] copyright 2001 EUMETSAT

the cloud above the ground and the direction of the apparent cloud offset is directly away from the subsatellite point (Johnson et al., 1994). Since Meteosat-6 is located to the west, there is a shift to the east in the apparent cloud positions as seen by Meteosat-6. This cloud displacement can be corrected if the height of the cloud, the satellite position, and the coordinates of the cloud are known (Kidder and Vonder Haar, 1995).

According to Johnson et al. (1994), a cloud top located at 40° north at a height of 4 km results in an offset of approximately 4 km. At 50° north the offset is already ~ 6 km.

Estimations reveal, that the amount of cloud displacement in our study is within the error of image rectification. Rectification includes a geometric correction process which transforms the image pixels to a nominal image geometry by removing deformations caused by the spacecraft's movement (www.eumetsat.de). According to EUMETSAT, the pixel displacement due to rectification varies between 1 and 2 pixels (personal communication Chris Hanson). In midlatitudes, the size of a pixel in the infrared and water vapor channel is ~ 5 x 8 km, resulting in a pixel offset between 5 km (minimum) and 16 km (maximum). For the visible channel (~ 2.5 x 4 km) the offset ranges between 2.5 and 8 km. In addition for the correction of cloud location the height of the cloud has to be guessed, which is another source of error.

The overall aim of this study is not to find the exact localization of convective centers, since it is known that low cloud-top temperature may not be directly located over the convection at lower levels (Adler et al. 1983, Heymsfield and Fulton 1988, Goldenberg et al. 1990). The final result of this study might be an estimation or a probability of the relative proportion of the convective/stratiform areas within a certain cloud region at a certain time. Therefore no parallax correction was done.

3.3 Data from the visible channel

Imagery from the visible (VIS) channel offers the highest spatial resolution of all three Meteosat channels (subsatellite point: 2.5 x 2.5 km) and contains information on the solar radiation reflected by the earth-atmosphere system. The VIS data is registered in the spectral band between 0.45 and 1.00 μm. The intensity of the pixels depends on the albedo of the underlying surface or cloud, highest reflectivities are shown in white, lowest in black. Water content and depth of the cloud are considered the most important factors on which the brightness of a cloud depends (Bader et al., 1995). Especially in the morning and evening scan VIS data exhibit distinct light/shadow effects which enhance cloud top structures.

The limitation to visible images is that they exhibit a pronounced time- and location-dependent diurnal and seasonal variability due to the changing illumination conditions given by the location of the pixel and the local sun position (Binder, 1989).

3.3.1 Normalization of VIS data

In order to make data from different times and geographical locations compatible with respect to insolation, a normalization procedure was used. This normalization procedure converts satellite visible channel data from Meteosat to a well-defined reference state (Binder, 1989) with a uniform level of illumination over the daylight sector of the picture (Bader et al., 1995). As a consequence normalized images contain no light effects.

In this study, the normalization procedure established by Binder (1989) was used. This procedure accounts for the solar zenith angle and produces reasonable results for solar zenith distances up to almost 90°. For each pixel of the analysed image the latitude and longitude as well as day and daytime were used as input parameters for the normalization. The normalization allowed an analysis of VIS images over a period starting from 07:00 until 17:00 UTC with a decrease towards the end of the SOP.

3.4 Identification of convective regions by satellite: Overview

For the identification and forecast of convective activity and its related severe weather phenomena (i. e. hail, strong precipitation, wind gusts) a big effort was and is made in scientific research of convection (e. g. COST-78, see Lagouvardos et al., 2001). Sprayd and Scofield (1984) describe satellite and radar data characteristics of different types of heavy convective rainfall systems. Especially for nowcasting purposes, the detection/identification and the forecasting of convective activity are important aspects (Riosalido, 1996).

In this study we use visible and infrared data from geostationary satellites in order to separate convective from stratiform cloud regions. Since visible and infrared radiation does hardly penetrate the cloud, the relationship between satellite-measured visible or infrared radiance and physical processes within the clouds are indirect. The basic assumption of convective-stratiform detection methods is, that cloud top structures are related to physical processes within the clouds.

Severe convection related to thunderstorm activity can be identified in the infrared data by cold cloud tops and rapid evolution. Cloud tops quickly extend to the top of the troposphere and rapid lateral expansion of the anvil region occurs (Kidder and Vonder Haar, 1995).

Using data from the visible channel, convection can be detected by a more detailed analysis of the cloud top structures due to the higher spatial resolution of the visible channel (e. g. Meteosat and GOES). While the coarser spatial resolution of the infrared channel smooths out the smaller convective cloud top variations, distinct cumuliform cloud-tops may be observed in the visible channel (Adler et al., 1985). Bader et al. (1995) gives an example, where the high spatial resolution of the VIS channel data and light/shadow effects allow an identification of strong convective updrafts within the anvil regions of cloud clusters in the Gulf of Biscay.

In both, infrared and visible images small convective features and larger convective cloud shields tend to have sharp edges on their upwind sides (Bader et al., 1995). These sharp edges are often used as criteria in order to distinguish between high cirrus clouds and convective clouds, since a pronounced cloud edge implies a thunderstorm (Adler and Negri, 1988). In Bader et al. (1995) the characteristics of convective regions in the visible and infrared channel are described in detail.

A broad number of software developments exist which aim to retrieve automatically convective cloud regions by means of satellite imagery. Some of these detection algorithms like the Convective and Stratiform Technique (Adler and Negri, 1988) aim to derive satellite-based precipitation estimations. However, these techniques are not universally applicable since techniques developed for the tropics may not perform well in the midlatitudes (Kidder and Vonder Haar, 1995). An overview of satellite precipitation estimation research is given in Adler and Negri (1988), Kidder and Vonder Haar (1995), and Levizzani (1998) and (2000).

The following section gives a short overview of some of these software products which rely on imagery input from geostationary satellites (i. e. Meteosat or GOES) elucidating the retrieval-techniques of convective regions.

3.4.1 USA: Convective-Stratiform Technique

Adler and Negri (1988) developed with infrared data the Convective-Stratiform Technique (CST). The technique provides an identification of convective centers and assigns precipitation rate and precipitation area to these features using GOES cloud-top temperature combined with a 1D cloud model.

Convective precipitation areas are separated from stratiform areas with the help of the spatial variation of brightness temperature around a localized brightness temperature minima. Regions with active convection are defined by a relative minima of brightness

temperature and a large slope parameter measuring the strength of the localized minimum value related to surrounding pixels. This slope parameter removes thin and nonprecipitating cirrus and is calculated by subtracting the average brightness temperature of the six closest pixels from the local brightness temperature minima. With the help of the brightness temperature minima, the slope parameter and an empirical linear discrimination line, convective cores are separated from thin cirrus points. According to them, a large slope parameter (i. e. strong gradients at the cloud borders) implies thunderstorm activity, while a weak slope parameter (i. e. weak gradients at the cloud borders) is associated with cirrus. The empirical discrimination line was established with the help of visible channel imagery and radar data.

Goldenberg et al. (1990) adapted the CST to an equatorial ocean area and found that the discrimination line would be rather accomplished by an exponential form because of the colder cloud tops in the investigated region. Reudenbach and Bendix (1999) adjusted the CST to midlatitude conditions for a quantitative estimation of summer convective rainfall.

Adler et al. (1985) used rapid scanning data with 5-minute interval from GOES to detect severe thunderstorms. For each individual storm, three rate of change calculations were made: 1. the cloud top ascent rate in the upper troposphere, 2. the cloud top ascent rate above the tropopause, 3. the maximum rate of expansion of area within temperature brightness isotherms. According to them, the separation between the cloud top ascent rate below and above the tropopause is necessary, due to the deceleration of overshooting parcels.

3.4.2 France: RDT/ISIS

Since 1999, Météo-France has been developing the Rapid Developing Thunderstorm (RDT) product of EUMETSAT's Nowcasting Satellite Application Facility (SAF). The software named RDT intends to provide information about significant convective systems from meso-α scale (e. g. Mesoscale Convective Complexes) down to smaller scales and possibly meso-γ scale (isolated storms) (Morel et al., 2000). Today, the software development is still proceeding.

The RDT product consists of numerical data where convective systems are described as "objects" with a list of their most relevant characteristics like cloud area, ellipticity, average temperature, velocity, cooling rate and area expansion.

For that purpose, Météo-France has further developed the software called ISIS (Instrument de Suivi dans l'Imagerie Satellitale) which allows a tracking and a documentation of convective systems from a sequence of infrared images. The ISIS output delivers a multi-parametric description of convective systems, including information on morphological (ellipticity, cloud area), radiative (average temperature, temperature gradients), and dynamic (cooling and expansion rate) characteristics (Morel et al., 2000). The software consists of three main modules:

1. Thresholding and detection of cloud systems: The analysis of pixels colder than a brightness temperature threshold and pixel areas greater than an areal threshold are recognized as "cells". The temperature thresholds are adaptive in order to account for the different development stages of the cloud systems (Morel et al., 2000).

2. Tracking of cloud systems: The tracking is performed by an overlapping technique, calculating the fraction of overlap between tracked objects in two consecutive images (cf. Morel et al. 1997, Morel and Sénési 1999, and Morel et al. 2000).

3. Discrimination of convective systems: The identification of convective systems is based on infrared images and analyses of the local temperature gradient on the edges of the cloud shield. Since young convective cells are related to strong cloud evolution, strong temperature gradients are located at their cloud edges. Simplified, a cell is regarded as convective, if the (peripheral) temperature gradient is larger than a predefined discrimination value. For more

details see Morel and Sénési (1998 and 1999) and Morel et al. (2000). The discrimination values vary monthly and have been tuned with lightning data as the ground truth for the design of convective samples on a five-year dataset.

The quality of the discrimination of convective systems has been quantified over France and shows a significant quality during the whole warm season (from April to September) for convective systems with a cold anvil exceeding 10 000 km^2 at a brightness temperature threshold of - 45° C. 80 % of the detected convective systems and even more than 90 % of the most active ones are correctly discriminated by the method, the rate of low false alarm was around 8 % (Morel and Sénési, 1999).

3.4.3 Austria: ASII

The Austrian Meteorological Service (ZAMG) has developed a nowcasting tool named "Automatic Satellite Image Interpretation" (ASII) within the framework of EUMETSAT's "Nowcasting and Very Short Range Forecasting" SAF. The aim of the ASII product is an automatic satellite interpretation in terms of conceptual models, providing a classification of typical cloud configurations and related key parameters and physical processes (Wirth et al., 2000).

ASII identifies convective cells by the brightness minima and their compact circular or elliptical shape. The successive steps for the detection of convective cells are (Csekits et al., 1999):

- Smoothing of calibrated IR images in order to eliminate small and not-significant brightness maxima.
- Extraction of the local brightness minima being colder than - 25° C.
- To avoid the detection of homogenous and fibrous structures, around each localized brightness temperature minima four concentric circles with different prescribed radii are constructed. For the classification as convective cell, 80 % of all pixels on at least one concentric circle have to exhibit a minimum difference to the localized brightness temperature maxima.
- Calculation of the development image, which is the motion-corrected difference image between two consecutive images separated by a time lag of 30 minutes. The development image can be interpreted as non-advective changes in the cloud field between two consecutive images.

The latter step allows an attribution of different development phases within the life-cycle of a convective feature. A life cycle characterization of convective cells recognizable in development pictures are given in Csekits et al. (1999) and Zwatz-Meise (2000).

3.4.4 Italy: NEFODINA

The Italian Air Force Meteorological Service developed a nowcasting product named NEFODINA (from the Italian: NEFOanalisi DINAmica), in order to detect and extrapolate strong convective phenomena from Meteosat infrared images. NEFODINA is an object-oriented product which uses statistical parameters from the objects identified as convective cells. The recognition of convective cells is established by calculating the slope index of the CST according to Adler and Negri (1988). Each identified cell is associated with a life cycle stage: e. g. a convective cell is regarded as developing, if the cloud top height is growing (i. e. cooling) and its area is enlarging. NEFODINA was used together with the MAP rapid scan data and it was found, that the detection of severe convective systems could be improved using images in a 5-minute interval instead of the operational 30-minute interval (Rosci et al., 2000). Today, NEFODINA is running operationally using 30-minute interval Meteosat images.

3.4.5 England: GANDOLF

In 1994 the UK Met. Office started a project which was aiming to improve the use of satellite imagery in quantitative forecasting systems, such as numerical weather prediction and nowcasting (Lagouvardos et al., 2001). The product of this project is a flood forecasting and warning system, called GANDOLF (Generating Advanced Nowcasts for the Deployment of Operational Land-based Flood forecasts).

GANDOLF is used to choose between advective and life cycle forecasting methods and for the latter, GANDOLF NNCC (Neural Network Cloud Classifier) was developed. The NNCC was produced in 1996 and used nearly 2200 samples of 17 x 17 pixel arrays of Meteosat visible and infrared imagery, as training class for an automatic cloud classification (Lagouvardos et al., 2001). These samples were subjectively labelled by an experienced meteorologist in four different classes: clear land or sea, dynamic cloud (frontal cirrus, thin cirrus, altostratus, nimbostratus and fog), shallow convective cloud (stratocumulus, cumulus and cirrus overlying stratocumulus) and deep convective cloud (cumulonimbus, MCS) (Pankiewicz, 1996a). The overall accuracy of this robust classifier from 730 independent test samples was 84 % including the analysis of textural pixel information (Lagouvardos et al., 2001). For further details of pattern recognition techniques see Pankiewicz (1995), for details of the NNCC see Pankiewicz (1996a and b). In 1999, NNCC was incorporated into GANDOLF and is regarded today as a key component for the distinction between convective and stratiform clouds (Lagouvardos et al., 2001).

3.4.6 Summary and comments

After presenting some techniques with infrared channel data, the main input parameters for the detection of convective cloud regions can be summarized as follows: the cloud top temperature minima and the surrounding pixel characteristics (e. g. the slope parameter of CST), the areal expansion of the anvil region in time, the cooling rate in time, the persistence of an analysed cloud region in time and its shape and size (e. g. extension of anvil region).

Neural networks, such as GANDOLF NNCC, use cloud patterns as input and compare them to templates of known cloud pattern values (e. g. size, shape, pixel brightness) as predefined in the training classes of cloud classification. Convective regions are identified by their spectral and textural appearance, emphasizing the analysis of cloud patterns within a region of interest.

The CST, RDT, ASII and NEFODINA use empirical discrimination functions for the identification of convective pixels/areas. By relating the strength of the localized minima brightness temperature to the surrounding pixels, convective centers are separated from cirrus clouds. One of the drawbacks of empirical discrimination functions and threshold techniques arises due to the adjustments required when applying the techniques to regions with different meteorological conditions, e. g. the tropics. Moreover, a fixed threshold, if set to a low value (e. g. cold temperature), may prevent the identification of young convection. Otherwise if a fixed threshold is set to a high value (e. g. warm temperature) the analysis may incorporate pixels which are not related to convective activity. Thus the results and the information gained of a threshold dependent analysis are strongly steered by the threshold value.

According to Yuter and Houze (1998), methods using an IR temperature threshold as a proxy for convective and stratiform precipitation overestimate convectivity below the clouds, since deep clouds contain stratiform and convective regions. Adler et al. (1985) found, that not all brightness temperature minima are thunderstorms (i. e. related to strong convective activity) and that not all thunderstorms have brightness temperature minima all the time.

Morel et al. (2000) implemented an adaptive temperature threshold detection algorithm taking into account the life-cycle dependent stage of a cloud system. They use an adaptive

temperature threshold value which is warm in the early stage of convective systems and colder during the development of the system.

All presented convective-stratiform methods rely on data from geostationary satellites. Anagnostou and Kummerow (1997) present a method using data from the Special Sensor Microwave/Imager (SSM/I) (see Ferraro et al., 1998). They defined a "variability index" defined as the mean absolute 85-GHz SSM/I brightness temperature difference between a pixel and the eight surrounding neighbour pixels. They found, that a low variability index is related to high probability of stratiform coverage, while a high variability index is related to high probability of convective coverage. Current meteorological information for the validation of the presented satellite-based systems are and were gained from radar, raingauge and lightning data.

3.5 Radar data

Analogous to satellite data, weather radar provide information on precipitation areas with high temporal and spatial resolution. Weather radar give an overall picture of precipitation systems from the synoptic to the storm scale, providing important information for short-term predictions (Germann, 2000). They operate within the 3 to 10 cm wavelength range and detect precipitation-sized particles and are not - like satellites - sensitive to small cloud particles (Bader et al., 1995). Thus radar data allow an interesting insight into physical processes within a precipitation cloud and are therefore an excellent complementary information for the validation of satellite-based convective-stratiform identification methods.

A precipitation radar measures the radiation power scattered back from water droplets or snow flakes in a volume of the atmosphere (Bader et al., 1995). The scattered radiation power is expressed in terms of reflectivity (Z), which is converted into corresponding rainfall rates (R). In this study, the conversion is based on an empirical predefined Z-R relationship with 16 intensity classes (see Table 3-1, p. 36) which is used operationally at MeteoSwiss.

The 5 cm Doppler radar is situated on the southern side of the Alps (Ticino) on a mountain named Monte Lema at 46.042° N/8.833° E at a height of 1625 m a. s. l. and was installed in 1993. The antenna scans the volume around the radar at 20 different elevations every 5 minutes with a 3 dBZ beam-width of 1° (Joss et al.,1998). During the MAP-SOP, the Monte Lema radar provided continuous operations and was used to construct a real-time radar composite with data from all operational radar around the Alps (Bougeault et al., 2001). A description of the operational available radar products from MeteoSwiss can be found in Joss et al. (1998).

For this study, reflectivity data in polar coordinates was used which provide the highest spatial resolution (i. e. 1 deg. x 1 deg. x 1 km). Since the width of a radar beam increases with distance, the spatial resolution is high at short range and low at wide range from the radar. The reflectivity of precipitation particles assigned to an image pixel in polar coordinates is representative for one cell with extension of 1 degree in azimuth and 1 km in range laying over the surface scanned during the given elevations (Joss et al., 1998). The cells reflectivity is coded in range 0 to 15 corresponding to a linear scale in dBZ and logarithmic rainrate scale, respectively (see Table 3-1, p. 36).

The earth's curvature, ground clutter and shadowing effects of mountains reduce radar visibility (Joss et al., 1998). Therefore, a correction is necessary to account for effects of reduced visibility. For each scan elevation visibility maps are created which give indication about the degree of non-occultation at locations scanned by the radar beam. The radar data used in this study is corrected for visibility reduction for each scan elevation. For further information concerning the correction of the radar visibility see Held (1995). Radar data used

in the present study was corrected with standard correction algorithms (i. e. ground clutter suppression, visibility correction, etc.) of MeteoSwiss.

TABLE 3-1. Classes of reflectivity and rainrate intensities according to Joss et al. (1998). Note the logarithmic scale of the rainrate.

Class	Reflectivity [dBZ]	Rainrate [mm/h]
00	< 13	< 0.16
01	13 - 16	0.16 - 0.25
02	16 - 19	0.25 - 0.40
03	19 - 22	0.40 - 0.63
04	22 - 25	0.63 - 1.00
05	25 - 28	1.00 - 1.60
06	28 - 31	1.60 - 2.50
07	31 - 34	2.50 - 4.00
08	34 - 37	4.00 - 6.30
09	37 - 40	6.30 - 10.0
10	40 - 42	10.0 - 16.0
11	43 - 46	16.0 - 25.0
12	46 - 49	25.0 - 40.0
13	49 - 52	40.0 - 63.0
14	52 - 55	63.0 - 100.
15	> 55	> 100.

4 Methods

In this chapter the methods for the identification of convective activity based on satellite data are presented, followed by preliminary results of the implemented satellite-based techniques and a description of the convective-stratiform radar algorithm.

As mentioned before, the basic assumption underlying the presented methods is, that the cloud top structure provides information on convective and stratiform cloud regions. For that purpose we use spatial and temporal information from infrared and visible rapid scan data. But first of all the requirements of the implemented satellite-based methods are defined.

4.1 Methodological requirements of this study

22.09.1992, Vaison-la-Romaine, France: several MCS generated a flash flood and produced 300 mm of rain in 24 h, with precipitation intensities reaching 220 mm in 3 hours causing big damages and loss of life. Meteosat imagery from this case shows a remarkable feature: a stationary V-shaped cloud structure (Benech et al., 1993). A V-shaped cloud is an unambiguous indicator for the occurrence of convection (Adler et al., 1985) and is produced when strong upper level winds are diverted around an overshooting top.

As pointed out in section 2.2 (p. 25) the convection encountered in the LMTA during the SOP can be described as "embedded" rather than "deep" convection and during the SOP no V-shaped cloud was observed in the LMTA. Since embedded convection is a part of a stratiform cloud, convective regions may not be clearly identifiable like isolated deep convective cells. Further, possible orographic effects triggering convection might be weak and therefore difficult to detect. Deep convective clouds can be recognized by their compact and elliptical shape of their cloud borders (cf. section 3.4, p. 31), in contrast embedded convective regions occur in stratiform clouds and are expected to exhibit a rather diffuse and fuzzy appearance within these cloud shields.

For the recognition of convective regions within satellite images, thresholding (i. e. fixed count/temperature thresholds, empirical discrimination lines) should be avoided, because of the loss of potential relevant meteorological information before a given threshold is exceeded. In this study, thresholds were only used to exclude warm pixels of land surfaces and warm clouds from the analysis as well as for classification purposes (cf. section 8.4, p. 77). The basic methodological requirements applied in this work can be summarized as follows:

- The analysis is restricted to cloud features on synoptic to the meso-β scale in a limited geographical area in the midlatitudes (LMTA) and shall exploit maximum benefit from the high time resolution of satellite and radar data.
- The analysis should account for the detection of "embedded" rather than "strong" convection within cloud areas in satellite images.
- The analysis investigates cloud patterns and no isolated cloud systems (i. e. no dependency on morphological characteristics of single clouds).
- Whenever possible, the use of fixed thresholds for the separation of convective and stratiform cloud regions should be avoided.
- The applied method should be fast, robust and easy to handle.

Based on these requirements, a methodology was developed which may allow to detect potential (embedded) convective regions using spatial and temporal information from cloud-top structures.

4.2 Spatial variance

In adaptation of the Convective Stratiform Technique (Adler and Negri, 1988) the satellite image is subdivided in 3 x 3 pixel arrays and for each array the count variance is calculated.

$$s^2 = \frac{1}{n-1}\sum_i (x_i - \bar{x})^2$$

s^2 = count variance of 3 x 3 array
$\bar{x}$ = mean count

The variance is a measure of the count variability of the pixels within a limited region: pixel arrays with low variances provide a smooth cloud top, high variance values indicate a strong textured cloud top. In accordance to the assumption, that cloud top structures give information on the cloud type below, stratiform clouds are characterized by a smooth cloud top, while convective cloud structures exhibit - due to up- and downdraft regions within the cloud - high spatial variances. As an exception, regions of strong up- and downdraft may occur below large anvil cloudiness, for example of a well-developed and mature convective system (e. g. MCS) and may be falsely regarded as stratiform cloudiness due to the shielding by a smooth cloud top. Apart from regions with strong vertical motion, high variance signals are encountered at cloud borders. Often individual borders of clouds are delineated and the change of size of these cloud borders in time gives hints about the intensity of cloud development. Therefore, the lateral expansion of clouds permanently observed over a period allows an indirect determination of their life stages (e. g. growing or dissipating stage).

The array size of 3 x 3 pixels was found to be a reasonable size, since larger arrays (e. g. 5 x 5 pixels) lead to spatially coarser signals and higher variance values. An example with results of the variance computation is provided in Figure 4-1 b).

4.3 Evolution/Tendency

In this study, the rate of change of individual pixel counts are calculated over a 10-minute period from the inverted infrared and water vapor data. The result reveals whether a pixel is either warming (i. e. decreasing count value) or cooling (i. e. increasing count value) and gives an indication about the magnitude of count value change within 10 minutes. Pixels with strong cooling may be an indicator of convective updrafts within a cloud shield. On the other hand pixels with a warming tendency denote regions of warming and possibly regions with cloud dissipation.

$$\left.\frac{dC}{dt}\right|_{n+1} = \frac{C_{n+2} - C_n}{2\Delta t}$$

C_n = count value at time n
Δt = time between two consecutive images

$$\left.\frac{dC}{dt}\right|_{n+1} > 0 \quad \Rightarrow \text{cooling}$$

$$\left.\frac{dC}{dt}\right|_{n+1} < 0 \quad \Rightarrow \text{warming}$$

It is important to note, that the calculated result of pixel evolution is centred between the images at time n and time $n + 2$, i. e. the image at time $n + 1$ contains the information on evolution rates over a ten-minutes period. The pixel evolution helps to delimit potential regions of cloud development and interesting time sequences of the rapid scan imagery. An

example of a rapid scan with results of the evolution computation is provided in Figure 4-1 a). Note that negative values of pixel evolution indicate a warming pixel, a cooling pixel reveals a positive value over the 10-minute period.

4.4 Preliminary results using described satellite methods

In this section, preliminary results from investigations with the spatial variance and tendency methods are described. Results from the temporal evolution of pixels reveal the magnitude of warming and cooling of a single pixel over a period of 10 minutes. The main difficulty of the tendency method is posed by advection which leads to seemingly strong cooling effects on the leading edge and seemingly strong warming effects on the back side of cloud systems. The putative warming and cooling signals result from the cloud motion since pixel count values change abruptly when cold cloud areas move over warmer areas like land and/or sea surfaces. In Figure 4-1 a) the seemingly warming signals are well established at the backside of the cloud shield moving from southwest to northeast. Seemingly cooling signals are located at the front side of the clouds, in the direction of cloud motion. This "double structure" of the calculation of pixel evolution is characterized by cooling effects at the leading edge of the cloud borders and warming effects at the backside of the clouds is typical of isolated cloud cells but also of entire cloud shields.

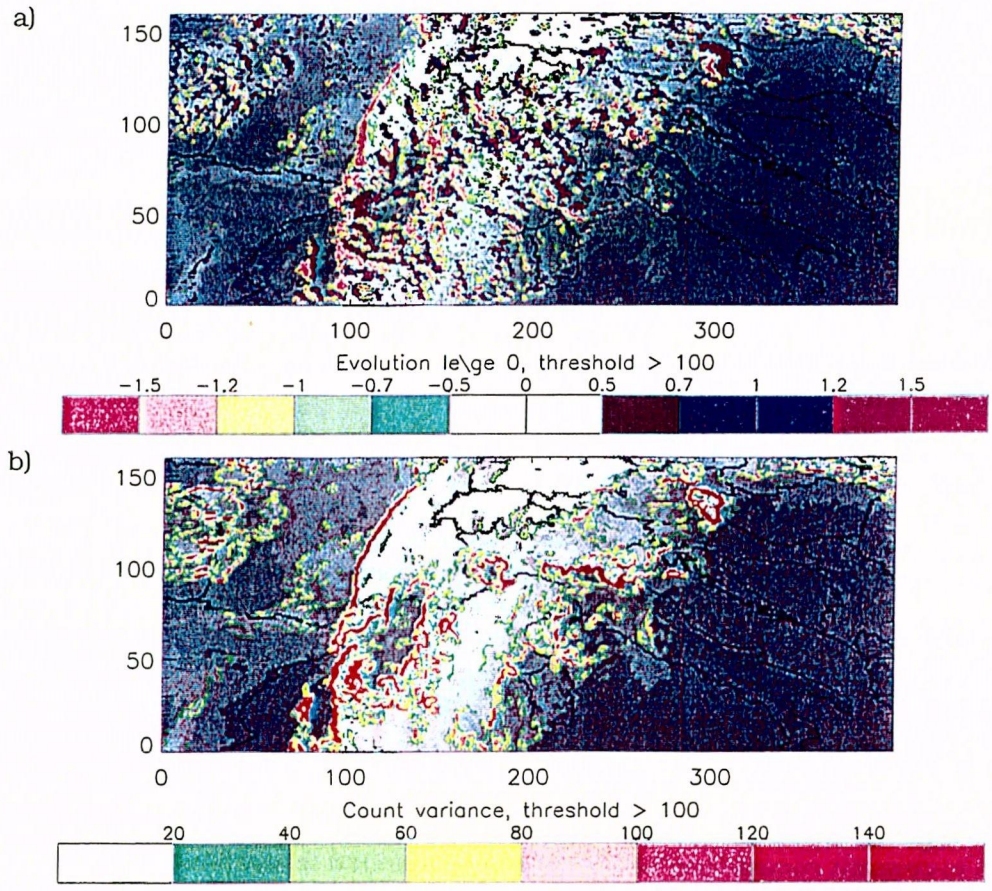

FIGURE 4-1. Examples of a) the temporal evolution of pixels over 10 minutes and b) the spatial variance within 3 x 3 arrays, 26.09.99, 09 UTC. Pixels exceeding the count threshold 100 were analysed. The magnitude of cloud development (negative: warming, positive: cooling), respectively of pixel variability is depicted with color. The clouds move from southwest to northeast exhibiting in a) putative strong cooling signals at the leading edges of the clouds and putative warming signals at the backside of the clouds and in b) strong pixel variances at the cloud borders.

The spatial variance is calculated for each image independently from the consecutive image and therefore there are no "artificial" signals due to cloud motion. As shown in Figure 4-1 b) the signals of the spatial variance are strongly accentuated at cloud borders since those arrays contain cold as well as warm pixels.

One of the basic questions at the beginning of the present study was, in which way convective areas would appear in satellite imagery through the application of the spatial variance and the tendency calculations. For that purpose, several isolated convective cells in the rapid scan region were investigated. The results of these investigations are summarized in Figure 4-2, which shows a conceptual model of signals provided by the tendency and the spatial variance occurring with convective clouds at different stages of life cycle. The inspection shows that the tendency and the pixel variance depend on the stage of life cycle of the observed cloud and its related convective activity. In a cloud containing young convection (i. e. before the generation of an anvil) the locations of the tendency and variance signals coincide with areas of strongest cloud development and areas of high pixel variability. After the generation of an anvil the tendency signals are characterized by the "double structure" meanwhile the signals of the pixel variance are situated around the border of the cloud. In this mature stage of cloud development, convection is completely hidden by the smooth anvil cloud top. Figure 4-2 gives an example of the characteristic appearance of isolated and deep convective features in satellite images. However, at that point in time it was unclear whether typical cloud top structures related to embedded convective activity could be identified, too.

In summary, first investigations of satellite data provide evidence, that the signals stemming from the temporal evolution consist of an "advective" part and of a "development" part. The first one is an unwanted artificial effect due to the cloud motion (advection) and must be reduced in order to enhance the signals of the latter one, the cloud development. The signals due to cloud development are supposed to be related in most cases with convective activity and are therefore of primary interest. For the reduction of the earth-relative motion of the investigated clouds in satellite imagery a tracking algorithm was introduced and is described in chapter 6.

5 Radar

In combination with the satellite information the radar observations indicate the point in time, where cloud systems start to produce precipitation. In order to verify satellite-derived information, we need to know whether the precipitation detected by the radar is convective or stratiform. In this section the necessary steps for a comparison between radar and satellite data are highlighted followed by a description of the radar-based recognition of convective and stratiform precipitation and of the implemented convective/stratiform separation radar algorithm.

5.1 Comparison radar and satellite

As outlined in previous chapters, there are many studies dealing with the detection of convective regions, either in satellite images or in radar images. However, studies with a direct and systematic comparison between convection found in satellite and radar images are rare.

Nagle and Serebreny (1962) compared radar precipitation echo and satellite cloud observations and found that at any particular instant in time a very low percentage of clouds precipitate in very limited areas. Negri and Alder (1981) defined individual thunderstorms by the location of the minimum brightness temperature with 5 minutes rapid scans from GOES and compared these locations with maximum radar reflectivity. They investigated one day

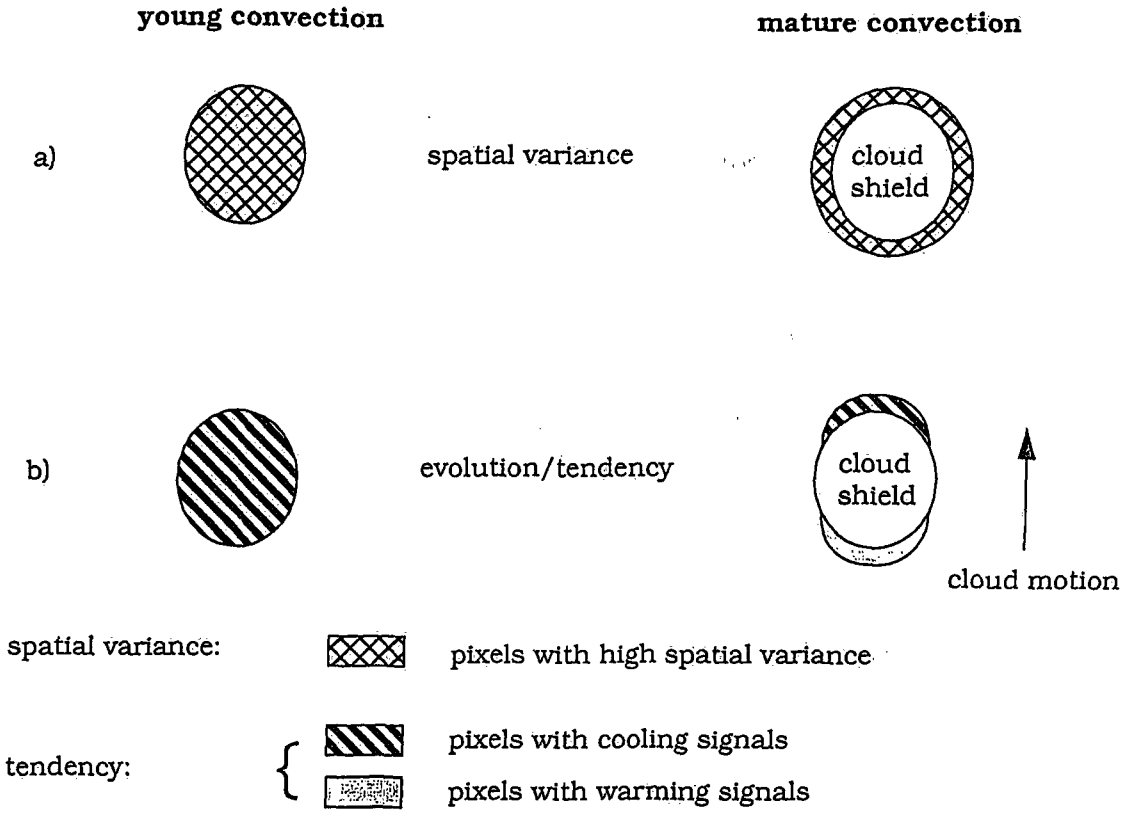

FIGURE 4-2. Signals of the spatial variance and the temporal evolution as shown by a single cloud at two different life stages: young (left side) and mature (right side) convection. In the stage of young convection (i. e. before the generation of an anvil) the signals of variance and temporal evolution coincide with the area of cloud development (left side of a) and b)). The generation of an anvil in the mature stage of the cloud excites strong signals at the cloud border, where the pixel variability is high (right side figure a)) and leads to seemingly cooling and warming tendencies at the front and rear side of the cloud, respectively (right side figure b)). In the mature stage the cloud shield is characterized by low spatial and temporal variability of the pixels.

with deep convection and found that the satellite-defined thunderstorms coincide with individual radar echoes, especially in the early stages of thunderstorm development. Wexler and Blackmer (1982) compared the behaviour of cloud tops inferred from GOES and radar reflectivity observations of three tornadic thunderstorms and found that the lowest brightness temperatures occurred with the formation of a mesocyclone when radar echo tops reached the maximum height. Adler et al. (1983) and Heymsfield and Fulton (1988) investigated the structure of thunderstorms using radiometric measurements from aircraft observations and compared those with radar data. They found, that the coldest infrared brightness temperatures do not always coincide with convective areas identified by radar. Vicente et al. (1998) computed a real-time precipitation estimation with a statistical analysis using radar derived precipitation and satellite derived IR cloud-top temperatures.

The equal temporal resolution of satellite and radar imagery allows a direct comparison at 5-minute intervals. The comparison is necessary in order to validate the results derived from methods based on satellite. First, the satellite pixels of the whole rapid scan area were georeferenced: for each pixel, the geographical latitude and longitude was calculated, whereas the geographical location refers to the center of the satellite pixel. For the comparison satellite-radar, a region of interest was defined (see Figure 5-1) and the Swiss military coordinates of the radar data were projected on a latitude/longitude Meteosat grid.

representing the spatial resolution of either the infrared or visible channel. The regions of interest represented by Meteosat grids in Figures 5-1 a) and b) cover almost the same geographical area and are of comparable size. The visible grid area (~ 27'540 km^2) is somewhat bigger than the infrared grid area (~ 25'696 km^2) extending further north and west. The grid area extension in north-south direction is approximately 176 km (infrared grid), respectively 180 km (visible grid), the west-east distance is approximately 146 km (infrared grid) and 153 km (visible grid).

The southernmost grid cell coincides with the most distant grid cell from the Monte Lema radar (infrared grid: ~ 139 km visible grid: ~ 141 km) and is located at the lower left corner of the Meteosat grids in Figures 5-1 a) and b).

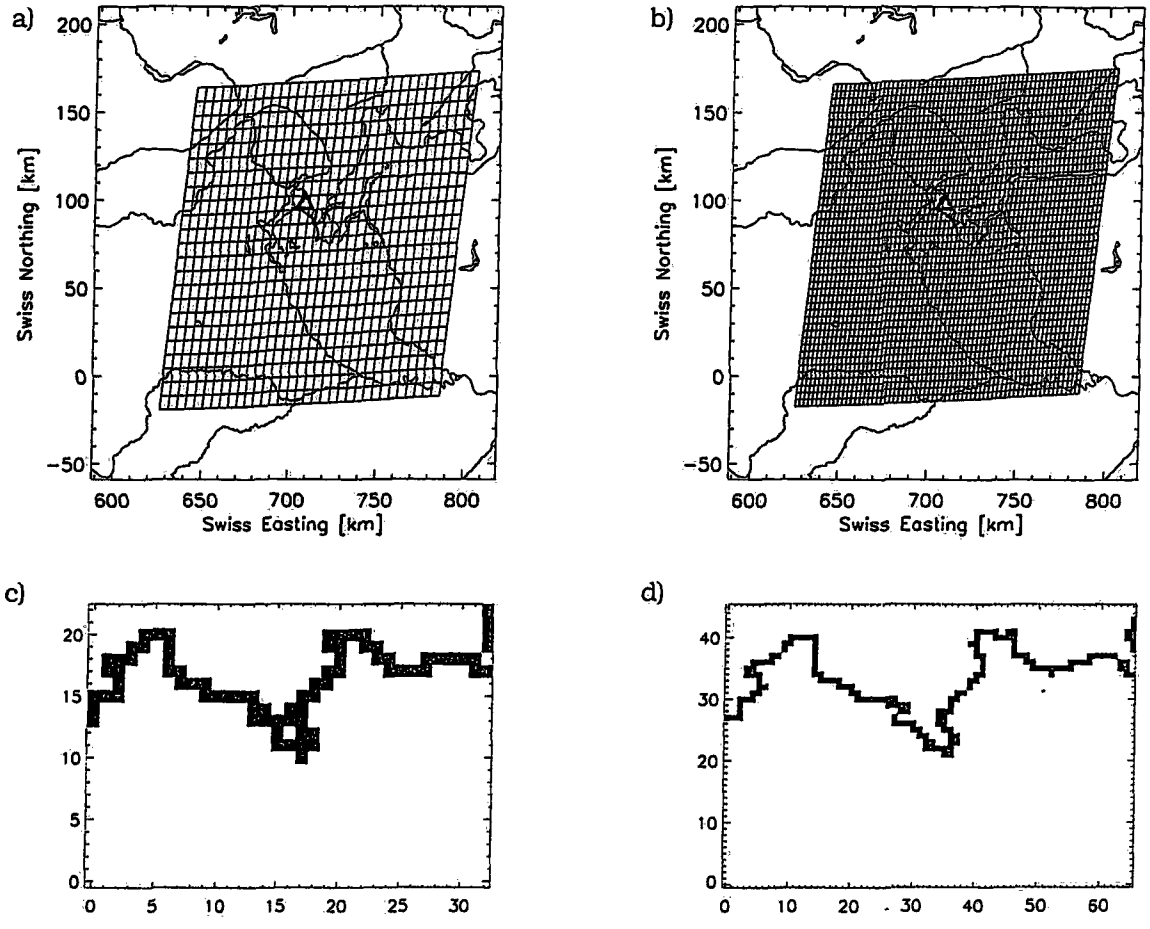

FIGURE 5-1. Region of interest of the present study pictured by Meteosat grids of the a) infrared channel and of the b) visible channel in Swiss coordinates. Panels c) and d) show the corresponding geographical areas in pixel coordinates, with black pixels indicating the southern border of Switzerland. In the upper panels, the location of the Monte Lema radar is represented by a triangle, rivers and country border lines are marked by thin black lines.

The higher spatial resolution of the visible channel provides more exact country border lines compared to the infrared grid as clearly depicted in the pixel-based images of Figures 5-1 c) and d).

The radar sample volumes of the atmosphere, the satellite two dimensional areas represented by pixels. Therefore, the verification of radar and satellite is based on the comparison between a volume (radar) and a two dimensional area (satellite pixel). However in satellite images, warmer and cooler count values in the infrared channel and light - shadow

effects in the visible channel provide information on the vertical structure of a cloud. The verification of the results will show, to what extent volume characteristics derived from radar is related to temporal and spatial cloud top structures as derived from satellite. We have to bear in mind, that the verification is restricted to precipitating grid cells since weather radar respond to larger precipitation-sized particles. Regions without precipitation can be identified in satellite images as evolving (e. g. cooling) but are not assigned to radar-defined precipitation classes. Strictly speaking, we analyse precipitation areas of clouds as detected by radar and cloud particles as seen by satellite.

5.2 Separation between convective and stratiform regions

A ground-based radar is an excellent instrument for the detection of precipitation in real-time, even in mountainous regions (Germann, 2000). Both precipitation types, convective and stratiform, exhibit different reflectivity patterns in radar images with distinct characteristics. Convective and stratiform precipitation differ in the magnitude of the in-cloud vertical air motions and the timescale of microphysical precipitation growth mechanisms (Steiner et al., 1995).

Convection

Strong updrafts in clouds with convective activity are usually narrow and can lift large particles upward and form well-defined vertical cores of maximum reflectivity (Houze 1993, Steiner et al. 1995). Within these updrafts, the vertical air motions are several meters per second and exceed the fall velocity of snow particles. In vertical cross sections of radar convective regions can be identified by cells, as tall, thin columns of high reflectivity, since the bulk of the precipitation mass falls out within a few kilometres of the updraft centers (Houze, 1997). Convective precipitation areas are therefore characterized by high reflectivity intensities and distinct horizontal echo structure with high spatial variability.

Stratiform

Houze (1993) defines stratiform precipitation in terms of the vertical velocity scales: *"Stratiform precipitation is defined as a precipitation process in which the vertical air motion is small compared to the fall velocity of ice crystals and snow."*

The terminal fall velocity of ice crystals and snow is ~ 1-3 m s^{-1} (Houze, 1993). In radar images, the stratiform precipitation is characterized by a horizontally orientated echo pattern with high reflectivity, called *bright band*. The bright band is the region where large snowflakes melt and is characterized by an intense echo in a horizontal layer about 0.5 km thick located just below the 0° C level (Houze, 1993).

Houze (1993) investigated the generation of convective and stratiform precipitation regions and their life cycles and found that stratiform clouds (nimbostratus) can become joined with convective clouds (cumulus and cumulonimbus) to produce the cooperative mechanism of stratiform precipitation. In one case, the *convection occurs in a shallow layer embedded in the upper portion of the nimbostratus* and drops ice particles into the layers of nimbostratus below. In the second case, the *nimbostratus is located next to an area of deep convective clouds*. Ice particles grown and carried up to upper levels by the strong convective updrafts of the deep convective clouds fall out in the neighbouring stratiform region (Houze, 1993). Therefore, convective and stratiform precipitation regions show different reflectivity patterns and stratiform precipitation is often accompanied by the occurrence of deep convection (Houze et al. 1990, Houze 1997) and develops as a decaying convective area (Houze 1993, Schiesser et al. 1995). For a description of dynamical and microphysical processes in convective and stratiform precipitation areas see for example Houze (1993, 1997).

A simple way to distinguish between convective and stratiform regions is the use of radar reflectivity thresholds. Hilgendorf and Johnson (1998) used for the definition of stratiform precipitation the reflectivity threshold ≥ 30 dBZ and for convective precipitation a threshold of ≥ 46 dBZ. Schiesser et al. (1995) defined a convective cell as a region enclosed by a 47 dBZ (30 mm h^{-1}) radar echo contour. Steiner et al. (1995) used the horizontal structure and radar echo intensity of the precipitation field to distinguish convective and stratiform regions.

Steiner et al. (1995), Houze (1997) and Hong et al. (1999) advise not to use the radar reflectivity bright band to identify stratiform precipitation. The bright band is clearly pronounced in well developed stratiform precipitation, but not in the early or late stage of development of stratiform precipitation. According to Houze (1997) the absence of a bright band does not imply the absence of stratiform precipitation structure. A strong bright band only will appear if some of the melting particles are in the form of large aggregates. Furthermore, the vertical resolution of the radar should be sufficiently fine. Typically a radar detects a bright band only at close range because the radar beam broadens with distance from the antenna (an antenna with 1° beamwidth of a C-band radar like the Mt. Lema has a vertical resolution of ca. 1.6 km at a distance of 100 km) and the melting layer is only ~ 0.5 km or less in depth (Houze, 1997).

The convective-stratiform separation algorithm in the present study relies on results of investigations from Smyth and Illingworth (1998). They used microphysical information from a S-band radar with polarization capabilities for a distinction between stratiform and convective precipitation in southern England. With the help of the linear depolarization ratio they discriminate between precipitation containing snow (i. e. stratiform precipitation) and precipitation containing graupel (i. e. convective precipitation). They found that the threshold 30 dBZ is rarely exceeded in snow 1.3 km above the bright band and is therefore an indicator of convective activity. These results were applied in the present study interpolating polar data from the Mt. Lema on Meteosat pixel grids (cf. Figure 5-1). For each individual grid cell the reflectivity at a height interval between 4.5 - 5.5 km was analysed and convective and stratiform precipitation cells were separated. The height interval of 4.5 - 5.5 km was chosen since the 0° reference height (i. e. the bright band region) was located in all investigated IOPs approximately at 3 km. The 0° reference height was derived from radiosounding profiles from Milano or when available from Claro (Ticino).

Investigations showed that the radar reflectivity data should not be averaged over the (grid) volume, as the areal extension of convective regions is probably in most cases smaller than the spatial resolution of a single Meteosat grid cell. Therefore, the 90 % quantile of the maximum reflectivity was chosen as threshold since it avoids the averaging of reflectivity over a volume and is more robust than the absolute maximum reflectivity.

In summary, convective precipitation regions were defined if the 90 % quantile (q_{90}) of maximum reflectivity in a height interval 1.5 km above the 0° reference height, i. e. 4.5 - 5.5 km, exceeded 30 dBZ (cf. Figure 5-2).

$$q_{90}\Big|_{4.5km}^{5.5km} > 30dBZ \qquad \text{Convective radar criterion}$$

With increasing distance from the radar, the vertical resolution deteriorates. A radar like the Mt. Lema with a 1° beamwidth has a vertical resolution of ca. 1.6 km at a distance of 100 km. At the most distant grid cell (~ 140 km) from the Mt. Lema the vertical resolution is ~ 2.25 km and therefore it might be possible to include bright band information from regions below the 0° reference height (3 km) in the analysis. Examinations of stratiform precipitation events during the MAP-SOP show that the most distant grid cells are not classified more

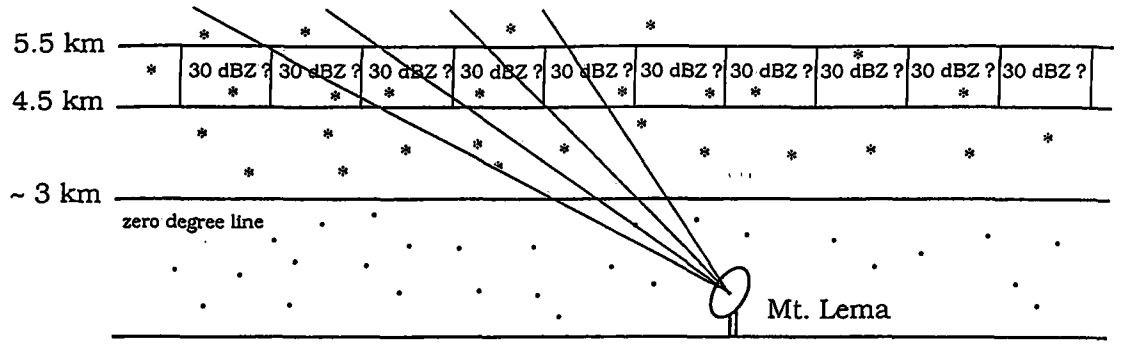

FIGURE 5-2. Conceptual model of the convective-stratiform radar algorithm used in the present study. The polar radar data from Monte Lema is interpolated on grid cells representing the spatial resolution of Meteosat pixels. The criteria of the algorithm rely on investigations from Smyth and Illingworth (1998). For details see text.

frequently as convective than grid cells nearby the radar and that the distribution of cells regarded as convective in stratiform precipitation areas is random and not systematic.

Stratiform precipitation regions derived from the radar data interpolated on the Meteosat grid were defined by a simple "precipitation threshold", separating between precipitating and non-precipitating grid cells. This "precipitation threshold" is an empirical value and depends on the spatial resolution of the used satellite grid.

A volume with the spatial dimension of the infrared grid containing interpolated radar data was regarded as precipitating (i. e. stratiform), if the sum of the precipitation rate intensities of the individual radar pixels, expressed in terms of reflectivity classes (see Table 3-1, p. 36), exceeded the value of 20 in a height interval between 4.5 and 5.5 km. Since the spatial resolution of the infrared and visible grid cells determines the sizes of the corresponding radar volumes, the "precipitation threshold" is exceeded faster in the larger volumes (infrared grid) than in smaller (visible grid). Therefore, an adaptation for the visible grid with its smaller volumes was necessary. The "precipitation threshold" for the volumes with the spatial dimension of the visible grid was set to 5 (infrared Meteosat grid: 20) corresponding to a quarter of the threshold used with the infrared grid[4]. The grid cells with no precipitation or too weak precipitation not exceeding the predefined threshold were considered as non-precipitating and remained unclassified. Visual comparisons of the areal coverage of the radar precipitation fields derived from the MeteoSwiss standard products and from the "precipitation threshold" as defined in the present study showed a good agreement.

The radar data interpolated on the spatial dimension of visible Meteosat grid cells show more distinct precipitation patterns than data interpolated on infrared grid cells (Figure 5-3) due to the higher spatial resolution. However, the qualitatively important information relevant for this study, the area and intensity of convective regions show a good geographical coincidence of the radar data interpolated on the visible and the infrared grid.

For the validation of the convective-stratiform algorithm ATD lightning data from the U.K. Meteorological Office (UKMO) was used. Figures 5-4 a) and b) illustrate a comparison between convective grid cells as identified by radar data interpolated on the infrared grid and recorded lightning over the same period. The locations of all registered lightning over a 5-minute period were plotted for each single rapid scan interval and compared to convective areas defined by radar. The lightning data was centred on each 5 minutes timestep of a scan image, e. g. for the timestep 20:00 UTC, all lightning records occurring from 19:58 until

[4] in accordance to the spatial resolution of the visible grid cells, which have the spatial dimensions of a quarter compared to infrared grid cells

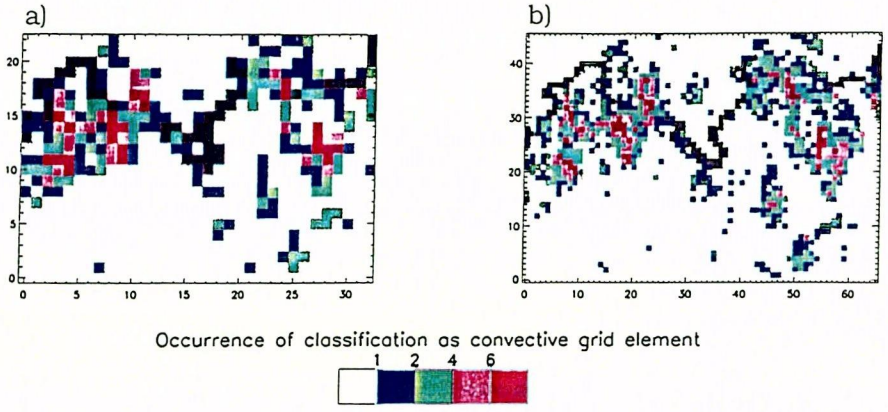

FIGURE 5-3. 20.09.99, 07:00-17:00 UTC: Frequency of occurrence of convective grid cells identified by the Mt. Lema radar using different Meteosat grid sizes a) infrared grid and b) visible grid. The colors depict, the number of times a grid cell was regarded as convective over the investigated period (10 hours). The black pixels indicate the southern border line of Switzerland.

20:02 UTC were taken into account. For Figure 5-4 raw lightning data were used and no correction concerning any possible error in location was made.

Figure 5-4 shows a reasonable geographical coincidence of convection as derived from radar and ATD lightning data during a period of strong convection in the LMTA. Generally, the radar algorithm worked well as visual comparison with non-interpolated radar data showed. The overall advantages of the convective-stratiform separation algorithm used in this study are its simplicity and its independency on the existence of a bright band.

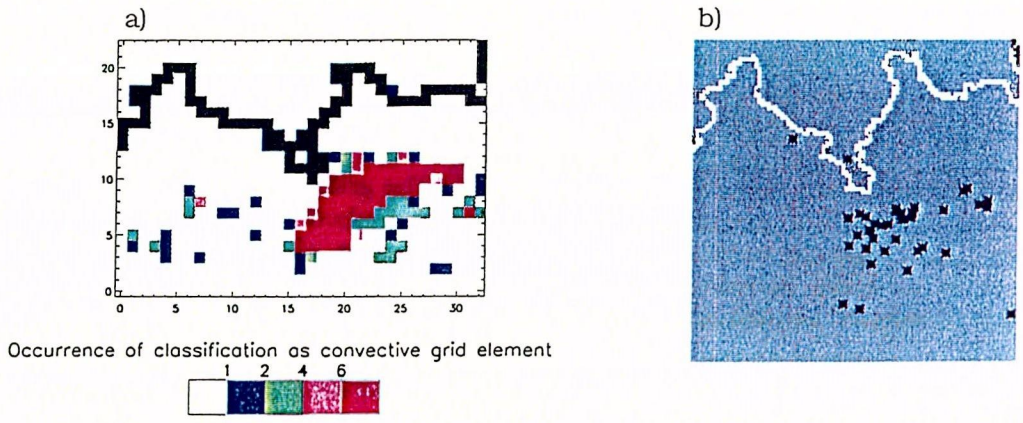

FIGURE 5-4. 04.10.1999, 19:15-23:00 UTC, a) Frequency of occurrence of convective grid cells identified by the Mt. Lema radar using the infrared Meteosat grid compared with b) ATD lightning data compared to the same geographical area (LMTA).

6 Tracking

In this chapter the tracking method is presented and results of sensitivity investigations are discussed. Investigations concerning the persistence of different cloud features are presented and the advantages of tracking multiple targets are illuminated.

Preliminary investigations (cf. section 4.4, p. 39) showed that signals from the tendency calculation (i. e. pixel evolution) result from cloud motion ("advective signal") and from cloud development ("development signal"). In order to distinguish between the "advective part" and "developing part" of the signal, a tracking algorithm was set up. Tracking eliminates the earth-relative motion of the clouds and enhances signals due to cloud development. An area with cloud development is characterized by strong pixel evolution, with either cooling (convective activity, generation of cloud) or warming (cloud dissolution). In this study, tracking of cloud systems is favoured by the high time resolution of the imagery, which allows an analysis of rapidly evolving systems.

Automatic tracking of clouds may be performed either by an object-oriented technique or by a pattern-oriented technique. An example of an object-oriented tracking technique is given by the ISIS tracking algorithm (Morel et al. 1997, Morel and Sénési 1998, 1999) which is based on the geographical overlapping between cells identified as convective in two consecutive images using Meteosat-7 images (cf. section 3.4.2, p. 32). The ISIS overlapping technique calculates the fraction of overlap of the tracked objects in two consecutive images and performs a satisfactory tracking of cloud systems covering an area of 1000 km^2 at any temperature threshold between - 30° C and - 55° C (Morel et al., 2001). Another example of a tracking algorithm using the "overlapping technique" is given by Machado et al. (1998).

The drawbacks in applying the overlapping technique is that the amount of overlap depends on the speed at which the features are moving and the image acquisition rate (Hodges, 1998). The application of the "overlapping technique" is limited to clouds, which are clearly identifiable in time and space. During the MAP-SOP most heavy precipitation events were characterized by embedded convection within stratiform cloudiness and only one case with an isolated convective cloud cell occurred in the LMTA. As a consequence, we concentrate rather on the tracking of cloud patterns (pattern-oriented technique) than on tracking of single cells (object-oriented technique). A description of the pattern-oriented technique used in this study is given in the next section, an overview of past and present cloud tracking by satellite data is provided by Machado et al. (1998) and Menzel (2001).

6.1 Pattern Correlation Coefficient (PCC) technique

According to Hodges (1998), the current techniques to perform cloud tracking and calculating the wind vectors are predominantly based on correlation techniques which are perfectly adequate for these purposes. In the present study the tracking is regarded as an additive means to extract cloud development and is not used for the derivation of cloud motion winds. Cloud systems are tracked with the help of a standard pattern correlation coefficient (PCC) technique using data from the infrared channel (Leese and Novak 1971, Schmetz and Nuret 1987). The advantage of infrared imagery is the availability over 24 hours and the distinct cloud patterns they reveal compared to data from the water vapor channel. Endlich and Wolf (1981) used GOES infrared and water vapor rapid-scan data to compute cloud motions with the cross-correlation technique. They found, that due to the lack of contrast in water vapor imagery, the tracking was presumably significantly degraded by noise while tracking clouds with infrared data was very successful.

The pattern recognition technique uses the spatial variability of pixels in a scene (e. g. standard deviation) which is referred to as texture parameter (Kidder and Vonder Haar, 1995) as an input for the tracking. For the PCC tracking, a sequence of successive images is used.

In the first image (timestep = 0) a cloud pattern is defined subjectively as a "target window". As common target window size we use is 15 x 15 pixels. This target window is sought for in the consecutive image (timestep = 1) within a search box by moving around until the best correlation match is found (cf. Figure 6-1).

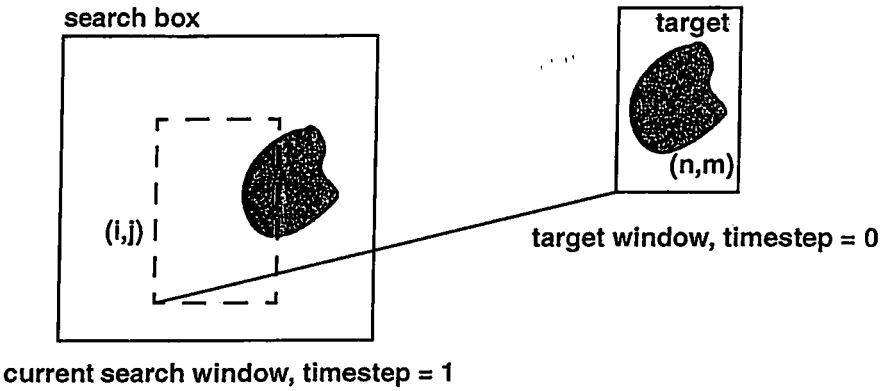

FIGURE 6-1. Concept of the pattern correlation coefficient technique (PCC). For details see text.

For different locations i and j within a predefined search window the standard pattern correlation coefficient PCC(i, j) is computed (Schmetz and Nuret, 1987). The Standard Pattern Correlation Coefficient is given by:

$$PCC(i,j) = \frac{\sigma_{st}(i,j)}{\sigma_s(i,j) \cdot \sigma_t}$$ **Standard Pattern Correlation Coefficient**

σ_t is the standard deviation of the pixel counts within the target area with n rows and m columns, σ_s is the standard deviation of the segment equivalent within the search area. σ_{st} is the covariance between the current search window and the target window.

$$\sigma_t = \sqrt{\frac{1}{nm} \cdot \sum_n \sum_m (x_t(n,m) - \bar{x}_t)^2}$$

σ_t = standard deviation in target window

$\bar{x}_t$ = average count of target window

$$\sigma_s(i,j) = \sqrt{\frac{1}{nm} \cdot \sum_n \sum_m (x_s(i+n, j+m) - \bar{x}_s(i,j))^2}$$

σ_s = standard deviation in current search window

$\bar{x}_s$ = average count of search window

$$\sigma_{st}(i,j) = \frac{1}{nm} \cdot \sum_n \sum_m (x_s(i+n, j+m) - \bar{x}_s(i,j)) \cdot (x_t(n,m) - \bar{x}_t)$$

σ_{st} = covariance between current search window and target

The largest PCC value found in the search box corresponds to the new location of the target window at timestep = 1. The size of the search box depends on the temporal resolution of the satellite images. With the decrease of time resolution, the size of the search box has to be increased, since the target window may cover a longer distance between two consecutive images. Since the target window displacement between two consecutive images is limited, we assume a maximum target displacement of one pixel per minute within a given time interval. Therefore, for images with 5 minutes intervals the size of the search box is chosen to be the target window incremented by 5 pixels in each direction, for images with 10 minutes intervals the increment is 10 pixels in each direction[5].

The displacement between the location of the target area at timestep = 0 and the new location at timestep = 1 corresponds to the (cloud) pattern motion. The new location of the target defines the new target area, which is moved in the search box of the consecutive image until the best correlation is found. Once the initial target is defined, the tracking algorithm runs automatically. The advantage of the PCC technique is that no object-specific definitions are required apart from the initial choice of the target window. Comparisons between results of tracked and untracked patterns in combination with the calculation of pixel evolution within a 10-minute period are presented in Figures 6-2 a) and b). Figure 6-2 a) represents a single cloud cell, Figure 6-2 b) a cloud area in the LMTA. Note that the results of the latter consist of pixel evolution calculated of multiple tracked cloud areas (cf. section 6.2.2, p. 52). The size of the target windows in both figures are comparable (i. e. ~ 20 x 15 pixels). Comparing the results of the tracked and non-tracked images show, that seemingly warming and cooling effects are minimized with the help of tracking.

In Figure 6-2 a) the apparent warming signals at the backside of the cloud cell and in b) at the backside of the elongated cloud shield almost disappear. The apparent warming region at the backside of the clouds results from the fast moving cloud borders with rapid changes of count values from cold pixels to warm cloudless pixels, exhibiting negative (i. e. warming) rates. In the untracked image of Figure 6-2 a) the leading edge of the cloud cell shows (seemingly) cooling effects, which can be reduced by tracking, too. The apparent cooling pixels on the leading edge of the cloud are related to rapid changes of count values from warm to cold, due to the cloud motion.

In summary, with the help of the PCC tracking the signals due to the earth-relative motion of the clouds are significantly reduced and signals due to cloud development are enhanced. The "double structure" of apparent evolution signals, typical of single cells as described in section 4.4 (p. 39), is minimized. Despite the fact that some ambiguity in texture matching between two consecutive images is always possible, the PCC provides very satisfying results with the use of rapid scan data. A recent example of the satellite-based application of the correlation technique together with MCS in the tropics is given in Carvalho and Jones (2001). Rossa and Binder (1997) and Mecklenburg (2000) provide examples of the use of the PCC technique with radar data.

6.2 Sensitivity of PCC tracking

The sensitivity of the PCC tracking was investigated depending on the time interval between consecutive images, the size of the search box, the pattern of the target and its persistence, and the size of the target window. The sensitivity investigations were carried out by tracking of single targets.

[5] In midlatitudes, the size of a pixel of the infrared channel is ~ 5 km x 8 km resulting in a maximum cloud displacement of 480 km/h what is unlikely to occur.

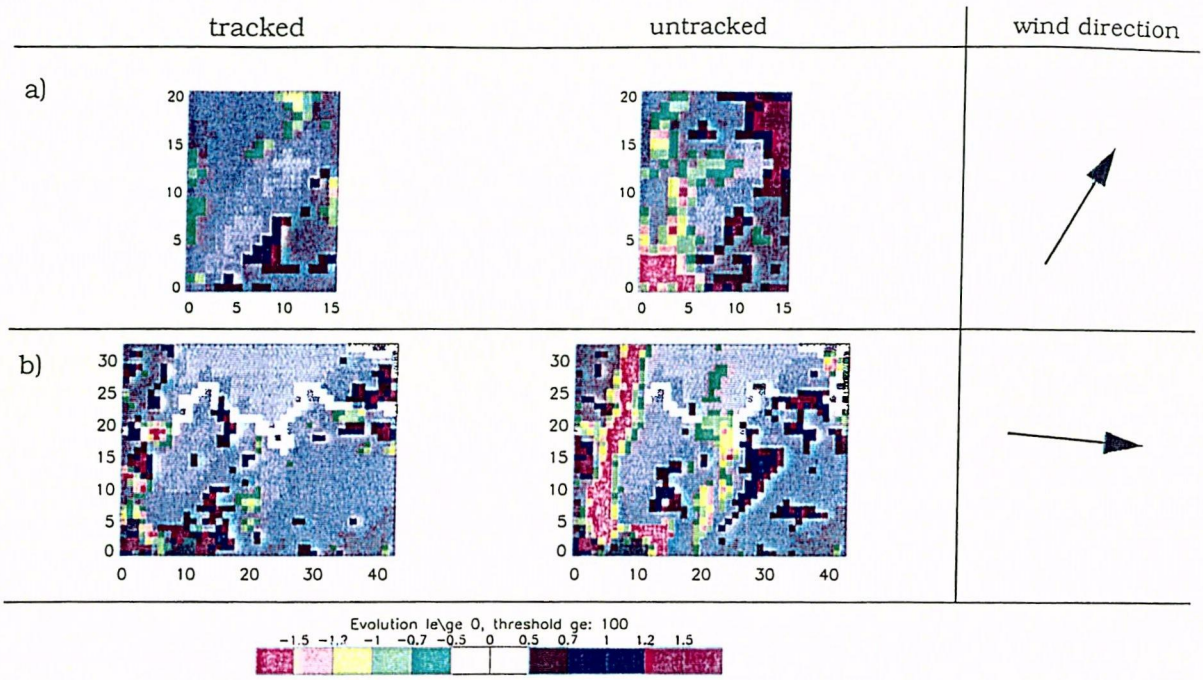

FIGURE 6-2. Examples of calculated pixel evolution signals over 10 minutes [counts/minute] of tracked and untracked cloud targets (negative values: warming, positive values: cooling), on 26.09.99. The upper row gives an example of a single cloud cell moving over the Ligurian Sea, the bottom row shows cloudiness moving over the LMTA. The thick white line delineates the southern border line of Switzerland (lower panels). The comparison between the tracked and untracked evolution signals are well recognizable: the untracked panels exhibit apparent cooling regions at the leading edge of the cloud and apparent warming regions at the rear edge of the cloud. These apparent signals are reduced in the tracked images (left panels). The general direction of cloud motion is indicated by the arrows depicted on the right side. As shown in the legend, only pixels exceeding the count value 100 were analysed.

6.2.1 Time interval and the size of the search box

Investigations prove that the time interval between two consecutive images is the most important factor for an accurate PCC tracking. The accuracy of the PCC tracking can be estimated from the degree of correlation between two patterns and the position of the target window. A steady progression of the positions of the target windows in combination with high correlation coefficients during a period is an indicator of an accurate tracking of an initially defined target pattern (compare Figure 6-3 b)).

Best results, i. e. high correlations and steady progression of target displacements are obtained with highest possible temporal resolution (i. e. 5 minutes). Figure 6-3 shows the target displacement of a weakly-textured target window (stratiform cloud pattern) using different time intervals between two consecutive images. A high temporal resolution of 5 minutes in Figure 6-3 b) allows a steady tracking of the target. When degrading the temporal resolution to 15 minutes as depicted in Figure 6-3 c), the target is tracked correctly up to the fifth position of displacement and from the sixth position (i. e. after 1 hour and 30 minutes), a new pattern is tracked. This new pattern was found within the search box and exhibits at this point in time the highest pattern correlation. From the sixth position the steady progression of the displacement positions is definitely interrupted. However note that the order of target displacement, illustrated with numbers within the triangles, is interrupted already at the third position (after 45 minutes). Comparing the third and the fourth position

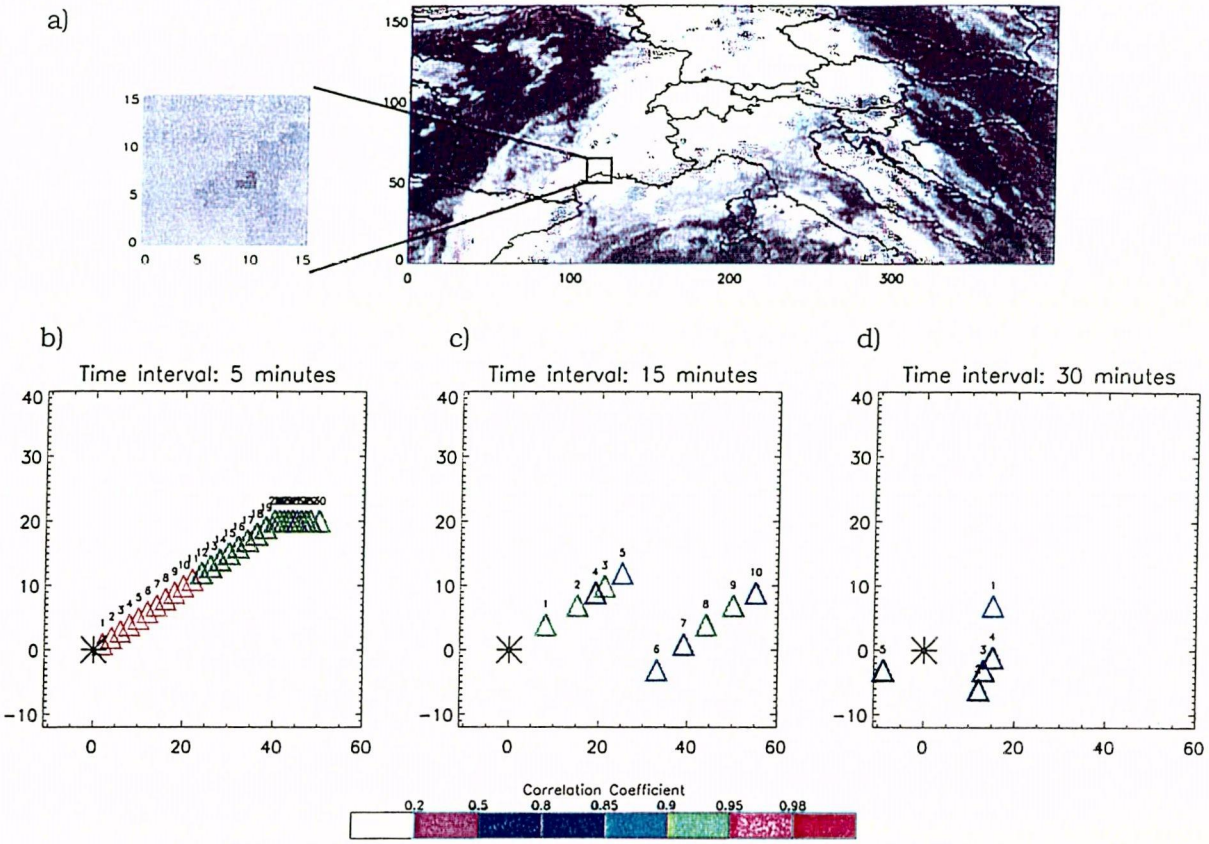

FIGURE 6-3. Results from PCC tracking on 24.10.99, from 12:00-14:30 UTC. In a) the cloud cover as seen by the Meteosat-6 infrared channel at 14:00 UTC is depicted, the black box represents the location of the tracked target at 12:00 UTC, the weakly textured 15 x 15 pixel stratiform target is shown by the small panel to the left. b) - d) present the target displacements (triangles) with varying time intervals between two consecutive images: b) 5 minutes, c) 15 minutes, d) 30 minutes. The star depicts the initial position of the target, the number above the triangles denotes the sequence of the displacement. High temporal resolution of images (i. e. 5-minute interval) allows a continuous tracking even of a small and weakly-textured cloud pattern. This continuity degrades with the increase of time between two consecutive images: panels b) and c).

of the target displacement, the latter is closer to the initial position of the target (depicted by the star) despite the continuous target displacement away from the initial target position (cf. Figure 6-3 b)). This shows that already after 45 minutes the initially defined target is lost what is confirmed by the decrease of the correlation coefficient.

A further degradation of the temporal resolution to 30 minutes, which is the operational mode of Meteosat, reveals that the interruption occurs earlier (Figure 6-3 d)) and when comparing to the results with 5-minute interval images, only the first position was tracked correctly. Note that a decrease in temporal resolution leads also to a decrease of the correlation coefficient values.

The decrease of time resolution between two consecutive images presumes an increase in size of the search box. Imagery with low time resolution (i. e. 30 minutes) requires a larger search box, since clouds may displace over longer distances between two consecutive timesteps. In combination with low temporal resolution of the images, the size of the search boxes may affect the quality of tracking, since a larger search box leads to a higher probability, that a similar cloud pattern is regarded as best fit (cf. Figures 6-3 c) and d)). In combination with high temporal imagery (i. e. 5-minute interval images) the size of the search boxes does not affect neither the correlation nor the location of displacement of the target.

This was tested with several target windows of equal size (15 x 15 pixels) and different sized search boxes (target window incremented by 15 x 15, 30 x 30 or 60 x 60 pixels in each direction).

In summary, the most accurate tracking results are provided by small search boxes with high temporal resolution of the images. In addition, small search boxes improve the computing time significantly.

6.2.2 The pattern and the size of the target window

Introducing the PCC tracking technique the question about the optimum size of the target window for the purposes of the present study raised. For cross-correlation tracking, Endlich and Wolf (1981) used target sizes of 7 x 7 pixels, Schmetz and Nuret (1987) performed the tracking with target segments of 32 x 32 pixels. According to our investigations, the size of the target has to meet two conditions: it must be large enough in order to include a reasonable quantity of textural information and it must be small enough to represent a region of homogeneous cloud motion which is advantageous for the accuracy of tracking.

The ability to track a cloud pattern is dependent on the intensity of cloud development and on the texture of the pattern. A distinct textured cloud pattern like an isolated convective cell can be tracked over a long period (e. g. 2 hours) exhibiting high correlation coefficients (e. g. over 0.9), even while developing. The high temporal resolution of the rapid scan images favours the tracking of rapidly evolving cloud patterns and does not affect the accuracy of tracking. Weakly textured targets (stratiform cloud patterns) evoke lower correlation coefficients (e. g. less than 0.8) and reveal, even if tracked over longer periods, reasonable target displacement locations (Figure 6-3 b)). The following Figure 6-4 demonstrates the dependency of tracking results using target windows with different sizes over a 2 hours period. The target windows were selected accidentally near the LMTA, the temporal resolution of the images was 5 minutes.

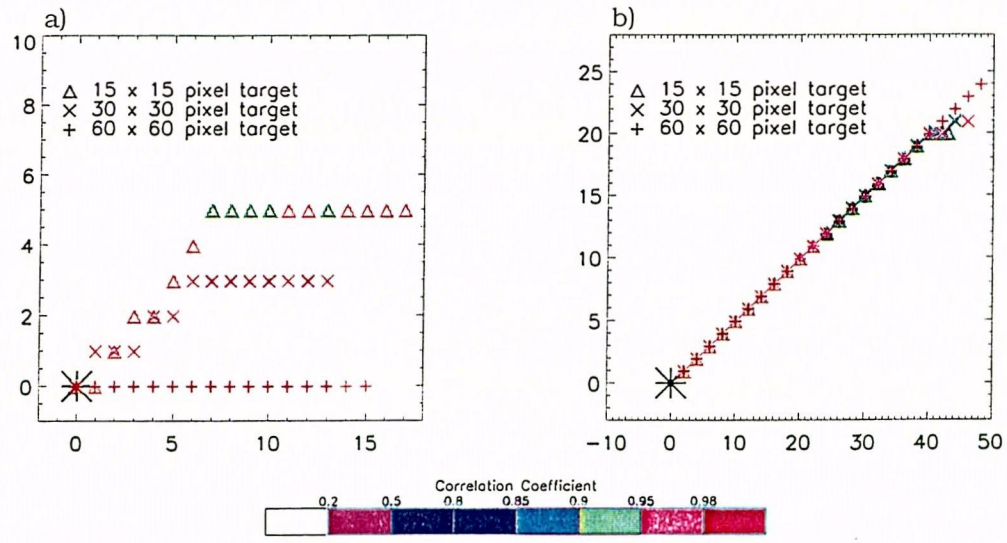

FIGURE 6-4. Location of target displacements with 5-minute interval images using target windows of different sizes: 15 x 15 pixels, 30 x 30 pixels and 60 x 60 pixels. The black star depicts the initial position of the target. a) 26.09.99, 14:55-16:55 UTC, b) 24.10. 99, 12-14 UTC, temporal resolution: 5 minutes. Note the different lengths of the x- and y-axis in a) and b).

In Figure 6-4 a), the target with the largest size (60 x 60 pixels) contains pixel information comprising the back side of a cloud shield located over the Po Valley, moving from west to east which is pinpointed by the displacement locations. The pattern of the smallest target window (15 x 15 pixels) in Figure 6-4 a) is positioned within the cloud shield showing different displacement locations moving first northeast and then east. The displacements of the medium sized target (30 x 30 pixels) indicates a dislocation of the target which is in between the large and the smallest target positions. Figure 6-4 a) is an example, where the locations of target displacements vary with the target sizes due to non-uniform cloud motion. On the contrary in Figure 6-4 b) all target windows with different sizes lie within a weakly-textured stratiform cloud layer with uniform cloud motion in northeasterly direction. The locations of target displacements are almost identical over the two hours period with slight variations in the last positions. In summary, Figures 6-4 a) and b) show, that the size of the target window may strongly influence the displacement of a pattern, in the Alpine region with non-uniform cloud motion.

It is probable, that the displacement locations found by the PCC method utilizing large target windows is a compromise between clouds moving at different velocities. Therefore, with a large target window the probability increases that we calculate *the average motion of an area of clouds*. Usually, wind velocity increases with height resulting in accelerated cloud motion. To account for this effect, height assignment to the tracked clouds may be used (e. g. Endlich and Wolf, 1981) in order to derive wind speed by cloud tracking. The operational method for deriving cloud-motion winds from Meteosat infrared images is described in Schmetz et al. (1993). They use a radiance windowing technique to tackle the height assignment problem by slicing the infrared images into different radiance classes representing different cloud layers (e. g. high cloudiness). Then, the cloud tracking is performed for the individual classes related to certain height levels. In this study, no height assignment was established since we aim to track whole cloud areas rather than to retrieve exact cloud wind speeds at different cloud levels, which is difficult. In addition it may be likely that a large target window in the Alpine area contains stationary cloudiness.

Figures 6-5 a) and b) point out the variability of the correlation coefficients over a two hours period of the target windows of Figures 6-4 a) and b). During almost all timesteps, the largest target window exhibits the highest correlation coefficients. A reduction in size of the target windows results in a decrease of correlation despite of the high temporal resolution of the images. The reason for decrease in correlation is that smaller target windows may not

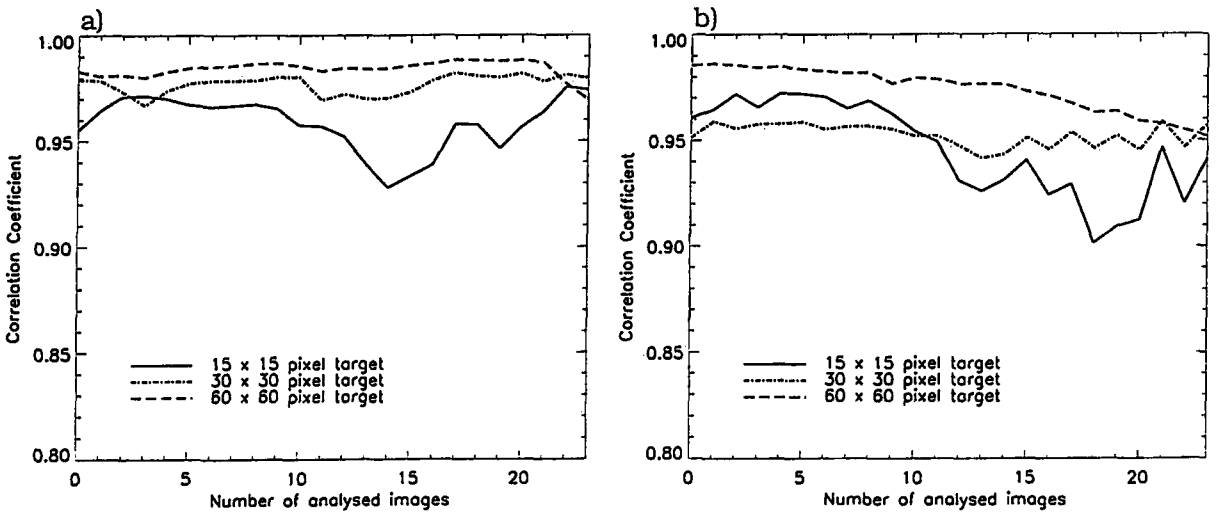

FIGURE 6-5. Corresponding correlation coefficients to Figure 6-4.

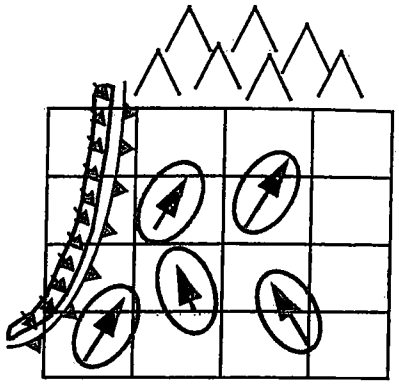

FIGURE 6-6. Conceptual model of a cold front crossing the Alps, moving from west to east, on 26.09.99. The big window, consisting of 4 x 4 subquadrants (target windows), depicts the analysed region. Within the analysed region clouds (mapped with blue color) move at different velocities ahead of the cold front in a southwesterly flow towards the Alps. The different velocities of the clouds are schematically represented by different lengths of arrows.

include distinct texture information like cloud borders to ensure the continuity of tracking. Therefore, the correlation between two consecutive timesteps may not be clear and without ambiguity. The ambiguity of the best correlation match can be seen in Figure 6-5 by the variability of the correlation coefficient of the smallest target window with a size of 15 x 15 pixels. A test using a smaller target window of 7 x 7 pixels proved that smaller target window sizes lead to a further decrease of correlation and a higher variability of the correlation. As shown in Figures 6-4 and 6-5 the smallest target size (15 x 15 pixels) is large enough to include the textural information required for a continuous track of the pattern. A continuous pattern tracking can be presumed, if the displacements of the targets show a continuous track and high correlation. This is the case for all targets in Figures 6-4 and 6-5. It was decided to perform the PCC tracking with target windows of a size of approximately 15 x 15 pixels. The main reason for choosing a small target window size in the present study is the aim to account for small scale variability of cloud motion within the region of interest (LMTA). Smaller target windows increase the probability of representing a region of homogenous cloud motion leading to more accurate tracking results.

Figure 6-6 schematically depicts an example of the 26.09.99 where a cold front moved over the Alps exhibiting different cloud motions in the region of interest: Ahead of the front, in the prefrontal area, the clouds move faster than in the postfrontal region. Since the aim of the present study is to investigate cloud patterns of the LMTA region and not only of one single target, the region of interest comprising an area of 56 x 48 pixels is subdivided into 16 smaller target windows of equal sizes (each 14 x 12 pixels) which are tracked for each timestep separately (Figure 6-6). The tracked target windows displace with the predominant cloud motion and do not permit the observation of clouds at a fixed geographic region. In order to allow cloud observations of a geographically fixed region a smaller area of the LMTA of 43 x 33 pixel is cut out for each timestep (Figure 6-7) from the 56 x 48 pixel area. The cut-out area remains geographically fixed in time and contains information from the 16 subarrays. This procedure allows a constant observation of tracked cloud areas from a fixed geographical region covering the Lago Maggiore region.

6.2.3 "Persistence" of a cloud pattern

The persistence of a cloud pattern depends strongly on the stage of life cycle and the associated intensity of evolution of the observed cloud system.

For investigations of the pattern persistence, sensitivity tests have been carried out. In the original tracking algorithm, the best matching pattern is used as new target for the subsequent timestep. Therefore, for each timestep the pattern of the target window is "reinitialized" over the investigated period allowing a tracking of cloud patterns which evolve. For examinations concerning the persistence of a cloud pattern, the redefinition of the target window for each timestep is suppressed. Instead of redefining the "reinitialized" target

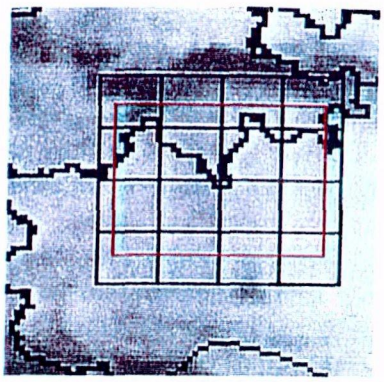

FIGURE 6-7. From the analysed region (56 x 48 pixels) a smaller area (43 x 33 pixels, red box) is cut out for each timestep from the 16 quadrants which represent the individually tracked target windows. The cut-out area allows a constant observation of the geographically fixed region of interest (LMTA) and contains information from the tracked cloud patterns of the 16 quadrants.

pattern in the consecutive image, the initially defined target pattern at timestep = 0 is used. This target pattern is referred to as "fixed" target containing texture information of the initial target window at timestep = 0. For each timestep, the pattern of the "fixed" target is compared to the patterns within the search box and the location of maximum correlation defines the target displacement between the two consecutive images.

There are two aspects for the interpretation of the results of investigations with "reinitialized" and "fixed" targets:

- The divergence of the "fixed" and "reinitialized" target positions: Coinciding positions of the "fixed" and the "reinitialized" target manifest a good tracking ability of the initially defined target pattern.
- The magnitude of the difference of the correlation coefficient between the "fixed" and the "reinitialized" target: Due to cloud development or ambiguity in matching, the correlation between the "fixed" and the "reinitialized" target degrades in time.

The difference between the correlation coefficients of the "reinitialized" and the "fixed" target is - apart from tracking errors (i.e. ambiguity in best match) - related to the magnitude of cloud development within the investigated period. Cloud development within short times leads consequently to a decrease of correlation between the "fixed" and the rapidly developing "reinitialized" target. In Figure 6-8 three cloud patterns of equal size (15 x 15 pixels) with different development rates and textural characteristics were investigated with 5-minute interval images over a period of 90 minutes. Figure 6-8 a) illustrates an isolated and slowly dissipating cloud over the Ligurian Sea, Figure 6-8 b) a rapidly evolving cloud cell at the eastern border of the Swiss Alps and Figure 6-8 c) a stratiform cloud pattern with weak evolution over the Po Valley. Comparisons of the figures demonstrate, that the displacement locations of the "fixed" targets coincide best in Figure 6-8 a) with the "reinitialized" target. In Figure 6-8 a) the coincidence of target displacement is recognizable up to the seventh position, corresponding to a period of 35 minutes. From this point in time, the positions of both targets begin to diverge. Despite the locations divergence this is a good example of a continuous tracking of a target defined once at the beginning of the period.

In Figure 6-8 b) an area was investigated, where convection was constantly triggered at a given spot. The "fixed" target remains more or less stationary whereas the "reinitialized" target displaces with the predominant southwesterly flow. The stationary position of the "fixed" target provides evidence, that the strong cloud development rate hinders a continuous tracking of the cloud pattern and its evolution. The stationary position is a consequence of the quick and geographically fixed generation of the (convective) cloud patterns. This is an excellent example showing the capability of the PCC method to track *rapidly evolving convective cloud patterns* by adjusting the tracked target pattern for each timestep.

Cloud development is not the only parameter affecting the suitability of a target pattern for "persistence" studies. In Figure 6-8 c) investigations of "fixed" and "reinitialized" target patterns within not evolving stratiform cloud regions show, that a rapid decrease in

correlation coefficients is observable, too. The stratiform region shows the limitation of a continuous tracking ability of weakly-textured "fixed" cloud patterns by the standard time interval (30 minutes) of Meteosat. The locations of target displacement diverge from the third position (15 minutes), corresponding to a correct tracking period of 10 minutes. By searching for the best correlation match of a weakly-textured target within a search box characterized by a weakly-textured cloud structure an unambiguous association might not be possible. The results are chaotic target displacements of the "fixed" target.

As a consequence, small and weakly-textured cloud patterns are not suited for pattern tracking over longer timesteps. This drawback of cloud regions with weak evolution can be minimized by defining larger target windows comprising more distinct texture information.

The trends of the correlation coefficients of all "fixed" targets in the bottom row of Figure 6-8 are characterized by changing correlation values in time. The decrease of correlation of the "fixed" targets is due to the cloud development, the increases of correlation can be explained by cloud patterns which are similar to the initial target pattern, i. e. target mismatching.

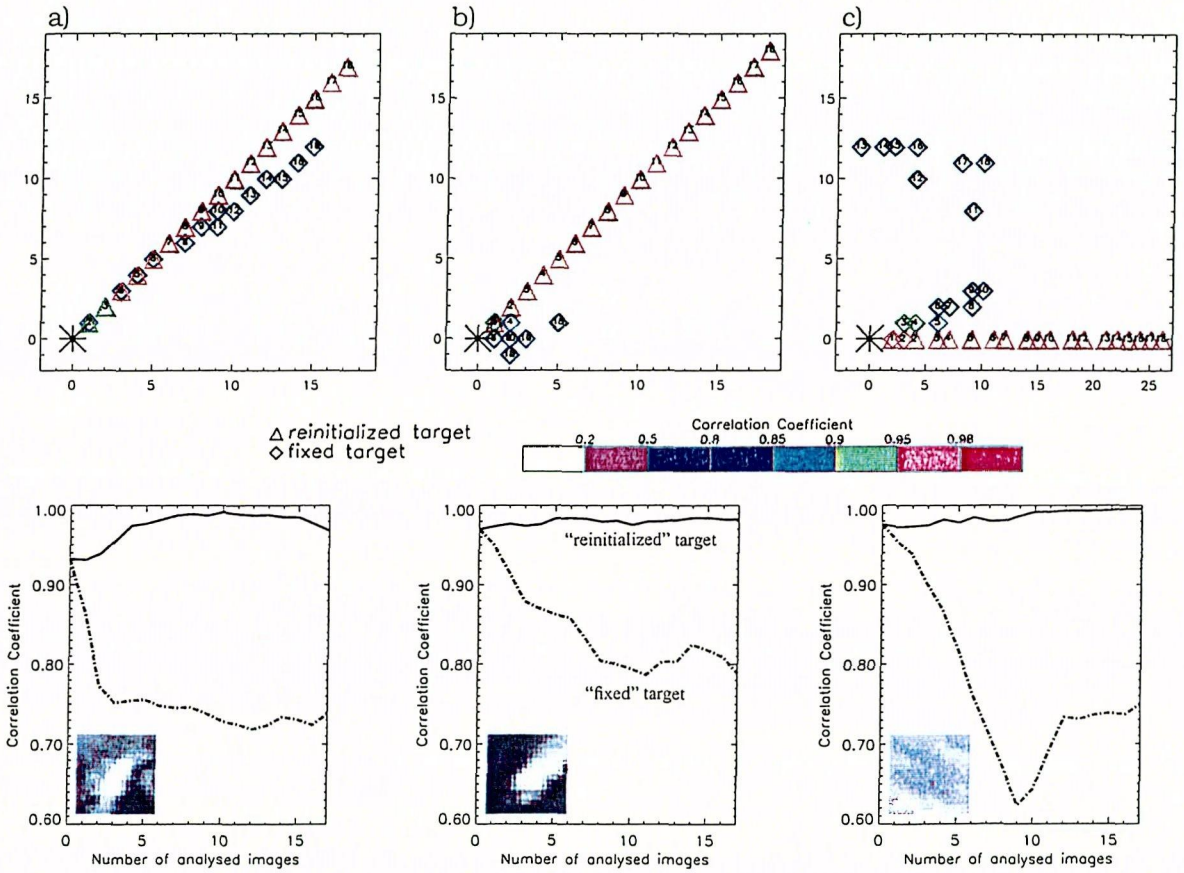

FIGURE 6-8. Ability to track differently textured cloud patterns of equal size (15 x 15 pixels) using "reinitialized" and "fixed" target strategy (see text for explanation) with 5-minute interval imagery. The top row shows the location of target displacements, the bottom row the corresponding correlation coefficients and the tracked target patterns. a) Cell-like pattern with moderate evolution, tracked from 10:30-12:00 UTC, 26.09.99. b) cell-like pattern with rapid evolution, tracked from 19:30-21:00 UTC, 03.10.99., c) weakly-textured stratiform pattern with weak evolution, tracked from 13:00-14:30 UTC, 20.10.99. The black star in the upper row depicts the initial position of the target, the number within the triangles denotes the sequence of the displacement.

The ability to track a "fixed" target pattern depends on the textural characteristics of the target area and of the search box. A more distinct texture pattern of a "fixed" pattern enhances the probability of a correct tracking, provided that the pattern of the search area in the consecutive image allows an unambiguous location of best correlation. As illustrated in Figure 6-8 a) the ability of a correct target tracking with respect to locations and displacements of an initially defined target area decreases with the magnitude of cloud development and with the associated loss of pattern persistency.

As an additional sensitivity study, the pattern of the "fixed" target was redefined - instead of only once - at half hourly intervals (i. e. 0, 30, 60, 90 minutes etc.), corresponding to the operational temporal resolution of the Meteosat satellites. The following Figure 6-9 presents the results of the "fixed" target now being redefined at half hourly intervals. Apart from the half hourly redefinition of the target, the tracking procedure and the initially defined target patterns are the same as with the "fixed" target being defined only once as presented in Figure 6-8.

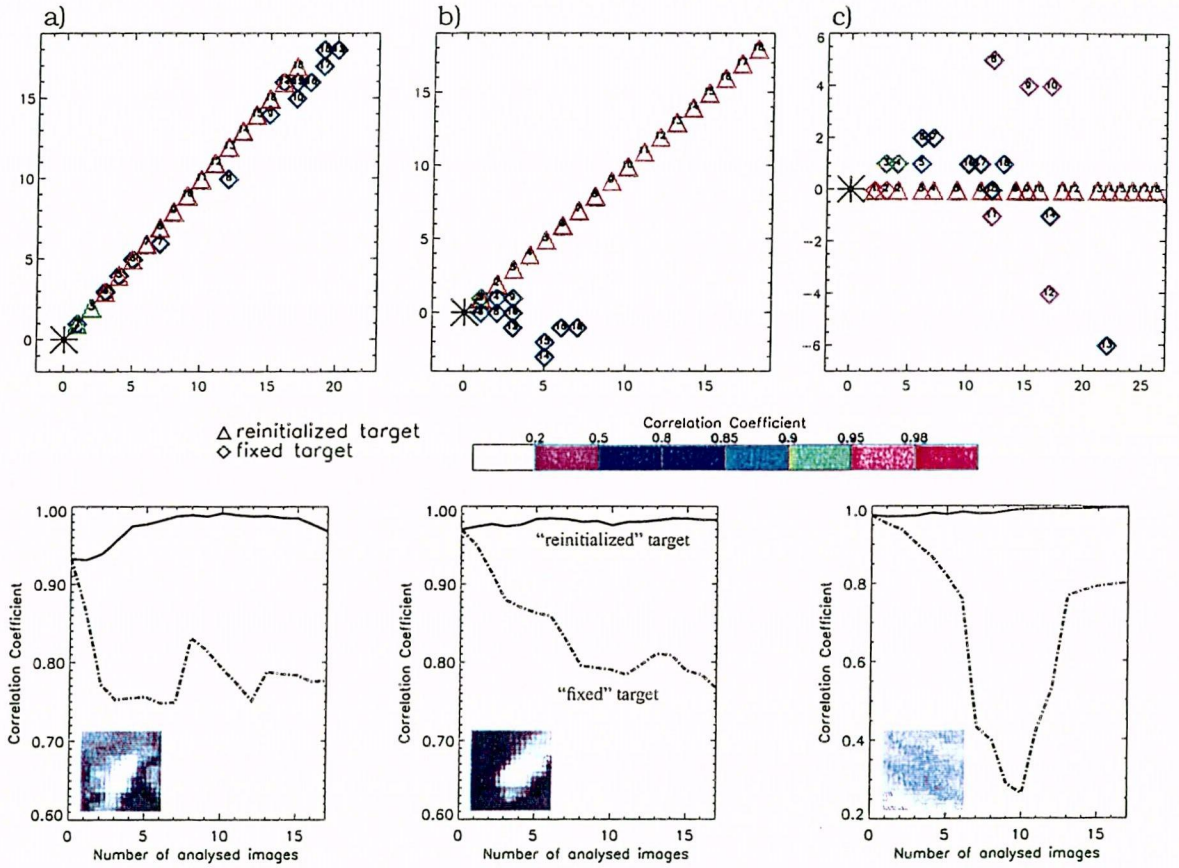

FIGURE 6-9. Same as Figure 6-8 but with a fixed target which is reintilialized at half hourly intervals. Note the different lengths of the x- and y- axes.

As illustrated by the localization of the "fixed" and "reinitialized" target positions and the corresponding correlation values, the results are not ameliorated by the half hourly redefinition of the "fixed" target (cf. Figure 6-8). Again, the best results are achieved with the pattern in Figure 6-9 a) where the coincidence of target displacement is recognizable up to the seventh position, corresponding to a period of 35 minutes. From this point in time, the positions of both targets begin to diverge. The results of Figure 6-9 b) and Figure 6-9 c) are comparable to those of Figure 6-8 b) and c) and need no further comment.

From Figures 6-8 and 6-9 it is recognized that it might be wrong to interpret a rapid decrease of the correlation coefficient in time as the only effect of cloud evolution. Thus for the interpretation of the "fixed" and "reinitialized" target comparisons the locations of the target pattern displacements *and* the correlation coefficient trends are required. The first parameter allows to judge the correct target displacement compared to the "reinitialized" target displacement, the latter gives an indication of the magnitude of the correlation. Provided that the target displacements of the "reinitialized" and "fixed" target coincide, the magnitude of correlation decrease of the "fixed" target is an indicator of the intensity of cloud evolution of the initially defined target.

In summary, the limited ability of tracking a "fixed" target - being defined once or redefined at half hourly intervals - compared to the "reinitialized" target is a clear indicator of the gain in information of images with high temporal resolution. This gain in information is especially precious when applying the PCC method with smaller scaled patterns.

6.3 Summary

The data of the infrared channel were used to implement an automatic cloud tracking algorithm by a pattern-oriented technique called PCC (Pattern Correlation Coefficient). In the present study tracking is not used for the derivation of cloud motion winds, but rather to extract development within the cloud fields since tracking reduces the earth-relative motion of observed cloud systems. Tracking of clouds in the Alpine area is challenging due to the complex processes related to topography resulting in stationary cloudiness or regions of non-uniform cloud motion. To account for non-uniform cloud motion, the region of interest was split into 16 target windows of equal size (14 x 12 pixels). Each target area was tracked separately and analysed with respect to its temporal evolution and its pixel variability of cloud top structures. From the overall region of these analysed targets a smaller box was cut out for each timestep permitting a constant observation at a geographically fixed region (LMTA). A number of studies were conducted to investigate the sensitivity of the PCC tracking results. These results show, that the quality of PCC tracking is dependent on the temporal resolution of the images, the search box and target window size and the target pattern persistence. The results of the sensitivity studies are summarized below.

6.3.1 Temporal resolution of satellite imagery

The temporal resolution of the images turned out to be the most important parameter determining the ability to track a cloud pattern and the tracking quality expressed in terms of correlation. The increase of temporal resolution from the operational 30-minute interval to the rapid scanning 5-minute interval allows continuous cloud tracking and helps to isolate information on cloud development. Images with high temporal resolution favour the tracking of smaller-sized cloud patterns, being rapidly developing convective cells, or weakly textured stratiform cloud areas. The latter can hardly be followed on a contiguous path by 30 minutes timesteps.

Using images with low temporal resolution, either a large target (e. g. 60 x 60 pixels) window is required or the target pattern must contain distinct cloud texture with weak evolution to ensure a steady tracking. The continuity in time of the displacement locations is, beside of the correlation, an indicator of tracking accuracy. The best continuity is achieved by the utilization of highest possible temporal resolution, i. e. 5 minutes. In the present study the tracking was performed with 5-minute interval imagery.

6.3.2 Search box

For the PCC tracking the size of the search box we made dependent on the temporal resolution of the images. Tracking cloud patterns in images with low temporal (i. e. 30 minutes) resolution requires a larger search box size since the observed cloud pattern may cover a longer distance between two consecutive images. In general, a larger search box leads to a decrease of correlation since the location of best matching of the target window patterns between two consecutive images is more ambiguous. The ambiguity of matching results from larger search boxes, since with large search boxes the probability increases, that a similar cloud pattern is regarded as best fit. The importance of the size of the search box diminishes with the increase of temporal resolution of the images. Results demonstrate, that the use of 5-minute interval images with different sized search boxes did not affect neither the correlation nor the location of displacement of the target.

6.3.3 Target window

Impact of the target pattern and the target size have been investigated. The examination shows, that the highest correlations with rapid scans are reached for isolated clouds since a distinct pattern can be better distinguished than a "smooth" stratiform cloud. The correlation of distinct target patterns result in the best matches (e. g ~ 0.95). However, together with images of high temporal resolution, correlations over 0.8 can be found for smooth cloud areas, too. With a decrease of temporal resolution, the structure of the target pattern has an increasing relevance for a correct tracking.

The use of the PCC technique together with images with low temporal resolution (e. g. 30 minutes) requires a larger target window (e. g. 50 x 50 pixels) that includes more texture information. Texture information of targets with a large extension are more persistent in time and contain probably more distinct cloud patterns. Larger target windows lead to higher correlation coefficients, since a synoptic-scale texture like cloud borders does not develop as fast as a small-scale cloud pattern. The conclusion is drawn, that for accurate PCC tracking a decrease in temporal resolution requires a distinctly textured cloud pattern or - if not available - a larger target window.

Smaller targets are more subject to rapid evolution and may not contain distinct texture information. Smaller target windows lead to a decrease in correlation between two images either due to cloud evolution or due to ambiguity in matching. Moreover, the ambiguity in matching leads to an amplification of the correlation trend over the investigated period. The high temporal resolution of the images allowed the tracking of smaller targets with a size of approximately 14 x 12 pixels in the present study. This size was found large enough to include the textural information required for a steady tracking and is considered small enough to account for accurate tracking in the Alps due to non-uniform cloud motion.

Results with different target sizes illustrate, that in the Alpine region the target window size may influence the target displacement and therefore the tracking accuracy. This is especially true when applying the tracking method for regions with non-uniform cloud motion in an Alpine region. Investigations reveal, that mainly extended cloud borders like cold fronts are associated with different cloud motions and different cloud motion velocities. In such regions, smaller targets lead to more exact target displacement values between two consecutive images since they account for the local variability of cloud motions within a limited geographical region. In contrast, the target displacements of larger target areas represent rather the mean cloud displacement and do not account for non-uniform cloud motion.

6.3.4 Cloud pattern "persistence"

The studies on persistence of cloud patterns provide evidence of the additional information gained by high temporal resolution of the satellite imagery. The gain in information is best observed with the analysis of the displacement locations and the correlation coefficient trends of the "fixed" and "reinitialized" targets.

Machado et al. (1998) confirmed that the pattern coincidence of two consecutive images works, as long as the time step between the satellite images is smaller than the time required for significant evolution of convective systems.

7 Meteorological cases

In this chapter, the investigated IOPs are described to point out the meteorological characteristics of the examined heavy precipitation events[6]. Only those time slots of IOPs will be considered where data from satellite and radar are available simultaneously and therefore limited periods within the official duration of the IOPs are described. Further and more detailed descriptions of the IOPs can be found in the MAP Field Catalogue (2000). An overview table with available rapid scan imagery and the official IOP duration can be found in the Appendix A. The chapter concludes with a table (Table 7-1, p. 66) listing all precipitation events investigated in the present study.

Figure 7-1 gives a time trace of days with strong precipitation and the corresponding IOP number during the SOP, based on the mesoscale precipitation analysis after Frei and Schär (1998).

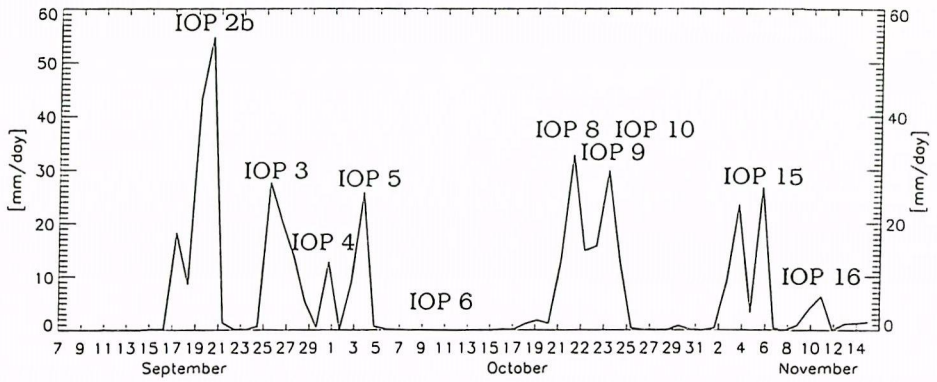

FIGURE 7-1. Mean precipitation (mm/day) for a ~ 150 x 150 km^2 domain in the Lago-Maggiore area during the MAP-SOP. Note that daily precipitation peaks at individual stations can be substantially larger than the grid point analysis of the subdomain (data from Frei and Häller, 2001). Only those IOPs are labelled which were relevant for the present study.

A total of 10 IOPs are described in chronological order starting with the "convective" (i. e. IOP 2b, IOP 3, IOP 4 and 5) and going over to the "stratiform" ones[7]. The major stratiform events were in descending order of importance: IOP 8, 9, 10, 15, 6 and 16. One additional case from 04 August 2001 was examined providing together with the 04 October (IOP 3) a further example of deep convection in the LMTA. Figure 7-2 portrays the geographical locations of the measurement site in the Ticino as described in the following sections.

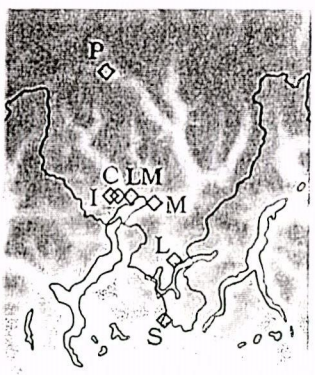

FIGURE 7-2. Locations of rain gauge measurement sites as mentioned in the following case descriptions (* are non-standardized measurement sites).

P = Piotta

I = Intragna*

C = Cavigliano*

LM = Locarno-Monti

M = Magadino

L = Lugano

S = Stabio

[6] The following sources were used as main input for the description: weather charts, radiosounding data from Milano, the MeteoSwiss database and the MAP Field Catalogue (2000).

[7] The separation between "convective" and "stratiform" IOPs is based on radar data.

7.1 IOP 2b: 19.09./ 20.09.1999

The IOP 2b lasted from 19.09. until 21.09. and is regarded as one of the most important IOPs featuring heavy precipitation events in the LMTA. Ahead of a deep trough extending into northern Africa and the associated cold front "Stau" precipitation was generated within a southerly airflow. On the southern side of the Alps from 12:00 UTC (19 September) stratiform precipitation started and intensified during the night and became more convective in the morning of 20 September. Between 09:00 and 10:00 UTC convective cells formed with an observed peak radar reflectivity of ~ 50 dBZ as observed by the Doppler radar on the Electra aircraft and the LMTA experienced the heaviest precipitation during this IOP.

Throughout the period of precipitation the airflow into the Lago Maggiore region at the 2 km level was generally from south impinging on the Alpine barrier and producing orographic precipitation with embedded convection tied to orography. The convective cells formed over individual mountain peaks but were not very deep since they rarely extended above 6 km. The accumulation of precipitation in the mountains on the western side of the Lago Maggiore region was particularly large. In Ticino, total precipitation amounts of 240 mm at Intragna and 170 mm at Locarno-Monti were registered. Referring to Figure 7-1 IOP 2b experienced the most intense precipitation event during the whole SOP. The precipitation over the LMTA ended in the evening of Monday 20 September.

From this IOP satellite data are available from 19.09. 18:00 until 20.09. 20:55 UTC and it is therefore very well documented. IOP 2b is an excellent example of heavy orographic precipitation with embedded convection over a mountainous region.

7.2 IOP 3: 25.09./ 26.09.1999

An upper-level trough situated over the Atlantic coastline of Spain and northern Africa led to southwesterly airflow related to heavy orographic precipitation in the LMTA. During September 25 the precipitation intensified and convective cells were observed in the LMTA in southwest-northeast oriented precipitation bands. The radar echoes extended up to about 6-8 km and exhibited cellular-like echo structures. These structures resulted in showery precipitation during the whole IOP and no bright band was discovered by the research radar. The predominant wind direction was southwest with a strong increase of wind speed with height. At low-levels the southwesterly flow continued throughout the 26 September forming convective cells on the west and north sides of the LMTA. The precipitation reached its maximum intensity in the night from 25 to 26 September, then decreased until midday. During these two days, large total precipitation amounts were accumulated in the mountains in the western and northern part of the LMTA (Locarno-Monti: 214 mm, Cavigliano: 440 mm). This event is well documented by radar and satellite data and provides another example of an event featuring embedded convection.

7.3 IOP 4: 30.09.1999

A fast moving upper-level trough associated with a cold front crossed the LMTA during the day of 30 September from west to east. As a consequence of the fast movement of the system, the LMTA experienced a brief period of precipitation in the afternoon with 15 mm/24 h in Magadino, 25 mm/24 h in Piotta and 22 mm/24 h in Locarno-Monti.

Most precipitation activity was recorded around 15:00 UTC where convective radar signals were detected embedded in stratiform echoes in the LMTA. The vertical structures of the radar had the form of small convective cells near local mountain peaks with maximum reflectivities of 30 dBZ at 6 km height as depicted by the RONSARD[8] ground-based research radar. Soundings at Milano showed a destabilization of the lower troposphere between 00:00

and 12:00 UTC connected with a change in wind direction from west to southwest above the 800 hPa level. Below, the wind direction changed from a westerly to a southeasterly airflow. Already by 18:00 UTC the Milano sounding depicted a strong inversion around 850 hPa with dry air above. Aloft, the winds turned in northwesterly direction transporting dry airmasses into the LMTA.

7.4 IOP 5: 03.10./ 04.10.1999

03.10.

After a south Foehn period on the north side of the Alps an active cold front hit the LMTA on Sunday morning 03 October. The precipitation started in the morning and intensified throughout the day. The northeastern part of the LMTA experienced heavy rainfall up to 100 mm (Magadino airport) causing flooded roads and one fatality. In the southwesterly airflow convective cells tied to orography were found. The U.S Doppler Radar on Wheels (DOW[9]), located at Magadino airport, observed the most intense precipitation between 16:00 and 21:00 UTC with radar echo tops reaching 8 km. Rapid scans are available from 19:30-22:55 UTC and the convective activity in the eastern part of the Ticino could be observed by the infrared channel data and compared to Mt. Lema radar data.

04.10.

On Monday evening 04 October starting from 19:00 UTC an intense convective cell formed to the east of the Ticino and progressed to the southwest towards Milano. This mesoscale convective system provided the only case with deep convection observed during the SOP in the region of Lago Maggiore and was completely missed by the numerical forecasts. From this case, rapid scans are available from 01:30-21:55 UTC with data from the beginning of the cell generation until the mature stage of the convective system.

IOP 5 provides excellent examples of both types, deep and embedded convective activity.

7.5 IOP 6: 13.10.1999

After a period dominated by a large scale high pressure system over central Europe, an upper-level low approached the Alps. The cyclonic system moved into the region of surface high pressure in the Po Valley and was weakening. The Mt. Lema radar showed from 06:30-15:30 UTC a well-defined bright band moving into the Po Valley indicating stratiform precipitation. As further shown by radar imagery, the precipitation moved from west to east slowly dissipating. As a consequence the observed precipitation in the Po Valley was weak and in the LMTA no precipitation was registered (cf. Figure 7-1). The Milano sounding at 00:00, 06:00 and 12:00 UTC showed a strong inversion at 800 hPa with a predominant westerly airflow above it and weak winds in the boundary layer. Moisture and warm air were transported by the westerlies into the Po Valley leading to a dissolution of the inversion at 800 hPa.

7.6 IOP 8: 20.10./ 21.10.1999

During IOP 8 the precipitation in the LMTA was stratiform with a distinct bright band observed by the ground-based radar network and no convective structures were detected (Houze, 2001). The most prominent feature of this IOP was the strong stability in the Po

[8] see MAP Implementation Plan (Binder et al., 1999)

[9] see MAP Implementation Plan (Binder et al., 1999)

Valley resulting in combination with the predominant southwesterly wind direction in a blocking effect. The stably stratified air was blocked by the Alpine chain leading to a cool counterflow in the lower atmospheric boundary running out of the valleys (Steiner et al., 2000a and b and 2002). From this case, satellite and radar data are available from the 20 and 21 October.

20.10.

An upper-level low pressure system moved into northern Italy accompanied by a change of wind direction from west to southwest and the onset of a deep Foehn on the north side of the Alps. In the Po Valley, an inversion situated at 800 hPa divided the drier stable airmasses below from the moist air above. During the day the inversion strengthened connected with a moistening of the air in the boundary layer. From 11:30 UTC the Mt. Lema showed stratiform precipitation moving towards the Alps. The precipitation was weak with daily totals of 14 mm (Locarno-Monti) and 12 mm (Lugano).

21.10.

In association with the cut-off low located over the Mediterranean, the wind direction turned from southwest (Milano sounding 00:00 UTC) to south (12:00 UTC) and finally to southeast (18:00 UTC) at higher levels (500 hPa). During the whole day, the Milano sounding indicated a stably stratified airmass residing in the Po Valley. The LMTA was covered by stratiform precipitation with daily totals of 54 mm (Locarno-Monti) and 50 mm (Lugano).

7.7 IOP 9 & IOP 10: 23.10.-25.10.1999

23.10. (IOP 9)

In front of an upper-level trough approaching western Europe warm airmasses and moisture have been advected towards the LMTA. From midnight until about 12:00 UTC stratiform precipitation moved rapidly across the area of the Mt. Lema radar towards the region of Venice. Afterwards the reflectivity echoes - still stratiform - were tied to the orography of the southern Alps. The recorded precipitation was 48 mm/24 h in Locarno-Monti, 35 mm/24 h in Lugano and 22 mm/24 h in Piotta. During the whole day, the predominant wind direction was from southwest as indicated by the radiosounding from Milano.

24.10. (IOP 9)

A weak upper-level trough associated with a frontal cloud system was retarded by the Alpine chain resulting in a south Foehn situation. The system proceeded slowly across northern Italy with main cloudiness and precipitation on the west-northwestern side of the Alps and Foehn on the northeastern side (Kuettner and Meitin, 2000). Radiosoundings from Milano showed a turning of the wind from west to southwest in all layers and an increase in humidity especially above 800 hPa during the day. The recorded precipitation amounts in the LMTA were 41 mm/24 h in Locarno-Monti and 30 mm/24 h in Lugano.

This case turned out to be an excellent case for the analysis of stratiform cloud top structures with satellite imagery. However, on this day the Mt. Lema provided limited data until 13:35 UTC, allowing only a direct comparison between satellite and radar imagery over a period of 1.5 hours.

25.10. (IOP 10)

The south-southwesterly flow throughout the atmosphere continued during the day transporting moisture towards the Alps. The precipitation amounts recorded in the Ticino were moderate: 18 mm/24 h (Locarno-Monti), 17 mm/24 h (Lugano) and Piotta: 52 mm/24 h. During the day, the Mt. Lema radar showed reflectivity echoes along the southern

foothills of the Alps and in the pre-Alpine region. The reflectivity echoes were of stratiform character and oriented in southwesterly-northeasterly direction. This day, rapid scan imagery was available from 06:00 until 23:55 UTC exhibiting southwesterly movement of the clouds and the generation of cloudiness related to the orographic barrier of the Alps.

IOP 9 and IOP 10 provide an example with stratiform precipitation in the LMTA associated with southwesterly wind direction.

7.8 IOP 15: 06.11.1999

IOP 15 featured a frontal passage over the Alps, inducing a lee cyclogenesis with a southwesterly flow ahead of it. Animation of infrared images show the generation of the lee cyclone associated with strong Mistral in the Rhone Valley starting from 12:00 UTC. Mt. Lema radar echoes showed a geographically fixed location of precipitation intensifying from 07:00 UTC with precipitation estimations of up to 30 mm/h. From 21:00 UTC the main precipitation area shifted towards south and did not affect the LMTA anymore. The daily precipitation amounts in the LMTA were 50 mm in Locarno-Monti, 22 mm in Lugano and 38 mm in Stabio. Further south, Milano reported 50 mm of precipitation. During the day, the radiosounding at Milano showed a turning of the wind below 900 hPa from south to southeast with constant southwesterly airflow aloft. From 06:00 until 12:00 UTC an inversion at approximately 925 hPa strengthened the decoupling of both airflows.

7.9 IOP 16: 11.11.1999

A cut-off low situated over the Gulf of Lion led to a southerly flow on its easterly flank. During the day the predominant wind direction at Milano was southeast below 800 hPa with southwesterlies aloft. Remarkable were the dry airmasses associated with the southeasterly airflow leading to a dry boundary layer up to 800 hPa. Rapid scans were available from 12:00 UTC and showed a slowly dissipating cloud layer over northern Italy. The cloud dissolution could also be observed by radar data from Mt. Lema which exhibited as maximum precipitation rate up to 10 mm/h but no bright band structure. Already by 16:00 UTC the radar echoes disappeared over the LMTA. The daily precipitation totals of this stratiform event were low with 18 mm in Locarno-Monti, 16 mm in Lugano and 3 mm in Piotta.

7.10 04.08.2001

This day was chosen as an additional case with deep convection in the LMTA, complementing the information from the MAP-SOP case of 04 October 1999. The data was made available by EUMETSATs' rapid scanning service on demand, providing ten-minutes scans. The infrared data was calibrated and analysed with the same applications as the images from the SOP.

Ahead of a trough extending from the British Isles to Spain, a thunderstorm with heavy precipitation developed in the evening of 04 August 2001 within the southwesterly flow. Several convective cells crossed the LMTA from southwest to northeast in the afternoon accompanied by gusty winds with maximum speed of 108 km/h in Locarno-Monti and 125 km/h in Magadino. The precipitation amount were 48 l/m^2 within 60 minutes registered in Magadino (Spinedi, 2001). Recorded daily totals of precipitation illustrate large differences in a limited geographical region typical of strong convective events. In Magadino 106 mm were measured, only 28 mm in Locarno-Monti which is located nearby.

The overview of the synoptic situation recalls the statements made in section 2.1.2 (p. 22) where the main "ingredients" for the generation of heavy precipitation were listed. Despite the similarity in the synoptic setting of the large scale flow of these events, differences are observed in terms of the specific mesoscale environment they occurred in. Especially in complex terrain the probability is increased, that small scale meso-β phenomena like winds in a single valley influence effectively the specific character of an overall precipitation event by determining e. g. the location of convection. Therefore, the aforementioned similarity must be considered with caution as long as the influences of small scale effects are not fully understood yet. The following table summarizes the relevant events, making reference to the predominant precipitation characteristics as derived by radar.

TABLE 7-1. Summary of all investigated precipitation events from MAP-SOP plus the event of 04 August 2001. The last row indicates the total number of events and their distribution with respect to the precipitation characteristics derived from radar observations.

IOP	Period	Description according to the POC Science Coordinator(*)	Precipitation characteristics
2 b	19.09. /20.09.	Frontal system and heavy rain over the LMTA*	embedded convection
3	25.09. /26.09.	Heavy orographic rain in the LMTA*	embedded convection
4	30.09.	Rapid frontal passage over the LMTA*	embedded convection
5 5	03.10. 04.10.	Frontal passage and cyclogenesis over Northern Italy* MCS to the east of LMTA	embedded convection deep convection
6	13. 10.	Upper-level low moving into a ridge over Northern Italy*	stratiform
8	20.10./ 21.10.	Persistent lifting of stable air during a frontal passage over the Alps*	stratiform
9	23.10. - 24.10.	Stratiform precipitation in frontal system passing rapidly over Northern Italy*	stratiform
10	24.10. - 25.10.	Stratiform precipitation in Northern Italy ahead of a slowly moving front with strong southwesterly flow aloft*	stratiform
15	06.11.	Cold frontal passage over the Alps and a lee cyclone*	stratiform
16	11.11.	Weak precipitation over the LMTA associated with a cut-off low	stratiform
-	04.08., 2001	Thunderstorm over the LMTA	deep convection
10			deep convection: 2 embedded convection: 4 stratiform: 6

The precipitation characterizations as derived from radar observations of the analysed events according to Table 7-1 (i. e. "deep convection", "embedded convection" and "stratiform") were taken over in the following chapter and the corresponding IOPs have been investigated resulting in the synthesis of the present work.

8 Synthesis

In this chapter, the satellite-based methods were applied to precipitation events described and classified in chapter 7 (see table 7-1, p. 66). In the first part of this chapter, the appearances of "deep convective", "embedded convective" and "stratiform" cloud features are presented and conclusions are drawn. In the second part a classification scheme is presented intending to quantify the magnitude of cloud development within four subregions centred over the LMTA. The quantification served as a major input for the overall characterization of the precipitation events helping to identify preferred areas of cloud development and allowing inferences from the life cycles of the analysed precipitation events. The insight gained helped to establish two conceptual models of heavy precipitation as encountered during the MAP-SOP. Finally the chapter concludes with the presentation of results based on radar investigations from the Mt. Lema. The radar data helped to determine location and the structure of convective areas. Furthermore, the dependency of preferred areas of convection on upstream conditions as denoted by Milano radiosoundings is discussed.

8.1 Deep convection

IOP 5 (04.10.1999) and the additional case from 04.08.2001 allowed studies on the appearance of deep convection in rapid scan imagery. Both days provide excellent examples of strong convective activity and enabled a detailed study by satellite and radar during different stages of life cycle of the observed cloud systems. Since convective activity occurred mainly in the evening of both days, visible satellite imagery was exploited only on 04.08.2001. Figure 8-1 depicts an image sequence demonstrating the evolution of a MCS east of Ticino beginning at 20 UTC, 04.10.1999.

The geographical location of the radar-detected convective echoes and the cooling satellite signals coincide in the developing stage of the convective cell (cf. Figures 8-1 a) and b)) before the generation of an anvil starts (Figure 8-1 c)). As soon as cloud top icing occurred the location of radar echoes and satellite signals did not coincide anymore and the strongest cooling effects in satellite images - as possible indicator of convection - were located at the cloud border because of the lateral expansion of the growing cloud (cf. Figures 8-1 c) - f)). The spatial variance accentuates the cloud border of the convective cell and provides information on the lateral expansion. The anvil region was characterized by a smooth and cold cloud top with very weak temporal evolution. It is interesting to see, that the area of convection in radar images was located at the leading edge of the cloud, moving southwestward in the upstream direction away from the Alps. The convective area was trailed by a precipitation area describing a common pattern for convective systems in the midlatitudes (Schiesser et al., 1995). An interesting mesoscale process could be recognized with the evolution of the MCS: Ahead of the convective edge of the cloud a region of cloud dissolution is observed, indicated by a warming area. This warming area is mainly shown in Figures 8-1 c) - e) ahead of the cloud around the arch-like cooling structure. This structure may be explained by a cold outflow produced by evaporative cooling of the convective system resulting in cloud dissolution.

On 04 August 2001 mature, isolated cells hit the LMTA from 00:00 until 08:00 UTC and between 15:00 and 21:00 UTC embedded within a southwesterly flow. From 15:00 UTC a mature MCS moved into the LMTA exhibiting a more or less pronounced structure with a leading convective edge and trailing stratiform area (cf. Figure 8-2, upper panels). Ahead of this MCS several smaller cells were generated joining the main system propagating towards the southern slopes of the Alps. Influenced by the orography, the typical cell structure of the MCS disappeared as seen in satellite imagery (cf. Figure 8-2, lower panels). The radar-detected convective signals changed from the structured leading convective edge of the MCS

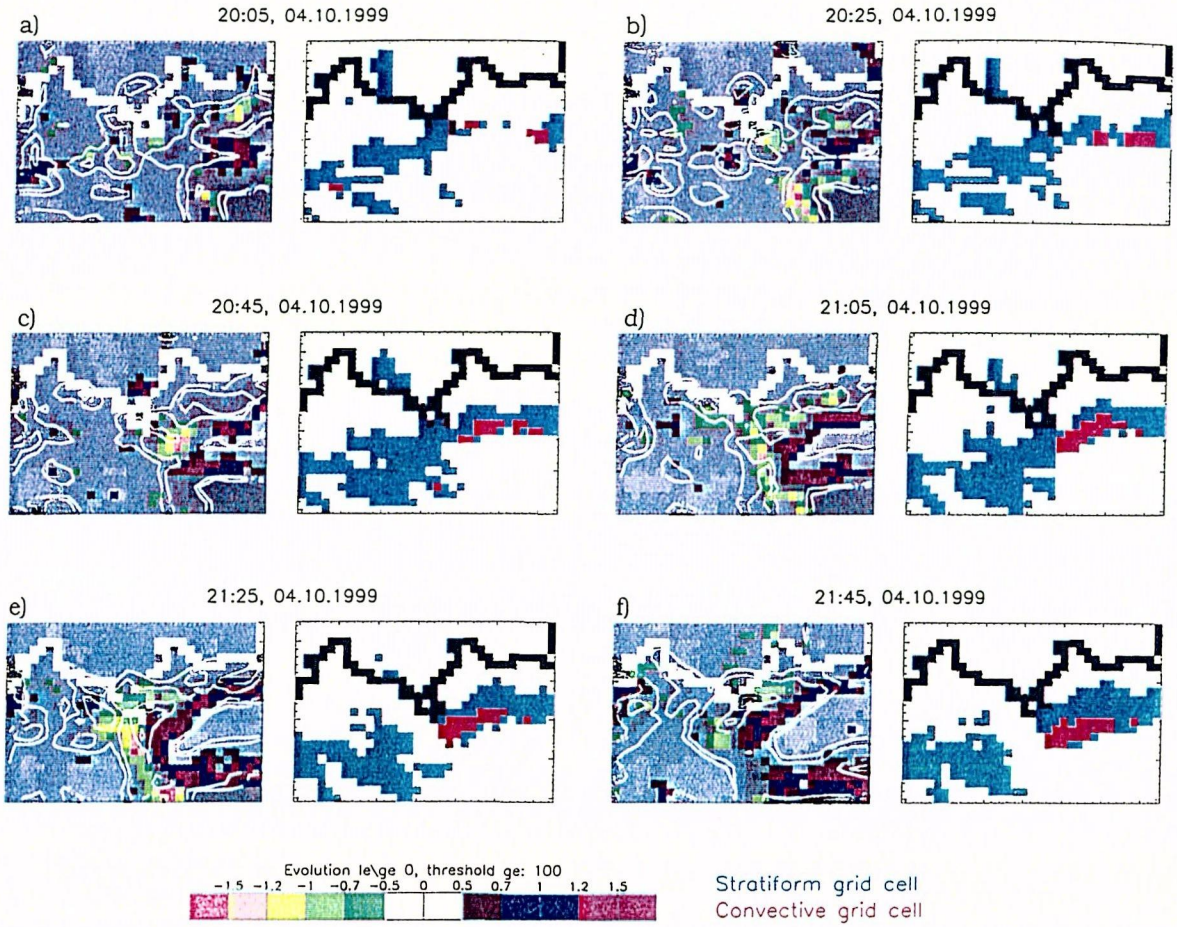

FIGURE 8-1. The generation of a deep convective cloud on 04.10.1999, 20:05-21:45 UTC, as seen by satellite (infrared channel) and radar images presented with 20 minutes interval imagery. In the satellite images the color depicts the magnitude of cloud development, the thin white lines delineate the regions of high pixel variability. In the radar images, stratiform pixels are colored in green and convective pixels in red. The thick white line (satellite images) and black line (radar images) depict the border line of Switzerland.

into scattered and sometimes band-like structures tied to orography (cf. Figure 8-2, lower panels). The MCS of 04 August 2001 is a good example illustrating the orographical modification of the appearance of deep convection systems in satellite and radar imagery.

Figure 8-2 summarizes the main results of investigations of deep convection by infrared satellite data and radar data. In this figure, the original satellite image (Figure 8-2 a)), the analysed satellite image (Figure 8-2 b)) and the radar-detected convective and stratiform signals are compared. The following conclusions can be drawn:

- The ability to detect the convectively active region in the satellite images is dependent on the stage in the life cycle of the observed cloud feature. As soon as an anvil is generated, the satellite signals representing strong cooling areas do not coincide with the convective radar signals anymore. Since the anvil is rapidly generated (e. g. within 0.5 hours) imagery of high temporal resolution allows an observation of the initial stage of a system which is relevant for nowcasting and potential warnings. After the anvil generation (mature stage) convection is hidden and the expanding anvil borders are characterized by strong cooling signals and high pixel variability. These areas seen in satellite imagery do not geographically coincide with the radar-detected convective echoes and would - if regarded as convective - clearly overestimate the convective activity.

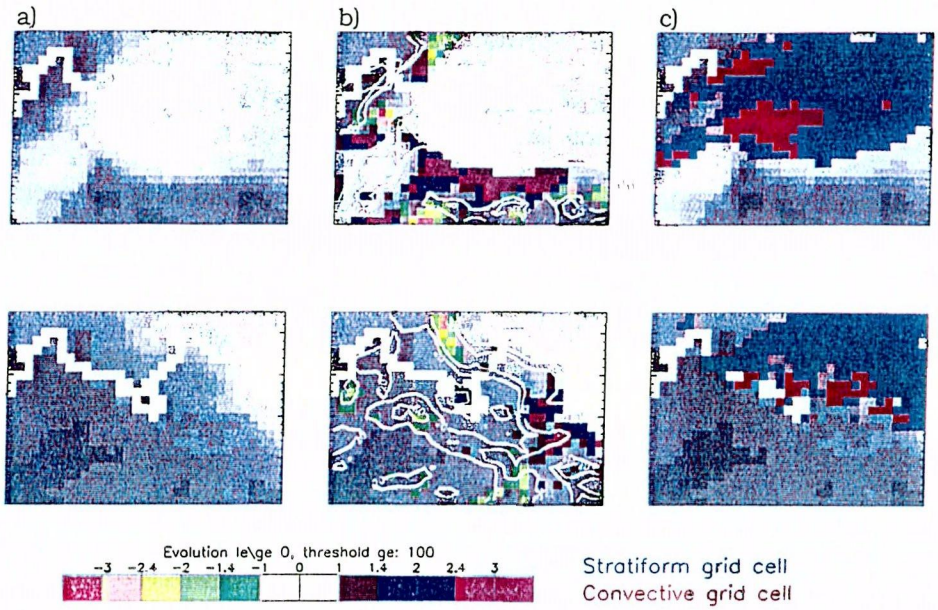

FIGURE 8-2. 04.08.2001, upper panels: 17:50 UTC, lower panels: 20:30 UTC, infrared channel. a) depicts the original satellite image, b) the analysed satellite image and c) the original satellite image with the classified radar data superimposed. Note the different cooling and warming classes in the legend due to the 10 minutes interval imagery compared to Figure 8-1. For a description of signatures see Figure 8-1.

- Compared to the horizontal extent of a mature MCS, the convective area detected by radar is limited in space (cf. Figure 8-2, upper panels). The echo structure showed in both cases a leading convective edge and a trailing stratiform area (cf. Houze, 1993). Remarkable is the geographical coincidence of cloud cover in satellite infrared images and precipitation regions - at a height interval between 4.5 and 5.5 km - as seen by radar. The precipitation area coincides quite well with the area of the MCS (cf. Figure 8-2, upper panels). The probability, that cold pixels contain precipitation as seen by radar increases with decreasing count values. However also warmer satellite pixels may contain precipitation particles (cf. Figure 8-2, lower panels).

Data from the visible and water vapor channels provide further information on the appearance of deep-convective cloud systems. Visible data were investigated from 09:00 until 18:00 UTC of the 04 August 2001 and variance calculations were applied. Special attention was directed to small areas of pixel variability within the MCS cloud and inferences from the comparison with radar imagery are drawn. Figure 8-3 a) illustrates fine structured areas of high pixel variability in the visible image within the large MCS cloud, Figure 8-3 b) shows the corresponding radar image. Apart from the cloud borders, regions of high pixel variances at the cloud top are depicted giving hints of potential areas of convection below. The areas of high pixel variability within the cloud may result from convection below but a clear attribution to radar-detected convective echoes is not possible. It is difficult to distinguish areas with high variability from pixel areas possibly related to convection. Regions of high pixel variability may coincide incidentally with convective areas detected by radar but no explicit identification of regions containing convective activity is possible. Therefore, the example of the 04 August 2001 shows, that the data of the visible channel are not suitable for the localization of convective areas despite the higher spatial resolution.

Generally, water vapor images provide less distinct cloud structures and suffer from a lack of contrast, but isolated convective areas with deep convection like the MCS observed on 04 August 2001 appear in water vapor imagery with distinct patterns (elliptical shapes). For the data of this channel, especially the pixel variability analysis was found very suitable for

the determination of the horizontal extension of the cloud. Figure 8-3 c) provides an example of an analysed water vapor image of 04 August 2001 with areas of high pixel variability accentuating the leading cloud edge of the MCS. Comparison of the areas of high pixel variability of this figure with the infrared channel (Figure 8-1 e)) shows that in the water vapor image the MCS is the only object pinpointed whereas in the infrared channel - due to more contrasting imagery - several areas of high pixel variability exist. As a consequence, water vapor images were exploited only with the occurrence of deep convection, since moderate and weak convection would not evoke enough contrast. In addition, low pixel contrast in water vapor images results in a lower magnitude of the pixel evolution as demonstrated in Figure 8-3 c).

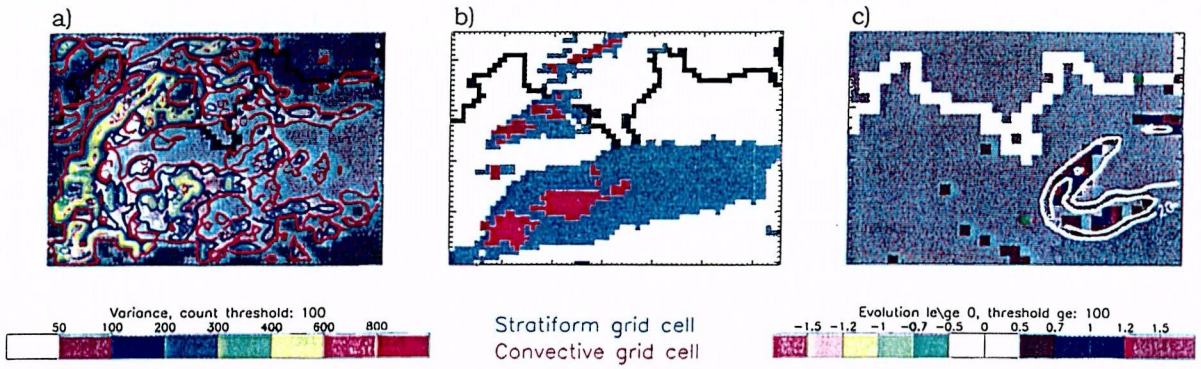

FIGURE 8-3. a) Normalized visible image, 04.10.1999, 16:40 UTC, colored thin lines depict regions of high pixel variances, b) the corresponding radar image with the grid resolution of the visible channel, c) water vapor image, 04.10.1999, 21:25 UTC. For a description of signatures see Figure 8-1.

In summary, the visible and water vapor channel provide the following additional satellite-derived information on cloud features related to deep convection:

- The higher spatial resolution of the data of the VIS channel provide more detailed information on cloud top structures compared to IR and WV data. Regions of high pixel variability accentuate potential areas of convection at the cloud tops but also the cloud borders. As a consequence thereof, a systematic attribution of regions of high pixel variability to the location of convective activity is not possible since non-convective areas like cloud borders exhibit strong pixel variability, too.
- The use of WV imagery is suitable for the identification of cloud features which are related to deep convection. Especially isolated areas of strong convection are well-recognizable in the low contrast imagery of WV by their elliptical patterns. The pixel variability depicts well the lateral borders of these isolated convective clouds and their horizontal expansion in time. Compared to IR data, WV images are characterized by a lower magnitude of pixel evolution as a result of the poor pixel contrast in WV imagery. In the present study, the poor contrast limited the use of WV imagery to cloudiness related to deep convection.

The knowledge of the appearance of deep convection is a helpful information in order to find embedded convection within satellite imagery as discussed in the next section.

8.2 Embedded convection

Compared to the cases with deep convection discussed in the previous section, embedded convection is supposed to be related to weaker updrafts within a limited vertical area in the atmosphere (cf. Figure 2-5, p. 26). As a consequence of the less intense updrafts within areas of embedded convection, the cloud development signals at the cloud top are expected to be weaker than cloud top characteristics evoked by deep convection.

During the whole period of IOP 2b the geographical coincidence of convective areas seen by radar and the areas of strong cloud development derived from satellite is poor. By noon on 20.09. the wind turned from a southerly to a southeasterly direction accompanied by an onset of convective activity in the eastern part of the LMTA. Figure 8-4 a) shows convection associated with southeasterly winds observed by radar and the corresponding satellite image. The satellite image illustrates strong cooling at the backside of a cloud moving over the LMTA. These cooling regions are not related to radar-detected convection. The poor coincidence of strongly evolving areas in the satellite image and the radar-derived locations of convection may be explained by the weak vertical extension of the convective cells which rarely extended above 6 km (MAP Field Catalogue, 2000). Moreover, IOP 2b was characterized by high reaching cloudiness with cold cloud tops hiding the areas of convective activity. The cloud cover was generated further south over the Ligurian Sea being transported with the southerly airflow towards the Alps. The stratiform precipitation was partly transported within this southerly airflow and partly generated within the LMTA above the Alpine mountains. During the whole IOP, convection as derived from radar was mainly located over the southern slopes of the Alps.

IOP 3 is a further example of convection related to orography in an unstable atmosphere. In the predominant southwesterly flow, strong convective activity was observed over the southern slopes of the Alps. Like in IOP 2b, there is a poor coincidence of the convective areas identified by radar data and areas of strong cooling in satellite imagery what is underlined by Figures 8-4 b) and c). Noteworthy is the strong cloud evolution ahead of the Alpine barrier on 25.09., as shown in Figure 8-4 b). A comparison with the corresponding radar image provides evidence that the cloud evolution depicted in the satellite image occurred in a precipitation-free atmosphere while the radar-detected areas of precipitation with embedded convection were located over the southern slopes of the Alps. During the night, over the Po Valley permanent and strong cloud evolution can be observed in satellite images. In the morning of the 26.09., the LMTA was covered by cloudiness exhibiting areas of weak cloud evolution changing to areas of strong cloud development and vice versa. Figures 8-4 b) and c) show strongly and weakly evolving clouds, both occurring - as depicted by radar - with convective activity. It is assumed, that - analogously to IOP 2b - the convection identified by radar is too weak to evoke signals on cloud tops.

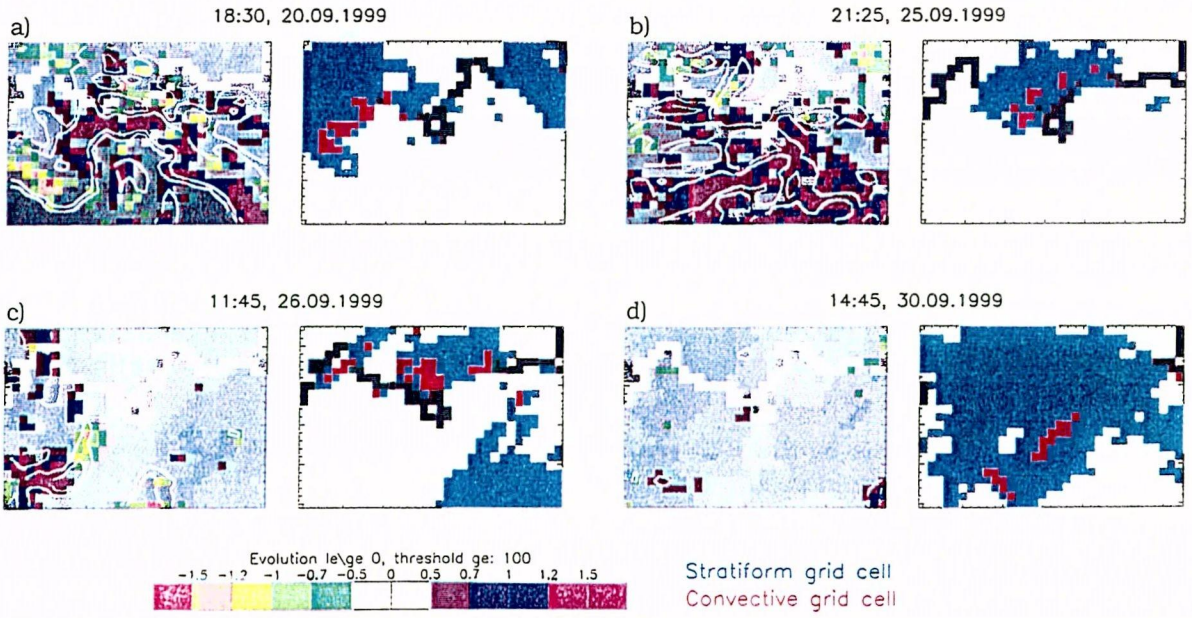

FIGURE 8-4. Examples of areas of cloud development seen by satellite (infrared channel) and convective/stratiform precipitation as derived from radar. a) 20.09., 18:30 UTC, b) 30.09., 14:45 UTC, c) 25.09., 21:25 UTC and d) 26.09., 11:45 UTC. For a description of signatures see Figure 8-1.

IOP 4 was associated with a fast moving cloud cover moving eastwards. Similar to IOP 2b the coincidence of satellite cooling areas and convection seen by radar is poor as shown in Figure 8-4 d). Most evolution signals in the satellite image are associated with cloud borders, meanwhile convection as detected by radar occurs below the smooth cloudiness.

In common with the previous IOPs, IOP 5 is characterized by an unstable atmosphere as indicated by the radiosounding from Milano. Convective activity in the northeastern part of the LMTA took place with radar echo tops up to 8 km (MAP Field Catalogue, 2000). Between 19:30 and 20:30 UTC a remarkable geographical coincidence of the areas with strong evolution and high count variability in satellite images and areas identified as convective by radar is found (Figures 8-5 a) - d)). The region of cooling and strong pixel variability remained geographically stationary tied to orography. Since the convection occurred in an environment of weak cloud development, the signals manifested by satellite are unambiguously attributable to convection within a precipitation region as shown by radar. Figure 8-5 illustrates this coincidence with an image sequence over a period of half an hour. IOP 5 is the only IOP where convection, favoured by an unstable atmosphere and by orographical forcing, evoked distinct signals in cloud top structure allowing a clear identification of embedded convection by satellite.

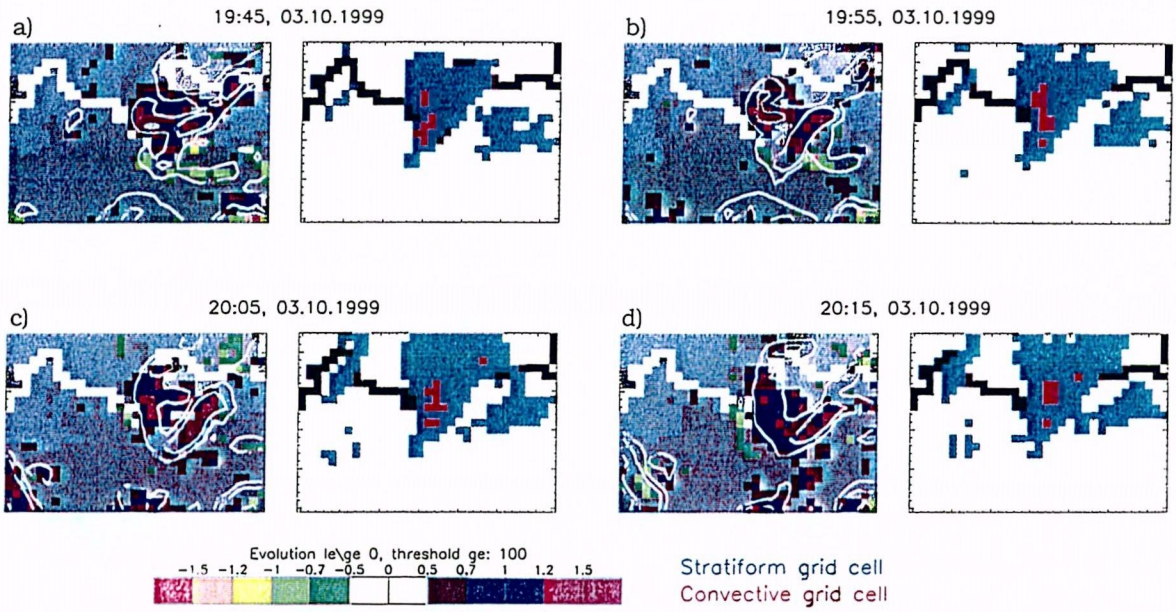

FIGURE 8-5. a)-d) 03.10., 19:45-20:15 UTC: Areas of convective and stratiform precipitation as derived from radar and areas of cloud development seen by satellite (infrared channel) shown with images in 10 minutes interval. For a description of signatures see Figure 8-1.

The following Figures 8-6 a) and b) show, that the VIS channel, despite the enhanced spatial resolution, does not permit the localization of updraft regions with embedded convection during IOP 3 and 4. For IOP 5 an investigation of normalized visible data is not possible due to daytime restrictions of normalized data.

From the investigations of the IOPs with convective cells embedded within a large-scale upslope flow in a predominant unstable airmass on the south side of the Alps we learn:

- A systematic geographical coincidence of areas identified as convective by radar and areas of strong cooling and high pixel variability derived from satellite is not recognizable, neither in the IR nor in the VIS data. Possible geographical coincidences of locations of potential convective activity observed by satellite and radar are regarded as incidentally.
- An exception to this general statement provided IOP 5 (03.10.) during a limited time (19:30 until 20:30 UTC). During this period cloud development signals derived from

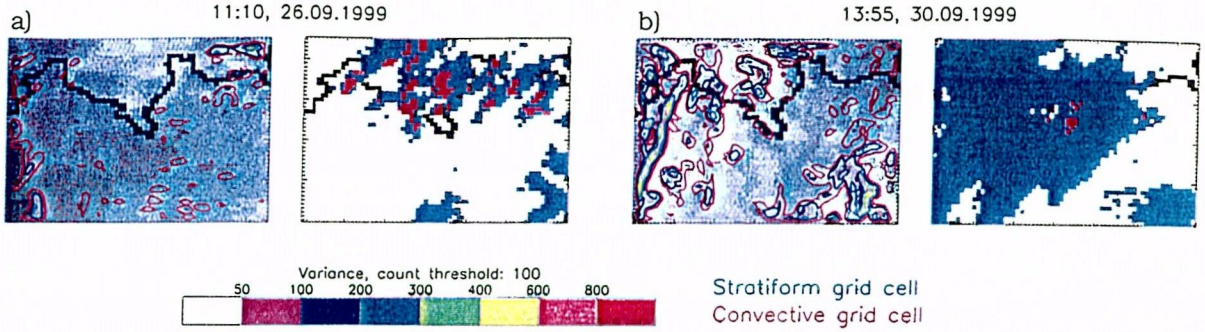

FIGURE 8-6. Pixel variability (colored lines) as derived from visible satellite data (left panels) and stratiform and convective regions identified by radar (right panels) of two cases with embedded convection. a) 11:10 UTC, 26.09. and b) 13:55 UTC, 30.09. The magnitude of pixel variability is indicated by colored lines.

satellite coincide geographically with the region of convection as identified by radar. In this case, the convection is strong enough to provide signals of strong cooling and high pixel variability recognizable in cloud top structures.

- The unambiguous identification of convection by satellite data is complicated by the fact that strong cloud development may occur also in an atmosphere without precipitation. The cloud development in a non-precipitating environment may be related to convection but the identification of convective areas is not possible by means of satellite or radar.

It is assumed that the intensity of convection related to orography determines the detectability of convective areas within satellite imagery. If the convection is strong, anvils are generated during short periods hiding the regions of convective activity as shown in the previous section. If the convection is too weak, no signals related to potential convective activity on the cloud top are detectable. It is hypothesised that in almost all cases with "embedded convection", the intensity of convection and the related vertical extension of the updrafts is too small to evoke signals at the cloud top. IOP 5 gives hints at the appearance of the "ideal embedded convection" allowing an identification by satellite imagery. During this case, the convective activity was obviously strong enough to generate cooling areas at cloud top. With echoes topping 8 km radar might give a possible reference for the intensity of the convection.

As a main result of this section we learn, that Meteosat data does not allow the systematic localization of embedded convective activity.

8.3 Stratiform precipitation

The investigated stratiform precipitation events in the LMTA were accompanied by a predominant southwesterly to southeasterly airflow in the lower atmosphere with the exception of IOP 6 which is characterized by a westerly airflow.

The appearance of cloudiness associated with stratiform precipitation is manifold. The classical stratiform cloudiness, characterized by weak cloud development and smooth uniform cloud tops is encountered only during a limited period during IOP 8 (21.10.) and IOP 9 (24.10.). During these IOPs, cloudiness with stratiform precipitation covered large areas of the Po Valley. The stably stratified atmosphere prevented an overflow of the clouds over the Alpine chain. As a consequence, the low cloudiness was blocked in the Po Valley by the orographic barrier resulting in weakly-textured and almost non-evolving cloud top structures. It is assumed, that such a situation of "orographic blocking of low cloudiness" strongly depends on the inversion height and its strength in the Po Valley. In satellite

imagery these situations can be recognized by sharp cloud borders extending along the southern slopes of the Alps as illustrated in Figure 8-7 a). In this figure, the northern edge of the smooth cloud shield is marked by areas of high pixel variability and mainly warming evolution. These evolution signals are caused by the movement of the cloud border which does not remain geographically fixed. The strong stability hinders a cloud development within the extended cloud shield, resulting in a more or less uniform cloudiness.

During most of the IOPs characterized as stratiform by the radar, the cloudiness exhibited time intervals with stronger or weaker cloud development and was not hindered from an overflow over the Alpine chain. Often, the overflow is combined with strong cloud development as seen in satellite images in the upstream region of the Alps in a precipitation-free atmosphere. Figures 8-7 b) - d) give examples of the manifold appearances of cloudiness accompanied by stratiform precipitation.

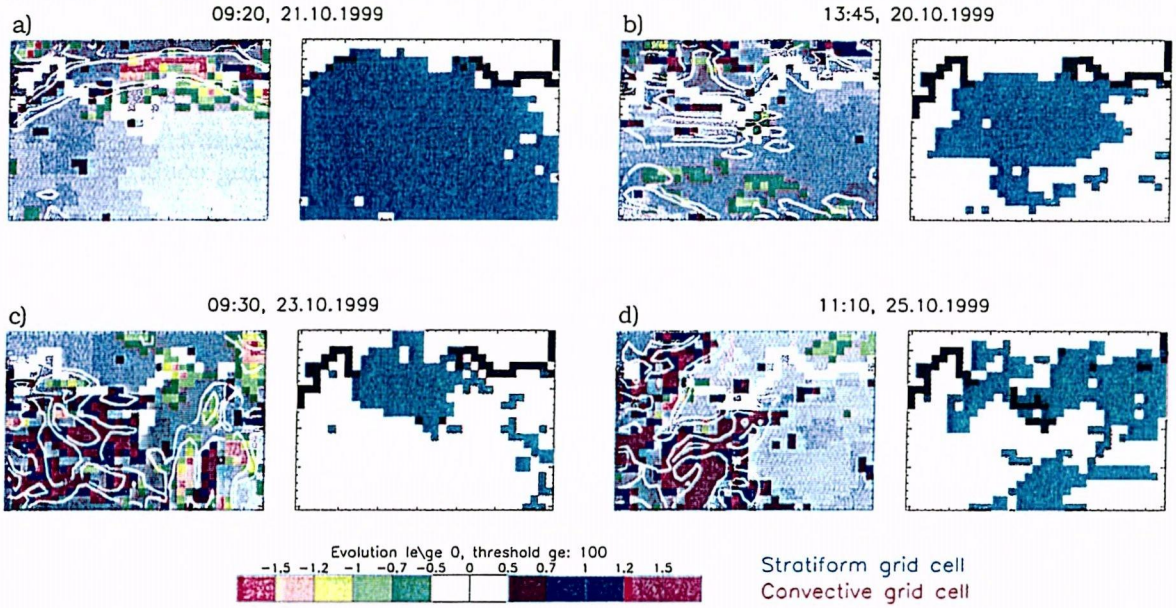

FIGURE 8-7. Examples of cloudiness as observed in the infrared channel associated with stratiform precipitation. a) 21.10., 09:20 UTC (IOP 8), b) 20.10., 13:45 UTC (IOP 8), c) 23.10., 09:30 UTC (IOP 9) and d) 25.10., 11:10 UTC (IOP 10). For a description of signatures see Figure 8-1.

Figure 8-7 b) represents a cloud structure frequently observed when analysing the stratiform cases. The cloudiness is characterized by weak to moderate evolution with a non-uniform cloud top. Though also periods with smooth and weak evolving cloud tops are found (e. g. IOP 9, IOP 15), no general characterization of the analysed IOPs with stratiform precipitation is possible. The spectra of appearances of cloudiness with stratiform precipitation in satellite imagery is too broad to allow a classification using cloud pattern characteristics as derived from the present methods.

Special attention was given to the results of Figures 8-7 c) (IOP 9) and Figures 8-7 d) (IOP 10) which show strong cloud evolution over the northern Po Valley. These results do not confirm the classical stratiform cloud patterns as expected originally with weak evolution and smooth cloud tops. Evidently, in stratiform precipitation areas strong cloud development is possible and in accordance to the cases with radar-detected embedded convection, the preferred area of cloud evolution is located over the Po Valley occurring in a non-precipitating atmosphere.

As inferred from radiosounding data from Milano, during IOP 9 and IOP 10 an unstable atmosphere favoured the cloud development observed in satellite imagery. The two radiosoundings in Figure 8-8 show a stable stratification at low levels with moist and unstable layers above.

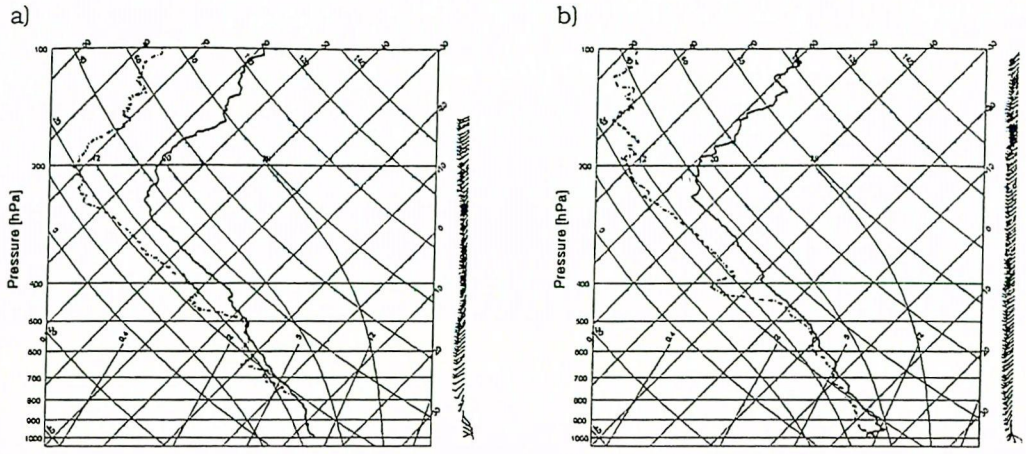

FIGURE 8-8. Radiosoundings from Milano with wind speed and direction indicated by wind flags, temperature (black line) and dewpoint temperature (dashed black line) from a) 23.10., 12:00 UTC (IOP 9) and b) 25.10., 12:00 UTC (IOP 10).

The results of the radiosoundings demonstrate, that the signals analysed from satellite imagery are plausible and underline, that strong cloud evolution may occur together with radar-detected stratiform precipitation. As derived from satellite imagery, the evolution proceeds mostly in a non-precipitating atmosphere and is not recorded by radar. In these cases, the satellite-based hypotheses are confirmed by radiosounding data from Milano.

One of the most striking feature of stratiform cloudiness is that its cloud tops are often colder than cloud areas with convective activity. As mentioned earlier, brightness temperature thresholds are often used for the separation between convective and stratiform cloud areas (e. g. Machado 1998, Carvalho and Jones 2001). Investigations of cloudiness associated with stratiform and convective precipitation prove that brightness temperature information is not a sufficient discrimination criterion. According to Figure 8-9 distinct differences in greyvalue distribution are observed between the cloudiness with stratiform and convective precipitation, respectively. The colder stratiform region in Figure 8-9 a) contains no convection whereas the warm cloud region in Figure 8-9 b) does. Obviously convection observed by radar occurs also in warmer cloud areas and the choice of a reasonably cold brightness temperature is no guarantee for the existence of convection within the observed cloud area.

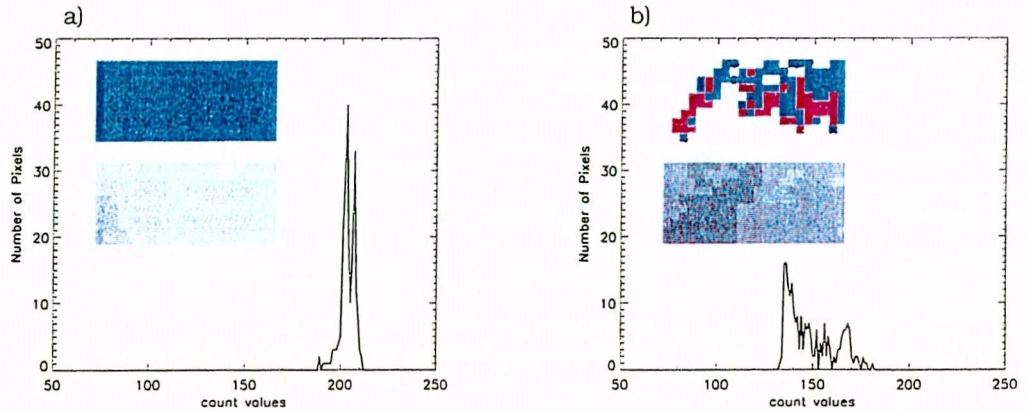

FIGURE 8-9. Histograms of the infrared channel: a) stratiform (06.11.1999, 21:50 UTC) and b) convective (04.08.2001, 21:40 UTC) cloud areas. The upper panels within the histogram plots depict the convective (red) and stratiform (green) pixels as classified by radar, the lower panels show the corresponding satellite area (size: 10 x 22 pixels).

Though the probability increases that with decreasing brightness temperatures a cloudy area contains convection, brightness temperature thresholds are not a sufficient criterion for the detection of convective regions for the purposes of the present study. It is conceivable to use brightness temperature thresholds for the detection of deep convective systems like MCSs in combination with additional information. Such kind of additional information for deep convective systems is provided with their distinct cloud patterns in the data of all channels (cf. section 8.1, p. 67). The main findings of cloudiness accompanied with radar-detected stratiform precipitation are as follows:

- There are many facets of cloudiness associated with stratiform precipitation. According to this, the appearances in satellite imagery are manifold, ranging from stratiform cloudiness with a smooth cloud top and weak temporal evolution (regarded as classical stratiform cloudiness) to cloudiness exhibiting strong evolution and high pixel variability. The regions of strong evolution are located over the Po Valley and occur in a non-precipitating atmosphere. It is questionable whether it is adequate to use a term like "stratiform cloudiness" since also in an area defined as stratiform by radar strong development occurs in a non-precipitating atmosphere. During IOP 9 and IOP 10 the unstable airmasses as gleaned from radiosounding data from Milano underline the results from satellite by showing strong cloud development.
- Analyses of brightness temperature demonstrate the limited capability of the brightness temperature or count thresholds for the detection of convective activity. Stratiform precipitation areas may exhibit cold cloud tops while precipitation in a convective environment may be observed with warm pixel areas.

The results point out, that *the* characteristic cloudiness accompanied by stratiform precipitation does not exist. As a consequence, separation between cloudiness with embedded convection and cloudiness with stratiform precipitation is not possible since the characteristics between the two are from a satellite's point of view not significant.

Summary

As shown in the first three sections of this chapter, it is difficult to separate between convective and stratiform cloud areas with the help of spatial and temporal information of cloud top characteristics only. The identification of locations of convective activity is limited with the established methods, depending on the life stage of the observed system and the intensity of convection. While deep convection shows distinct characteristics in terms of shape and evolution/pixel variability, the appearance of embedded convection in cloudiness could not be recognized. The coincidence of convective radar signals and potential embedded convective cloud areas as seen by satellite is regarded as incidental. A probable reason for that is the limited vertical extent of embedded convection producing weak signals at cloud top level aggravating its identification with the methods used in the present study. Therefore, in most cases the embedded convection is a too weak phenomenon to produce distinct signals in terms of cloud shape or (cooling) evolution/pixel variability at the cloud top. IOP 5 can be regarded as the only exception during the whole SOP, where within a limited period of an hour a coincidence of satellite- and radar-derived convective signals is recognizable.

The expected classical stratiform cloud top structure with weak evolution and pixel variability is encountered but can not be regarded as the predominant cloudiness associated with stratiform precipitation. Several IOPs, classified as stratiform by radar, show moderate to strong cloud evolution with areas of high pixel variability. It must be assumed that significant vertical motion within the atmosphere, related to an unknown extent to convection, without the generation of precipitation, occurs also in an area characterized as "stratiform" by radar. According to the POC Science Coordinator (MAP Field Catalogue, 2000) IOP 9 and IOP 10 provide examples of stratiform precipitation events. However, both cases

revealed strong cloud evolution in satellite imagery suggesting an unstable atmosphere. The radiosounding data from Milano confirm the evolution signals derived from satellite describing rather convective than stratiform airmasses in the Po Valley. On the other hand, an event like IOP 2b is characterized in satellite imagery mainly as stratiform, while radar identifies convection below the high cloudiness associated with the precipitation system.

Usually, brightness temperatures are used to identify convective regions. For the purposes of the present study, count thresholds would not allow a correct discrimination between convective and stratiform cloudiness. It is shown with the help of radar data, that convection may occur in warm cloud regions without an indication of cold cloud tops. On the other hand, stratiform precipitation in cloudiness with very cold tops without the presence of convection is observed.

In summary, the classical stratiform cloudiness with uniform cloud top is in most investigated cases not confirmed by the analyses of the satellite imagery. Therefore, the separation between convective and stratiform areas is not possible by satellite, as long as convection is not deep. As a consequence we propose instead of an estimation of convective activity an estimation of cloud development of a precipitation system. With cloud development we refer to cloud evolution due to convective *and* non-convective processes. In the next section, an automated quantification of the magnitude of cloud development will be presented.

8.4 Classification/Quantification of cloud development

In this section a quantification of the cloud development within the Lago Maggiore area is derived. The quantification of cloud development helps to characterize the predominant cloud structures of one or more precipitation events and allows an identification of preferred areas of strong cloud development.

For the quantification, an area centred over the Lago Maggiore is divided in four subregions of equal size (17 x 22 pixels), covering different geographical areas (cf. Figure 8-11, p. 79). The northern two subregions lie within the pre- and Alpine region of southern Switzerland, the southern subregions cover the northern part of the Po Valley comprising the southern slopes of the Alps. The division in subregions helps to localize the preferred regions of strong cloud development allowing inferences from the different stages in the life cycle of observed cloud systems. The total area covered by the four quadrants is somewhat bigger than the originally defined LMTA in order to include larger cloud areas as input data for the classification. Empirical thresholds are set in order to classify and quantify the magnitude of cloud development within each of these four subregions for each image of a rapid scan sequence. The count threshold set to 100 ascertains the classification of pixels containing cloudiness. As classification input, several parameters are analysed individually for each subregion:

- cloud development: the number of cooling and warming pixels respectively, and their magnitudes
- the magnitude of pixel count variability
- histograms including information on mean count value and histogram width

These input parameters are combined and seven different classes are established (cf. Table 8-1, p. 78) with one additional class for unclassified input data. As illustrated in Table 8-1 the main criterion for the classification is the information on cloud development with the associated indications on magnitude and number of evolving pixels for each of the four subregions. Limited use is made of the count variability of the pixels as classification input. High count variability is induced by all cloud borders independently of their evolution and

are not necessarily related to cloud development. Note that the class definitions and examples of each class in Table 8-1 are provided in the Appendix B.

TABLE 8-1. Established classes for a quantification of cloud development attributed to each of the four subregions.

Classes	Main characteristics	Abbreviation
strong cooling cloud development	prevailing strong cooling	CD ++
moderate cooling cloud development	predominant cooling with moderate magnitude	CD+
balanced cloud development	balanced relation between warming and cooling	B
weak cloud development	weak temporal evolution either warming or cooling	W
non-evolving	cold and smooth cloud top with low pixel variability and weak evolution	NE
moderate warming cloud development	predominant warming with moderate magnitude	CD-
strong warming cloud development	prevailing strong warming	CD--
unclassified	pixels below a count value of 100/ no evolution	UC

The following Figure 8-10 presents the classification scheme and the relation of the classes to each other. The x-direction depicts the magnitude of evolution and the y-direction the cooling or warming trend. The class "B" stands for balanced evolution, i. e. the number of cooling and warming pixels are more or less balanced within a subregion. Note that within this class, strong but balanced cooling and warming pixel evolution may be encountered as illustrated in Figure 8-11 a) in the lower left corner. "B" separates the classes with moderate and strong evolution (CD) from classes with weak or balanced evolution. The classes with strong cloud development (cooling: "CD +", "CD ++", warming: "CD -", "CD --") depict the trend and magnitude of cloud development. The signs "+" and "-" stand for cooling and warming, respectively, whereas a duplication of the signs separates areas with moderate development (e. g. "CD +") from areas of strong development (e. g. "CD ++"). The classes "W" and "NE" are characterized by weak pixel evolution. The first class "W" (Weak) is characterized by weak temporal evolution with no major cooling/warming trends. The latter ("NE" = Non Evolving) represents a typical stratiform cloud top with cold count values, low pixel variability and a narrow histogram width. "NE" is the only class respecting the pixel variability and its magnitude, both supposed to be weak. The class "UC" (UnClassified) is assigned to subregions with count values lower than 100 or to subregions with no evolution and is rarely

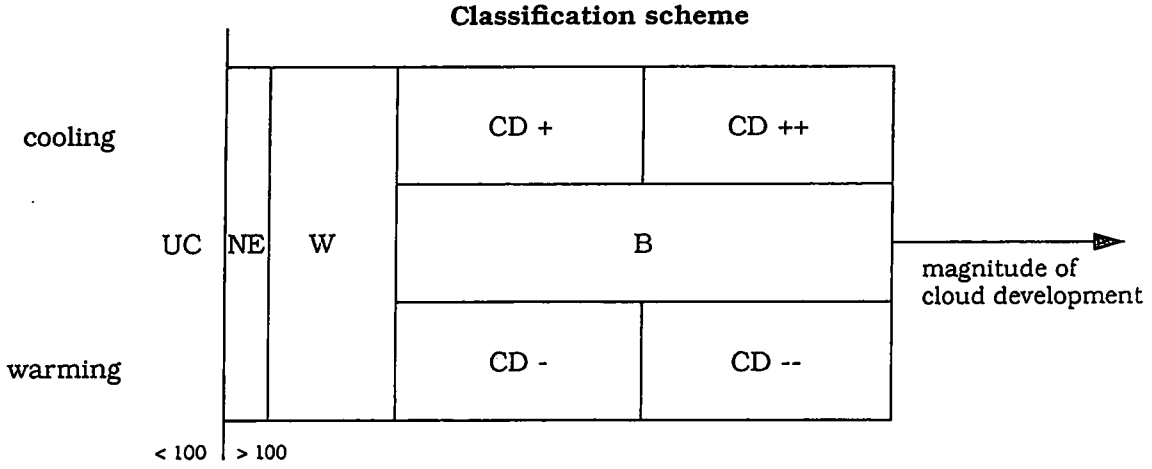

FIGURE 8-10. Classes used for the quantification of cloud development within the four subregions (cf. Figure 8-11) according to the abbreviations in Table 8-1. The magnitude of cloud development is derived from the intensity and number of cooling/warming pixels within each of these four subregions. Pixels warmer than the count threshold 100 are not analysed. For the empirical thresholds of each class refer to the Appendix.

used. Figures 8-11 a) - c) show the region of interest, the subdivision in four quadrants and the classification as result of the satellite-derived information. The figures provide examples of all classes listed in Table 8-1, except the class "unclassified" ("UC"). Since strong emphasis is put on the information from the pixel evolution, the colors representing the magnitude of evolution and the extension of evolving areas give a good impression of the characteristics of each single class.

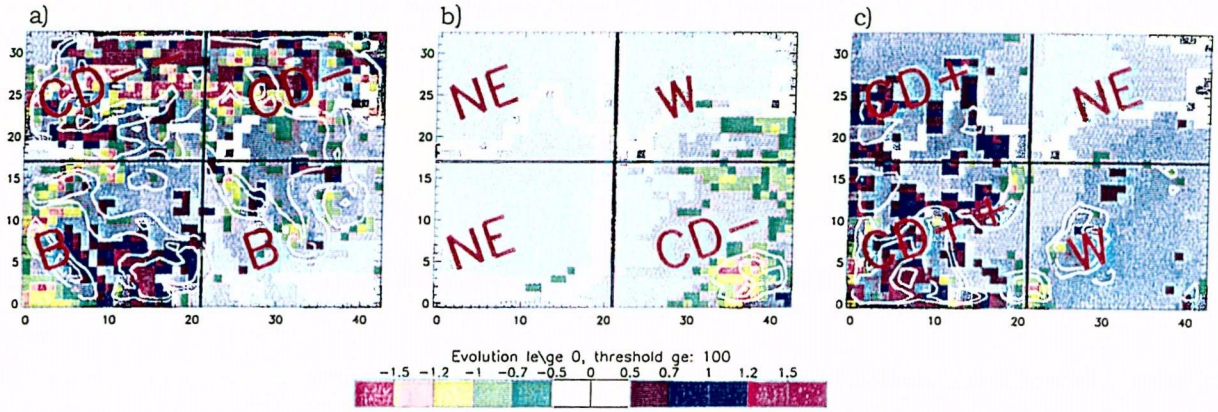

FIGURE 8-11. Examples of classification, infrared channel, a) 20.09., 02:45 UTC, b) 24.10., 12:30 UTC and c) 26.09., 11:50 UTC. The four quadrants are separated by a black line, the red letters within indicate the classification according to Table 8-1. For a description of signatures see Figure 8-1.

The classification results established for each timestep of a time series are summarized in overview figures over selected periods. These figures serve as major input for investigations concerning the life cycle of cloud systems in the LMTA aiming at a geographical localization of preferred areas of cloud evolution. In the next section these results are discussed.

8.4.1 Life cycles related to orography

One of the most pronounced feature is to observe the moving of areas of cloud development being transported over the Alps. As seen in the previous sections, strong cloud development in satellite imagery may occur during all types of precipitation derived from radar, being characterized as "deep convection", "embedded convection" or "stratiform" type. Of major interest is the question, whether during these precipitation types specific cloud development characteristics over longer periods are recognizable and where the preferred area of cloud development is located.

In many cases, the strong cloud development over the Po Valley gives evidence, that clouds are generated *before* they reach the southern slopes of the Alps. This implies that the clouds are produced over the Po Valley and move with the predominant airflow towards the Alps. While moving over the Alps the magnitude of cloud development is often decreasing indicating that over the Alps the intensity of cloud development is less than over the Po Valley.

The following Figure 8-12 summarizes the results of the class distribution of the three precipitation types with respect to cloud characteristics over long time sequences with 5-minute interval imagery. Figure 8-12 a) refers to embedded convection showing strong cloud evolution over the Po Valley with a maximum occurrence of the classes "CD+" and "CD++" in the lower left quadrant. The class "CD+" denotes the frequency maximum of class distribution with the peak frequency in all four subregions. Apart from the class "UC"

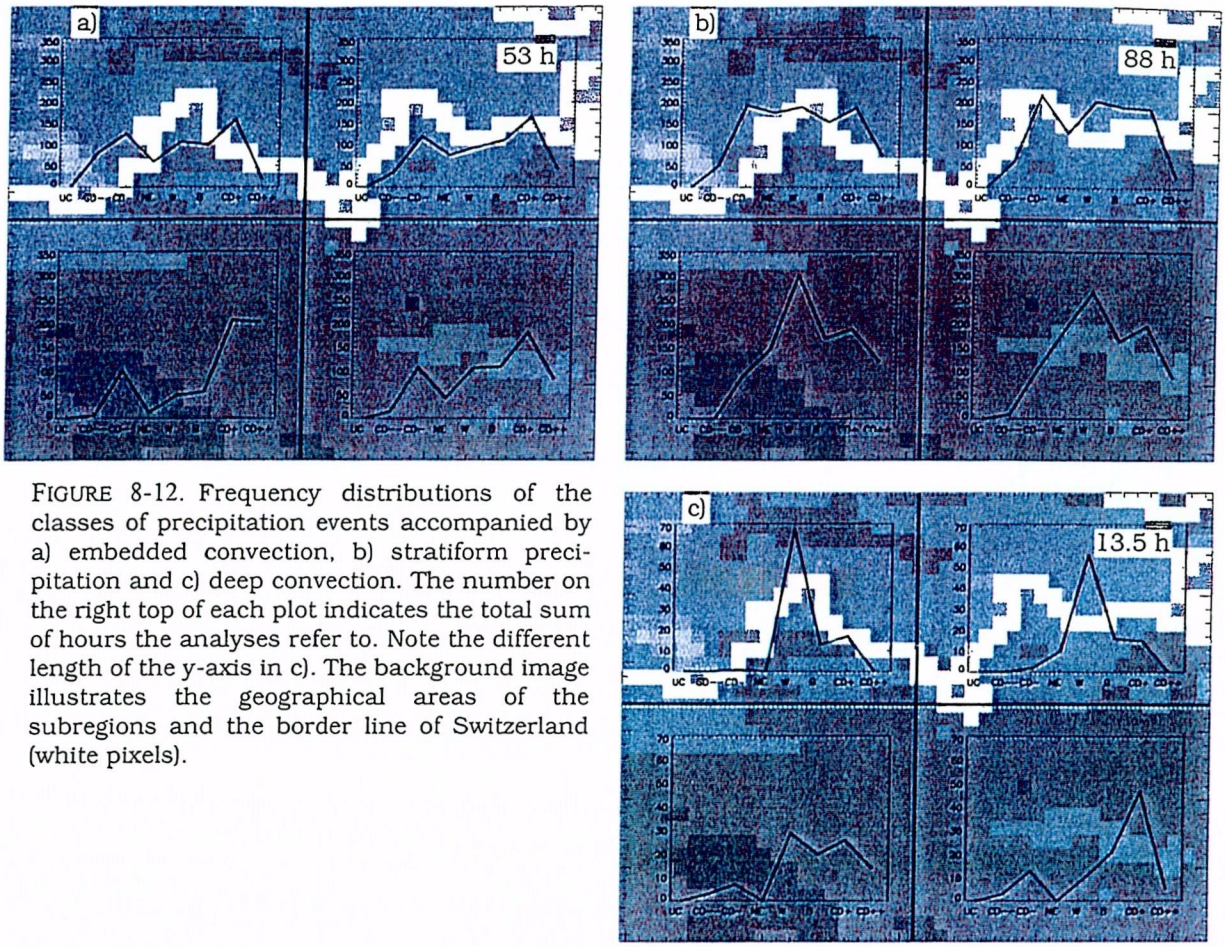

FIGURE 8-12. Frequency distributions of the classes of precipitation events accompanied by a) embedded convection, b) stratiform precipitation and c) deep convection. The number on the right top of each plot indicates the total sum of hours the analyses refer to. Note the different length of the y-axis in c). The background image illustrates the geographical areas of the subregions and the border line of Switzerland (white pixels).

(unclassified), the classes "NE" (non-evolving) and "CD--" (strong warming) are identified as minima in all quadrants. A total of 53 hours are included in the investigations.

Figure 8-12 b) depicts the result of 88.5 hours of cloudiness which is dominated by stratiform precipitation. Also here, the lower left quadrant manifests the highest frequency of classes related to strong cloud development, followed by the lower right and upper left quadrants. While the frequency distribution of quadrants located over the Alps show no predominance of a certain class, the class "W" standing for weak evolution dominates the lower quadrants. The different facets of cloudiness associated with stratiform precipitation is well underlined by the large variety of classes especially in the northern subregions located over the Alps. It is remarkable, that the class distributions tend to be similar over the Alps (upper two panels) and similar over the Po Valley (lower two panels). It might be argued, that the stratiform cloudiness experiences a modification while being transported over the Alps, thus as a result of the orography. However, cooling cloud development is observed over the two subregions located over the Alpine chain as well since evolving cloud areas are being transported over the Alps with the prevailing wind direction. In comparison to Figure 8-12 a) the classes of the cloudiness with stratiform cloudiness show a more frequent occurrence of the classes with weak or balanced cloud development. The class "CD++" is classified less frequent in the regions over the Po Valley confirming a less intensive cloud development of stratiform cases.

Figure 8-12 c) presents the classification results of the two precipitation events with deep convection. Since deep convection occurred only during short periods, the total sum of analysed hours is small (i. e. 13.5 hours) compared to the cases with embedded convection

(53 hours) and stratiform precipitation (88 hours). At first sight it becomes clear, that an inference from the class distribution to the presence of cloudiness related to deep convection is not possible. Strong cloud evolution is not observed in the four quadrants, though the lower right one is characterized by cooling cloud development. A problem arises by the fact, that the encountered MCSs are moving and may consequently drift over several quadrants affecting the classification results. Furthermore, the associated anvils are not recognized as convective areas and are rather classified as "W" (weak), "B" (balanced) or even "NE" (non-evolving). This accentuates the importance of object-oriented information on clouds related to deep convection, which is not included in the present classification scheme. During both analysed events the convective activity is mainly concentrated over the Po Valley where both subregions give hints of the occurrence of cloud development associated with cooling. The subregions over the Alps illustrate a predominance of the class "W" and are not affected by strong cooling cloud development.

It is evident, that the classification distributions give a general overview over the predominant classes of the varying precipitation type. Investigating one single event or even a few hours of it, the class distribution may vary significantly from the "climatological" results illustrated in Figure 8-12.

In summary, the automated classification enabled an analysis of cloudiness associated with different precipitation types identified by radar. In accordance to the results of the first three sections of this chapter, temporal and spatial characteristics of cloudiness integrated into a classification scheme do not allow a distinction of different types ("deep" and "embedded convection", "stratiform") like radar. The subdivision in four subregions helped to identify the areas of preferred cloud evolution. Especially with predominant south/southwesterly airflows of the investigated events it is clearly illustrated, that the main cloud evolution occurs over the Po Valley, *ahead* of the Alpine barrier. The lower left subregion is characterized by the presence of a high proportion of the classes "CD+" and "CD++" representing cooling cloud development. Within this subquadrant located to the southwest of the LMTA the preliminary generation or evolution of clouds occur in a precipitation-free environment which will result, while being transported, in precipitation over the LMTA. Therefore, the life cycle of precipitation systems hitting the LMTA initiate already over the Po Valley with the generation or evolution of clouds that will produce precipitation and convective activity over the orography. It is interesting to see, that this cloud development often takes place several tens of kilometers ahead of the south Alpine slopes and may be considered as an effect evoked by the orography (cf. Figures 8-13 and 8-14).

This is underlined by Figure 8-13 which shows a comparison between satellite and radar data and demonstrates the complementary character of the information of both systems. According to this figure, within the northern part of the Po Valley strong cloud development occurred *without* the generation of precipitation in a precipitation-free atmosphere as depicted by the satellite images. The localization of strong cloud development is lying to the

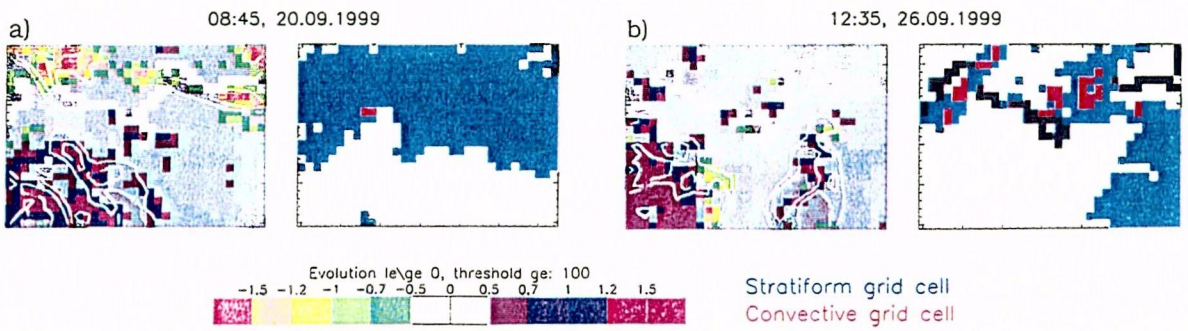

FIGURE 8-13. Analysed IR satellite images (left panel) and radar images (right panel) from a) 20.09. and b) 26.09.1999. In both cases, the prevailing wind direction was southwest. For a description of signatures see Figure 8-1.

southwest of the LMTA in accordance with the classification results of the lower left subregion in Figure 8-12. The radar data in Figure 8-13 provide evidence that the precipitation starts over the southern slopes of the Alps as a result of the clouds developed in the upstream area. In most cases associated with convection, the areas of convection are tied to orography over the southern slopes. This will be discussed in the next section. Further inferences from the classification results, e. g. the prevailing precipitation type, are speculative due to the limited capabilities of the classification scheme with respect to the identification of cloud development related to convective activity. The main benefit from the classification is the identification of the area of preferred cloud development. The preferred area of cloud development give hints at the influence of orography and the life cycles of precipitation systems. The insight gained by the automated classification helped to establish conceptual models which attempt to condense the information derived from satellite and radar.

The following Figure 8-14 summarizes two conceptual models of two different types of cloudiness associated with precipitation encountered during the MAP-SOP. Emphasis is put on the analysed signals from satellite and radar illustrating the complementary data character of both systems. Figure 8-14 a) illustrates the strong cloud evolution over the Po Valley as seen by satellite and the radar-detected area of convection within the precipitating area. In Figure 8-14 a) the atmosphere over the Po Valley is unstably stratified with strong cloud development observed in satellite images ahead of the Alps. The precipitation and the convection within detected by radar is located over the southern Alpine foothills.

In Figure 8-14 b) the airmasses over the Po Valley are stable with stratiform precipitation, and no convection is derived from radar data. The cloud tops are low and uniform with weak evolution being blocked by the Alpine chain. Only at the cloud borders along the southern foothills evolution can be observed in satellite images (cf. Figure 8-7 a), p. 74).

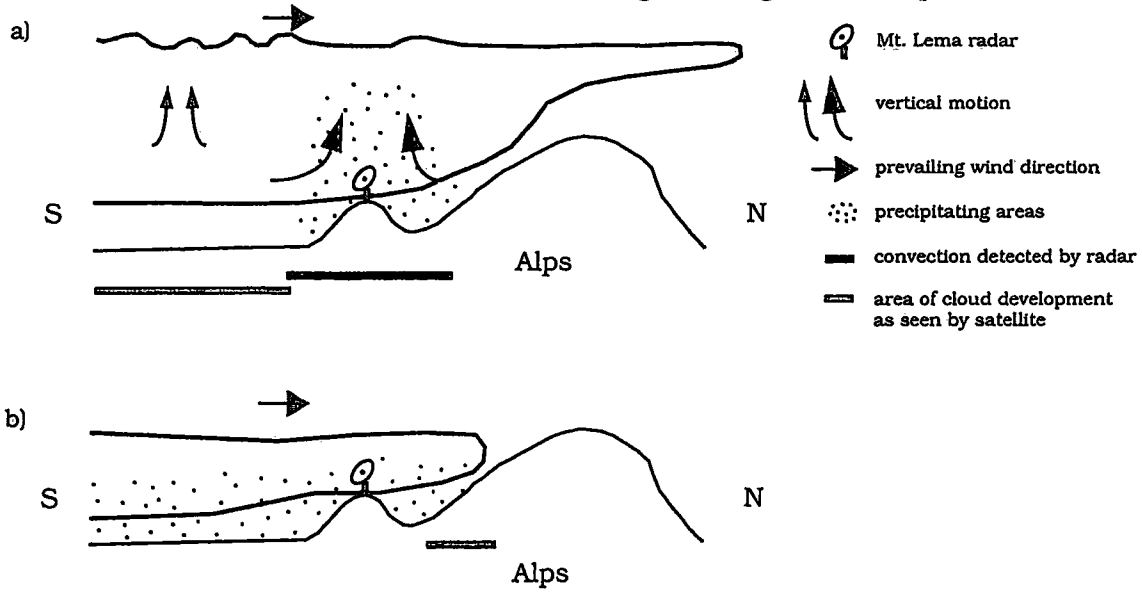

FIGURE 8-14. Two conceptual models summarizing information derived from satellite and radar for precipitation events on the southern side of the Alps. The figure depicts a cross-section from south to north across the Alps, cloud borders and precipitation are blue-colored, radar-detected convective areas are in red and regions of strong cloud development as seen by satellite are in grey color. In a) the stratification of airmass in the Po Valley is unstable in b) it is stable.

These two contrasting conceptual models result from the investigated precipitation events. Figure 8-14 a) shows the life cycle of precipitation systems with cloud generation/cloud development ahead of the Alps. The precipitation falling along the southern foothills of the

Alps is being developed already over the precipitation-free northern Po Valley where radar data is not available. On the other hand, Figure 8-14 b) presents the classical stratiform cloudiness with weak evolution at the cloud borders and smooth cloud tops. Further information on this type can be found in section 8.3 (p. 73). With these conceptual models of precipitation systems in the LMTA we conclude the exploitation of satellite data.

8.5 Radar

In contrast to many other satellite investigations, the present study includes the analysis of radar data for the validation of the results derived from satellite. The radar analyses provide numerous important facets of heavy precipitation events on the southern side of the Alps which help to complement the meteorological puzzle as depicted in Figure 1-1 (p. 11). In the analysed satellite imagery, evolving cloud systems move over the LMTA and shift with the prevailing wind direction. In contrast, precipitation in radar imagery in the Alpine region remains often geographically fixed over several hours, preferably along the southern slope of the Alps.

As pointed out in chapter 2, the precipitation potential of cloudiness being transported into the LMTA is influenced by the large scale setting of the synoptic wind field. The change of wind field affects the precipitation potential as demonstrated by IOP 6. During this IOP small precipitation amounts were registered in the LMTA due to the prevailing westerly airflow. All other IOPs were predominantly accompanied by winds from southwesterly to southeasterly directions. The following section tries to give some answers with respect to the location of convection as seen by radar and the associated wind fields.

8.5.1 Convection and its localization

The preferred locations of convection as identified by radar of events with "deep convection" and "embedded convection" are presented in Figure 8-15. The colored lines resume the preferred areas of convective activity in the LMTA depicting the frequency of classification as convective grid cell by radar during selected periods. Figure 8-15 a) shows the geographical

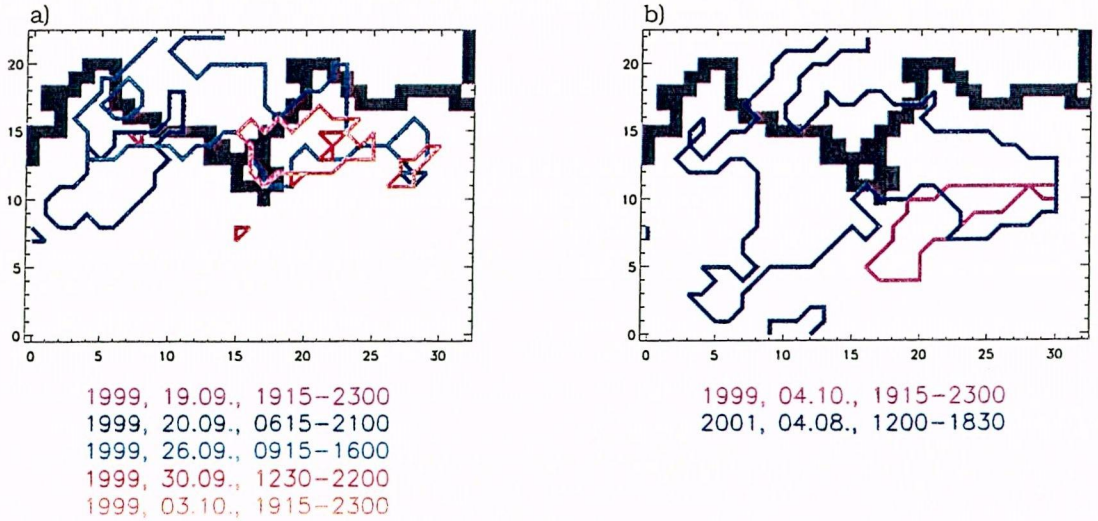

FIGURE 8-15. Preferred areas of convective activity as identified by radar interpolated on a IR Meteosat grid. Events with a) embedded convection as identified by radar and b) deep convection. The colored lines represent pixels which were classified at least 6 times as convective during the investigated period of each individual event indicated by color. Note that the analysed period of each event varies. The thick black line denotes the southern border line of Switzerland.

area of preferred locations of "embedded convective" activity. In most cases, these areas are located along the southern slopes of the Alps with exception to IOP 3 (26.09.) with convective activity extending into inneralpine regions. The convection during IOP 5 (03.10.) was concentrated on the eastern side of the Ticino, while the areas of convection at the beginning of IOP 2b (19.09.) and during IOP 4 (30.09.) show only small areas of preferred locations of convection. The characteristic of all IOPs with "embedded convection" is the remarkable connection to orography when compared to satellite data. During IOP 2b (20.09.) the area covered by convection lies mostly ahead of the south Alpine slopes due to the strong counterflow in the valleys (Steiner et al. 2000a and b and 2002). This counterflow, a consequence of evaporative cooling, relocated the area of convective activity away from the Alps into the Po Valley.

Figure 8-15 b) presents the main areas of convective activity associated with MCS. Apart from the southwest-northeast oriented band of convection during 04.08.2001 the convection was evoked by distinct cells characterized by a leading (convective) edge and a stratiform trailer. Compared to Figure 8-15 a) the location of convection is further south over the Po Valley. The location of convection in Figure 8-15 a) is quite consistent with the results of Frei and Schär (1998), Germann (2000) and Houze et al. (2001). They found that the area of most intense precipitation occurred over the southern slopes of the Alps rather than over the highest peaks over the Alpine chain which coincides with the preferred areas of convection found in the present study.

The following Figure 8-16 shows the dependency on the location of convective areas from the mesoscale airflow. All Figures 8-16 a) - d) show the frequency of occurrence of radar-defined convective grid cells during a 4 hours period compared to wind data as derived from radiosounding from Milano. In Figure 8-16 a) (20.09., IOP 2b) southeasterly winds in the lower atmosphere impinge on the southern flank of the mountains to the west of the Ticino and produce convection ahead of it. It may be concluded, that the location of convection in this case is the result of the relatively weak easterly winds at low levels, combined with the orography (steep slope) and the above-mentioned downvalley counterflow. In Figure 8-16 b) (26.09., IOP 3) a large southwest-northeast oriented line of convection is produced within a south-southwesterly airflow. Such "bands" are often observed with both types of precipitation, convective and stratiform, while animating analysed radar images with predominant southwesterly winds. The preferred location of convection in Figure 8-16 c) (30.09., IOP 4) is concentrated to the east with southwesterly flows aloft and has a rather small extension. In addition, the wind directions at 850 and 700 hPa have a more westerly component associated with a (stratiform) precipitation field moving from west to east over the LMTA. Comparing the preferred location of convection in Figure 8-16 d) (03.10., IOP 5) to Figure 8-16 c) it is evident, that the patterns of the grid cells classified as convective are similar. However, wind direction and wind speed at all height levels of Figure 8-16 d) resemble more the wind field characteristics of Figure 8-16 b). From these comparisons it becomes evident, that the preferred areas of convection in the LMTA may not be inferred from radiosounding data from Milano alone. The location of the convective grid cells in Figures 8-16 d) and b) differ completely despite the almost identical airflow. In Figure 8-16 d) the convection is limited to the areas lying to the east of the LMTA and no convection was observed in the west

From these investigations it is concluded, that the use of radiosounding data from Milano is of limited use for the determination of the areas of preferred convection in the LMTA. We assume that small scale effects like local wind fields which are not represented by radiosounding data from Milano interact with orography and determine the locations where convection is triggered. However, there is an increased probability of the occurrence of convection to the west of the LMTA in association with winds from southeasterly directions shown by Milano soundings. This statement is underlined not only during IOP 2b but also with former heavy precipitation events like the Brig case in 1993 and the Piemonte flood in

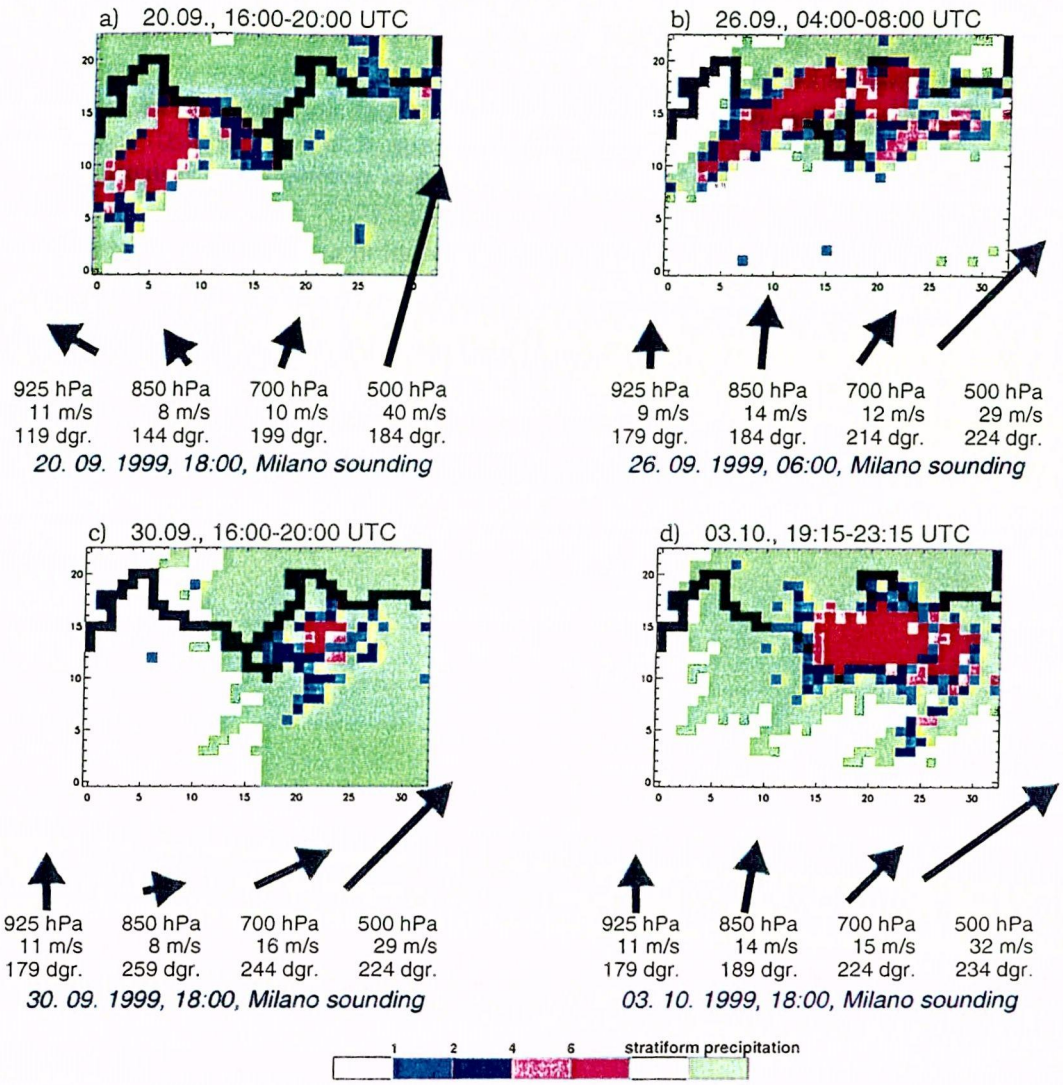

FIGURE 8-16. Frequency of occurrence of convective grid cells identified by the Mt. Lema radar over a 4 hours period in comparison with radiosounding data from Milano at different heights. a) 20.09., 16:00-20:00 UTC (IOP 2b), b) 26.09., 04:00-08:00 UTC (IOP 3), c) 30.09., 16:00-20:00 UTC (IOP 4), d) 03.10., 19:15-23:15 UTC (IOP 5). The stratiform precipitation areas are colored in light green, the black line depicts the southern border line of Switzerland. Note that the radiosounding data is centred within the 4 hours period, except in c).

1994 (Binder and Rossa, 1995). The events with deep convection (not shown) present both different wind fields with respect to locations of convective activity (cf. Figure 8-15b)). In common are the mainly weak winds at 925, 850 and 700 hPa, with a southwesterly wind aloft. Of course these two cases do not allow investigations concerning the determination of preferred areas of convection with the help of radiosounding data.

In summary, the following conclusions can be drawn from analyses of radar data:

- The events characterized by "embedded convection" exhibit geographical fixed radar echoes on the southern slopes of the Alps, with a predominant southwest-northeast orientation of the precipitation patterns. The convective activity is located mainly along the southern foothills of the Alps, towards the Alpine crest, the occurrence of convective activity decreases when approaching inneralpine areas.

- The events characterized by "deep convection" were accompanied by large cloud cells with a leading convective edge and a stratiform trailer, with the main convective activity located in the northern Po Valley.
- Localization of convection of the events with "embedded convection" showed a weak dependency from wind direction from Milano sounding. It is assumed, that small scale effects are relevant determining the preferred location of convection requiring data from the meso-β scale.

As pointed out in the previous sections, radar data complements the information derived from satellite providing additional insight into precipitation systems in a complex terrain like the Alps.

9 Conclusion

In this chapter, the major conclusions from the case studies summarized in the previous chapter are discussed. According to section 1.3 (p. 17), the overall aim of this study is to gain *additional information on heavy precipitation events observed during the MAP-SOP* with the help of data from the geostationary satellite Meteosat-6. The established pixel-based methods combine spatial (pixel variability) and temporal (pixel evolution) information and use non-calibrated pixel data as input. As a consequence thereof, the methods concentrate on the analyses of relative differences in pixel characteristics and are not based on absolute thresholds.

In the first two sections, the results of the climatological studies and the main benefits from the high temporal resolution of the satellite data are briefly pointed out. After a discussion of the results regarding the identification of convection by satellite and the radar-based investigations, the chapter concludes with personal views of the potential of the new generation of geostationary satellite systems.

9.1 Some key ingredients for heavy precipitation

Investigations of the occurrence of heavy precipitation on the south side of the Alps from 1961-2001 reveal, that there is a clear frequency maximum in autumn and a secondary maximum in spring. The sum of observations of heavy precipitation is subject to a large year-to-year variability as shown in Figure 1-4 (p. 15), confirming the tendency towards a frequency increase starting in 1976.

The ensemble of past events with heavy precipitation and cases which occurred during the MAP-SOP show similar characteristics with respect to the synoptic and mesoscale flow setting leading to strong precipitation on the southern side of the Alps. Some key ingredients for the occurrence of heavy precipitation are listed in section 2.1.2 (p. 22). Despite the similarity in the synoptic setting of the large scale flow of these events, differences are observed in terms of specific mesoscale environment they occurred in. Especially over complex terrain the probability is increased, that small scale meso-β phenomena like winds in a single valley influence effectively the specific character of an overall precipitation event by determining e. g. the location of convection. Therefore, the aforementioned similarity must be considered with caution as long as the influences of small scale effects are not fully understood.

The mesoscale flow setting is investigated with the help of long-term radiosounding data from Milano. The results show a veering of the wind with height in the warm conveyor belt ahead of the cold front, confirming the conceptual model of Kappenberger and Kerkmann (1997). The radiosounding data show further, that the mean wind direction and wind speed of the selected pre-SOP and SOP cases are in accordance with the long-term radiosounding climatology.

9.2 Rapid scan data: a general gain in information

The availability of rapid scan imagery has provided a unique way to monitor cloud evolution associated with heavy precipitation in complex terrain. For investigations of short-term atmospheric processes like the generation of convection related to orography the continuous availability of satellite imagery with high temporal resolution is of great support. The high temporal resolution of the rapid scan imagery compensates at least partially the moderate horizontal resolution of the geostationary satellite. Though it is difficult to give a quantitative measure of the information gained by rapid scan imagery there are mainly two aspects. These two aspects underline the advantage of the 5-minute interval imagery compared to 30-

minute interval imagery, which are in operational use today. The high-temporal resolution allows for:

- the detection/observation of fast evolving convective clouds
- tracking of cloud patterns in complex terrain

Satellite imagery can be used for the detection of areas with rapidly evolving deep convection. As shown in the present work, supplemental information from satellite data of high temporal resolution allows a continuous observation of convective systems from the very beginning of their life cycle. The attribution of a stage of a life cycle to an observed system is of major interest for forecasting and warning purposes.

As a direct benefit from the high temporal resolution of satellite imagery the introduced PCC tracking algorithm allowed the analyses of cloud pattern evolution in complex terrain. In the present study tracking is used for the extraction of the magnitude of cloud development because tracking reduces the earth-relative motion of observed cloud systems. With the PCC technique, based on texture information, it is possible to determine the temporal evolution of a limited pixel area during a 10-minute period. The implemented tracking algorithm accounts for different speeds of cloud propagation, including stationary effects like the triggering of convection at a fixed geographical spot. The high temporal resolution of satellite imagery permitted a tracking technique and corresponding results, which could not be achieved with the currently operational resolution of 30 minutes. The tracking technique used and the results of sensitivity studies are described in chapter 6.

A further benefit from rapid scan images not investigated in the present study would be the satellite-based derivation of cloud winds. Purdom (1996) demonstrates the potential of rapid scan imagery for the derivation of cloud motion winds resulting in more accurate cloud drifts with the help of high temporal resolution. However, orography may greatly disturb such a procedure, since air and cloud motion may not correspond over mountainous areas (e. g. lee-wave clouds).

9.3 The discrimination of convective and stratiform regions

One of the main foci of the present study has been to examine whether cloud top structures provide characteristics allowing a differentiation between convective and stratiform cloud areas. Initially it was supposed, that convection in the rapid scans exhibits a distinct temporal evolution and high pixel variances due to strong up- and downdrafts within the clouds. In contrast, stratiform cloud regions were thought to possess a weak cloud development and a smooth cloud top.

The results reveal, that an unambiguous identification of convective regions by satellite is restricted to the occurrence of deep convection. The major advantage of cloudiness containing deep convection are the well-developed cloud shapes facilitating the recognition of convective areas. The localization of convection is possible during a very limited period within the life cycle of a deep convective system, since the region of convective activity is rapidly hidden by the generation of an anvil. Before anvil generation, the convective region is characterized by strong cooling of the cloud top within areas of high pixel variability. After the generation of an anvil, the cloud development signals are concentrated at the border of the isolated cell exhibiting strong cooling while, according to radar data, convection occurs within a limited region of the MCS. At this stage of life cycle, the geographical coincidence of convective radar echoes and strong cloud development is no longer true and the use of the satellite-derived information as indicator for the location of convection is not sufficient.

In contrast to deep convection, cloudiness containing radar-detected embedded convection or radar-detected stratiform precipitation lacks of typical temporal and spatial cloud top characteristics. The distinct cloud shape which allowed an unambiguous identification of areas with deep convection is not observed with the occurrence of embedded convection.

From the investigations it must be concluded, that the phenomenon "embedded convection" is in most cases too weak to evoke temporal and spatial cloud top characteristics. The appearance of cloudiness with radar-detected stratiform precipitation is manifold and comprises a wide range of cloud characteristics. Though stratiform cloudiness with weak evolution and smooth cloud tops are encountered, no criteria could be defined which permitted a general identification of cloudiness with stratiform precipitation as seen by radar.

In contrast to other satellite studies, no fixed count threshold is used for the detection of convective activity within clouds. This lack of an absolute threshold involved the analysis of warmer pixel areas without restricting the analysis to cold cloudiness. The inclusion of warm pixels accounts for the detection of potential embedded convective activity which is weaker in terms of intensity compared to deep convective systems. Furthermore, convective cloud areas might be recognized in their initial stage of development. However, the distinction between cooling signals of cloud evolution associated with convective and non-convective processes is not explicit. Often, stratiform regions identified by radar may exhibit strong cooling areas in satellite images. On the other hand, cloudiness containing convection derived from radar may exhibit a smooth cloud top with weak development since convection is hidden by the anvil. As a consequence, regions of strong cooling cloud development as seen in satellite images *may* contain convective activity but it remains open to what extent the cooling signals are related to convection. Therefore, to infer temporal and spatial characteristics of cloud top structures from the prevailing precipitation type (i. e. convective or stratiform) is not possible. The methods used in the present study do not allow a separation between convective and stratiform areas, but a differentiation between regions with strong or weak cloud evolution.

It is important to note, that the detection of convective areas by conventional weather radar is limited to regions with precipitation. In a non-precipitating atmosphere a distinction between convective and stratiform cloud evolution is not possible by means of radar observations. To regard regions with strong cloud development in a non-precipitating atmosphere as convective areas may also be wrong since cloud development in an environment without precipitation may be caused by a slanted uplift of airmasses. Therefore an unambiguous identification of convective areas not exhibiting characteristic cloud shapes like deep convective systems could not be achieved. For the verification of satellite-based hypotheses in a precipitation-free atmosphere supplemental data are required (e. g. numerical model output).

Furthermore, the limited potential of brightness temperature/count thresholds as the only discriminator between convective and stratiform cloud regions is demonstrated. Convection is not restricted to cold cloud areas, whereas cold clouds are not necessarily accompanied by convection. Brightness temperature or count thresholds for the detection of convection can be used with the occurrence of deep convective systems, where the associated distinct cloud shapes provide the required additional information for the recognition of convective systems.

Comparing satellite and radar data, different characterizations result from both information sources. While the satellite derives cloud top characteristics from space, radar detects precipitation within and below clouds. The different locations and sensitivities of the instruments result in different views and characterizations of heavy precipitation events. For instance, the classification subdividing the MAP-SOP heavy precipitation events in cases with "embedded convection", "deep convection" and "stratiform" characteristics relies on information derived from radar. While areas with "deep convection" can be recognized by characteristic cloud shapes, cloudiness with "embedded convection" or "stratiform precipitation" are not distinguishable by satellite data.

It is one of the major findings of this study, that in several cases being classified as stratiform by radar, strong cloud development is observed in satellite imagery. The strong cloud development detected in satellite imagery emphasizes that some of the precipitation events

classified as stratiform by radar are accompanied by strong cloud generation and strong cloud development in a precipitation-free atmosphere. In some cases, the strong cloud development is underlined by radiosounding data from Milano, exhibiting an unstably stratified atmosphere. The classical scheme of stratiform cloudiness with a smooth cloud top and weak evolution is only partly encountered. The analyses of satellite data do not confirm the classical schemes of cloudiness associated with convective and stratiform precipitation as derived from radar and do not allow a systematic separation between the two.

The fact that strong cloud development occurs together with stratiform precipitation accentuates the complementary character of the information derived from satellite and radar data. It must be assumed that significant vertical motion within the atmosphere, related to an unknown extent to convection without the generation of precipitation, occurs also in cloud areas characterized as "stratiform" by radar.

9.4 Quantification of cloud development and life cycle

Meteorological processes like convection triggered by orography and the related life cycle of convective systems are of primary importance for fore- and nowcasting purposes. The goal of investigating life cycles of precipitation systems is achieved by the quantification of cloud development. Instead of quantifying the convective activity within a cloud system as initially intended, the magnitude of cloud development - independently from the presence of convection - is quantified. As main classification input served the intensity of cloud evolution. In addition histograms, spatial pixel variability and count maxima are used as criteria. The classification is established for each image of a rapid scan sequence.

Four subregions centred over the LMTA were defined to account for different geographical areas, two located over the northern Po Valley and two over the Alpine region. The subdivision allows a regional analyses of the magnitude of cloud development what is advantageous in a complex terrain like the Alps. A drawback of the geographical partitioning in subregions is, that in many cases the classification of the analysed signals refers to fractions of cloudiness of a whole frontal cloud system. Signals evoked by larger cloud systems may appear in more than one subregion and clouds are not recognized as entities. A recognition of clouds as entities presumes a classification technique treating the various clouds as objects. Especially for the identification of deep convective systems the distinct cloud top structures can be used as input for an object-oriented classification. This additional information on cloud structures is not included in the present classification scheme. The frequency distributions of the classes allow the localization of the preferred areas of cloud development over the Po Valley but a systematic derivation of cloudiness associated either with "deep convection", "embedded convection" and "stratiform precipitation" is not possible.

The applied classification scheme is based on empirical thresholds which help to separate the different classes. As pointed out in section 4.1 (p. 37) the use of thresholds involve the risk of missing relevant information for the classification. The results of the classification depend on whether the predefined empirical thresholds are exceeded or not. Already small differences in the input data may result in different classifications. Despite that, we suppose to have included the relevant information in the classification scheme. The classification results can be easily verified by visual inspection of the analysed images with the main input parameter of the classification, the evolving pixel areas and their magnitudes.

It is likely, that the classification results are, at least to some extent, related to the atmospheric stability. During several IOPs, moderate and strong evolution could be attributed to unstable airmasses with a predominance of the classes "CD +" and "CD ++". In contrast, classes like "NE" and "W" represent cloudiness in a more stable atmosphere with weak evolution. However, no systematic conclusions can be drawn from the magnitude of cloud development with respect to the stability of the atmosphere as shown by IOP 2b.

During this case, weak cloud development was observed though the atmosphere was unstably stratified.

In summary, the results of the automated quantification of cloud development localize the preferred area of cloud development over the northern Po Valley ahead of the Alpine barrier. Especially in the subregion lying to the southwest of the LMTA strong cloud development occurred during IOPs characterized by "embedded convection" and by "stratiform precipitation" (radar classification). The cloud development in this subregion is an upstream effect induced by the Alps and highlights the life cycle of clouds related to orography. Apart from cases where cloudiness is being advected from south, this area represents the initial stage during a life cycle of a precipitation system affecting the LMTA. Thus, we observe by satellite the generation and/or development of clouds which result in precipitation over the LMTA.

9.5 Radar

Most satellite studies lack of an independent information source used for the verification of satellite-based hypotheses. The results of this work provide evidence, that data from additional meteorological instruments like the radar give insight into mechanisms of heavy precipitation and complement satellite-derived information. Sensitive to precipitation, the Mt. Lema radar provides important results concerning the predominant precipitation type separating convective and stratiform precipitation patterns over a complex terrain like the Alps. The significance of independent data for verification of satellite-based results is underlined when focusing the results from the two investigated deep convection cases. Both cases showed MCSs associated with a leading line of convective precipitation trailed by a stratiform region. Compared to the cloud shield area, only a small part is covered by convective precipitation demonstrating the small area covered by convection in a mature system[10].

Furthermore, radar data provided interesting information with respect to the preferred location of convection and patterns of stratiform precipitation. In many cases, both were tied to orography and showed in association with the predominant southwesterly winds southwesterly-northeasterly oriented rainbands. The dependency of the preferred areas of convection on the mesoscale flow setting was investigated with radiosounding data from Milano. The results showed no dependency from the wind field from the Milano sounding and it must be concluded, that the location of convection is driven locally and can not be inferred from radiosounding data from Milano. However, only a small number of events were investigated, constituting a major limitation for the interpretation of these results.

The use of radar data from a height interval between 4.5 and 5.5 km is twofold. On the one hand, ground clutter occurs only, if ever, at long distance from the radar, on the other hand it is possible that relevant information from regions below the analysed height level might be missed. For instance Houze (2001) found, that the convective radar echoes occurring during the IOPs 2b, 3, and 5 were characterized by maximum reflectivity at low altitudes, especially over peaks and ridges in the lower windward regions of the Alpine barrier. As a reference height, the elevation of mountain peaks in the region of Locarno-Monti rise up to 2.4 km, i. e. below the lower limit (4.5 km) of the analysed interval. Further, the radar data was interpolated on Meteosat grid cells representing either the spatial resolution of the infrared or visible image grid. By the interpolation the radar data was degraded resulting in a loss of information. Despite the restrictions concerning the height level of occurrence of convection and the degradation in spatial resolution we suppose to have seized all relevant convective regions, as visual inspection with non-interpolated radar data confirms.

---

[10] Houze (1993) found that in tropical MCSs the convective area is only 10 % of the precipitation area.

In summary, the analyses of radar data provide insight into precipitation characteristics which could not be derived from satellite data alone. This additional source of information is regarded in the present study as necessity, especially for the investigations of phenomena occurring at the meso-β scale like the embedded convection. Data from both systems (i. e. satellite and radar) complement each other and the information derived from one instrument is not capable of substituting the information derived from the other. Radar is regarded as an optimal instrument for the detection of convection in precipitation. As previously mentioned in sections 9.3 (p. 88) and 9.4 (p. 90) the evaluation of radar information is restricted to precipitation areas since strong cloud development occurs in a precipitation-free environment. As a consequence, the satellite-based hypotheses on convective and non-convective regions from non-precipitating areas remained unverified. Despite the complementary character of the information of both systems, the radar provided an excellent data set for the verification of satellite-based hypotheses. It is likely, that without the radar information, different conclusions would have been drawn only from satellite data. Especially for investigations on the mesoscale, complementary information from different measuring systems are required helping to understand complex processes over complex terrain.

9.6 Methodological limitations

There are four limitations to the capabilities of the presented satellite-based methods and the associated results, listed in descending order of importance:

- The relation between the temporal and spatial characteristics of the investigated meteorological phenomena and the physical properties of the satellite and radar data is a limiting factor.
- The verification of satellite-based hypotheses by radar is restricted to precipitating areas.
- The cooling or warming evolution signals, caused by the advection of the cloud systems, may not be completely eliminated by the tracking algorithm.
- The areas of cloud development as seen in satellite images might be hidden due to the presence of high cloudiness.

The challenging task of finding characteristic cloud top structures evoked by meso-β scale phenomena is strongly dependent on the spatial resolution of the satellite imagery. A limited intensity and horizontal extent of phenomena like embedded convection searched for in satellite imagery require instruments being capable of seizing small scale cloud top structures. As schematically depicted in Figure 2-5 (p. 26), the vertical and horizontal extent of the convective region is limited resulting, as shown in section 8.2 (p. 70), in weak signals at the cloud tops. It is assumed that the poor coincidence of convective regions derived from satellite and from radar are due to the limited spatial resolution of the satellite data. Especially data from the infrared channel has moderate spatial resolution (midlatitudes: 1 pixel corresponds ~ 5 km x 8 km) which is obviously to coarse to permit the recognition of cloud top structures associated with embedded convection. The visible channel offers a better spatial resolution (midlatitudes: 1 pixel corresponds ~ 2.5 km x 4 km) but is restricted to daytime. In contrast to the satellite data, radar has a high spatial resolution and was interpolated to infrared and visible Meteosat grids. Despite the degradation in spatial resolution caused by the interpolation, radar is regarded as the optimal instrument for the identification of convective regions within precipitation. Therefore, the limitations regarding the spatial resolution of the used instruments in the present study, radar and satellite, result from instrumental properties of the latter.

The restriction of verification of the satellite-based assumptions by radar to areas containing precipitation is another important methodological limitation. As pointed out in the sections 8.2 (p. 70) and 8.3 (p. 73), the "classical" (embedded) convective and stratiform cloud characteristics could not be confirmed preventing a separation between the two cloud types.

Remarkable is the strong cloud evolution over the Po Valley, associated with both, stratiform and convective cloud regions. It is hypothesised that within the area of the Po Valley convection occurs initializing the generation of clouds in a precipitation-free environment. Since this evolution occurs in most cases without the generation of precipitation, no verification by means of radar is possible. It is conceivable that this gap of knowledge could be filled either by radar which is sensitive to cloud particles or by data from numerical models.

The tracking algorithm in the present study was implemented since it is regarded as a methodological prerequisite for the extraction of signals evoked by cloud evolution (cf. section 4.4, p. 39). Despite accounting for effects resulting from a complex terrain like the Alps, the tracking algorithm does not completely eliminate signals caused by the motion of the analysed cloud system, but reduces them significantly. Therefore, tracking errors can not be completely excluded and affect the result of the calculation of cloud development of the analysed target pattern. These errors are most likely due to target mismatching between two consecutive images. Possible tracking errors can be identified by animating satellite imagery with development signals (warming or cooling). The calculated development signals may change sign within a short interval of 10 minutes from a strong warming to a strong cooling area and vice versa. Such kind of change is observed with single pixels but also with larger pixel areas. Rapid changes of warming and cooling of larger cloud areas within such a short period is not feasible in reality. Such an inconsistency in time of the development signals give a hint about possible effects caused by tracking errors.

High and thick cloudiness in satellite imagery prevents from the detection of evolving cloud areas subject to evolution. An example is provided by IOP 2b, where convection derived from radar occurred below the cold and smooth cloud top seen in satellite imagery. However considering all investigated events, the shielding effects caused by the presence of high and thick cloudiness are supposed to play an inferior role. High cloudiness can be recognized easily while animating visible imagery at high temporal resolution and did not occur often.

10 Final remarks

As pointed out in the previous section, the current limitations for the use of geostationary satellite data for research purposes on the meso-β scale result from the spatial and spectral resolution of Meteosat-6. As shown, meteorological phenomena like the occurrence of "embedded convection" can not be inferred from Meteosat-6 data systematically. For investigations of small-scale features like the "embedded convection" the importance of the spatial and spectral resolution of the satellite system increases.

The initially defined challenges of the present study allow rather specific than general answers since the nature of cloudiness associated with heavy precipitation events and their characteristics is versatile and complex and does not permit generality. The gained results can be considered as a bundle of aspects which contribute individually to complement a complex puzzle illustrating a phenomena like heavy precipitation (cf. Figure 1-1, p. 11).

In most of the investigated cases, the coincidence of convective regions detected by radar and regions with high temporal evolution seen by satellite is poor or restricted to a limited period in time. As a consequence, the potential use of rapid scan data for nowcasting purposes of weak convective activity is limited. However, the use of rapid scans for the detection of regions of strong cloud development may be of primary interest for a forecaster especially in a precipitation-free atmosphere where no radar observations are available.

As pointed out in section 9.2 (p. 87) one of the main benefits from rapid scan images is the potential for the early detection of deep convective systems. With the help of distinct cloud shapes, areas with deep convection can be recognized *before* the generation of precipitation.

i. e. before a possible detection by radar. Moreover, with the help of tracking, the magnitude of cloud development between two consecutive images can be calculated. Of course, for the operational use of such kind of information an immediate operational availability of rapid scan data is required to allow a fast data processing. Collier and Lilley (1994) noted a time lag of one or two hours between the onset of cloud-top temperature decrease of large thunderstorms and the subsequent increase in of maximum precipitation rate as recorded by radar. This may show the potential of a combined use of satellite and radar data on the meso-β scale. The combination of both kind of instruments, satellite and radar, both being further developed, is considered as a great means for now- and forecasting purposes now and in future.

Seeking for an answer concerning the necessary requirements allowing the detection of small-scale phenomena by satellite three aspects need to be mentioned:

- enhanced spatial resolution;
- enhanced temporal resolution;
- enhanced spectral resolution.

These requirements will be met by future geostationary satellites - like Meteosat Second Generation (MSG) - the successor of the current operational Meteosat-7. According to EUMETSAT, the MSG will be launched in mid 2002 and is expected to run operationally from the beginning of 2003. Currently, parallel operations of Meteosat-7 and the MSG system are planned until at least the end of 2003. The successful rapid scanning of Meteosat-6 during the MAP-SOP initiated the introduction of an operational rapid scanning service that will probably last at least until the end of 2003 (Image, 2001).

With the MSG the operational availability of images changes from 30 to 15 minutes which is considered as a big improvement. In addition, MSG has the capability of providing data of limited scans of any predefined area and the temporal resolution of the imagery will be proportional to the number of scan lines (www.eumetsat.de). It is conceivable to establish a PCC tracking mode as presented in the current study fitting the demands of 15-minute interval imagery. The adaptations of the present tracking software for imagery with a temporal resolution of 15-minute interval is straightforward.

The higher spatial resolution of MSG (IR: 3 km, VIS: 1 km) will favour further examinations of small-scale phenomena being related to orography. Further, MSG will provide multispectral data of 12 channels and will offer unique possibilities to gain insight into microphysical precipitation processes. Microphysical structures permit a quantitative measure of cloud properties like radii of cloud particles and can be directly related to physical processes. With the help of these microphysical measurements the relevance to the precipitation potential of clouds may be retrieved (e. g. Levizzani et al., 1999). Rosenfeld and Lensky (1998) inferred microphysical characteristics of precipitation forming processes of continental and maritime convective clouds from NOAA AVHRR imagery.

Despite the bright future in satellite meteorology it will be always advantageous to complement satellite data with additional datasets like radar or other supplemental information on a phenomenon to be investigated. Referring to the present study, meteorological phenomena occurring on the small-scale require data from a corresponding scale. Especially over complex terrain like the Alps, small-scale processes may modify expected destinations of convection in a still unknown matter. Therefore, the knowledge of these processes has to be increased complementing the existing. For that purpose, meteorological field experiments like MAP are a necessity for a steady progress on the path of meteorological science.

APPENDIX

A. MAP IOPs: an overview

TABLE A. IOP duration and rapid scanning operations during the MAP-SOP (after Hanson et al., 2000). The missing images due to the eclipse period are not listed.

IOP	IOP start	IOP end	Rapid scan imaging start	Rapid scan imaging end	Scan duration [h]
1	15.09., 00:00	16.09., 06:00	-	-	-
2a	17.09., 12:00	19.09., 00:00	18.09., 02:00	18.09., 22:00	21
2b	19.09., 00:00	21.09., 00:00	19.09., 18:00	20.09., 21:00	27
3	24.09., 10:00	27.09., 00:00	25.09., 15:00	26.09., 17:00	26
4	30.09., 00:00	01.10., 18:00	18.09., 02:00	01.10., 12:00	24
5	02.10., 00:00	05.10., 06:00	03.10., 19:30	04.10., 22:00	26.5
6	24.09., 10:00	14.10., 00:00	13.10., 02:00	13.10., 23:00	21
7	17.10., 12:00	19.10., 00:00	17.10., 18:00	19.10.,00:00	30
8	20.10., 00:00	22.10., 06:00	20.10., 06:00	22.10., 06:00	48
9	22.10., 18:00	24.10., 00:00	23.10., 00:00	23.10., 22:00	22
10	24.10., 00:00	25.10., 18:00	24.10., 12:00 25.10., 06:00	24.10., 18:00 26.10., 00:00	6 18
11	26.10., 12:00	27.10., 18:00	26.10., 18:00	27.10., 18:00	24
12	29.10., 12:00	31.10., 00:00	29.10., 18:00	30.10., 18:00	24
13	01.11., 12:00	03.11., 00:00	02.11., 00:00	02.11., 18:00	18
14	02.11., 18:00	05.11., 00:00	-	-	-
15	05.11., 00:00	10.11., 00:00	06.11., 00:00 08.11., 06:00	07.11., 18:00 08.11., 06:00	42 36
16	11.11., 12:00	14.11., 00:00	11.11., 12:00 13.11., 06:00	12.11., 18:00 13.11., 18:00	30 12
17	15.11., 00:00	16.11., 00:00	15.11., 00:00	16.11., 00:00	24
					479.5

B. Quantification of satellite derived information

In the following, the input parameters for all 8 classes are listed as referred to in section 8.4, p. 77. The criteria used for the classification base on empirical thresholds. The criteria comprehend information on the grey value distribution (i. e. width of histogram and mean), the number and magnitude of cloud development (warming or cooling) and the pixel variability within each subregion as presented in Figure 8-11, p. 79. The following figures present the characteristics of each class and depict:

a) the analysed subregion with the corresponding evolution signals (colored pixels), the areas of high pixel variability (thin white lines) and the result of the classification written with red colored letters (i. e. "CD++" etc.).

b) the greyvalue distribution of the subregion as derived from the original satellite image with the vertical red line marking the mean greyvalue.

c) the number of cooling and warming pixels of each cooling/warming class according to the classes of the legend indicating the magnitude of cooling/warming.

d) cooling and warming pixels within each class of the legend (x-axis) and the pixel greyvalue variability within 3 x 3 arrays around these pixels (y-axis). Note the different lengths of the y-axes.

25.09.1999, 22:30 UTC: "**CD ++**"

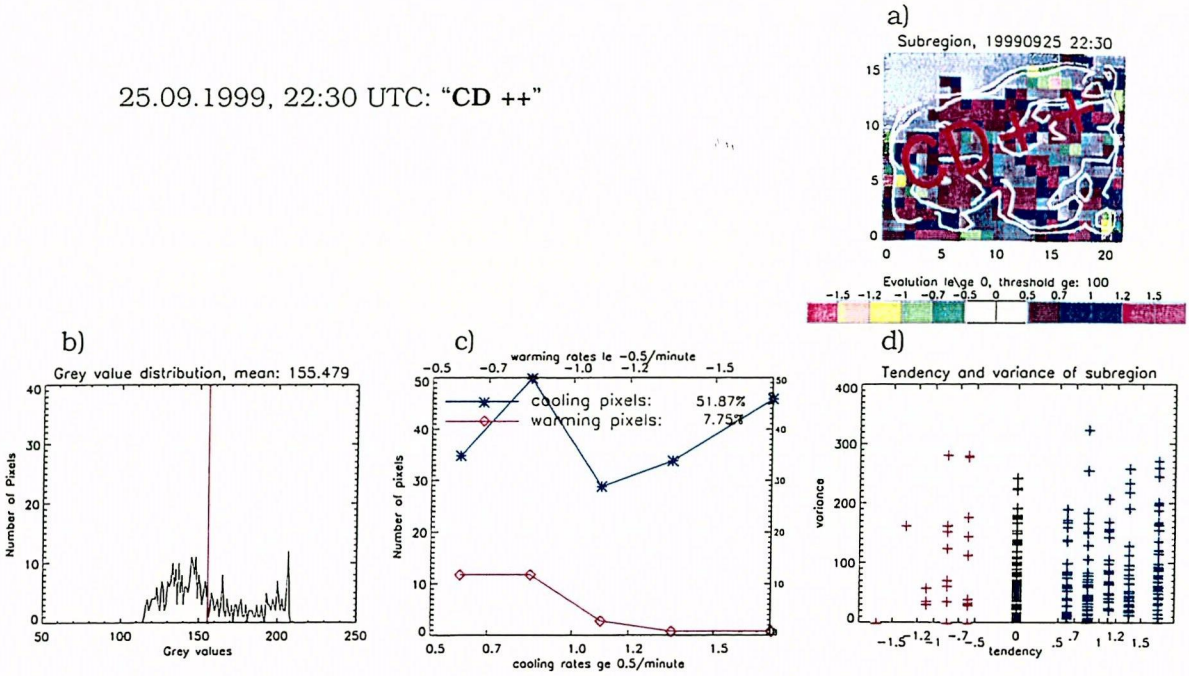

20.09.1999, 16:55 UTC: "**CD +**"

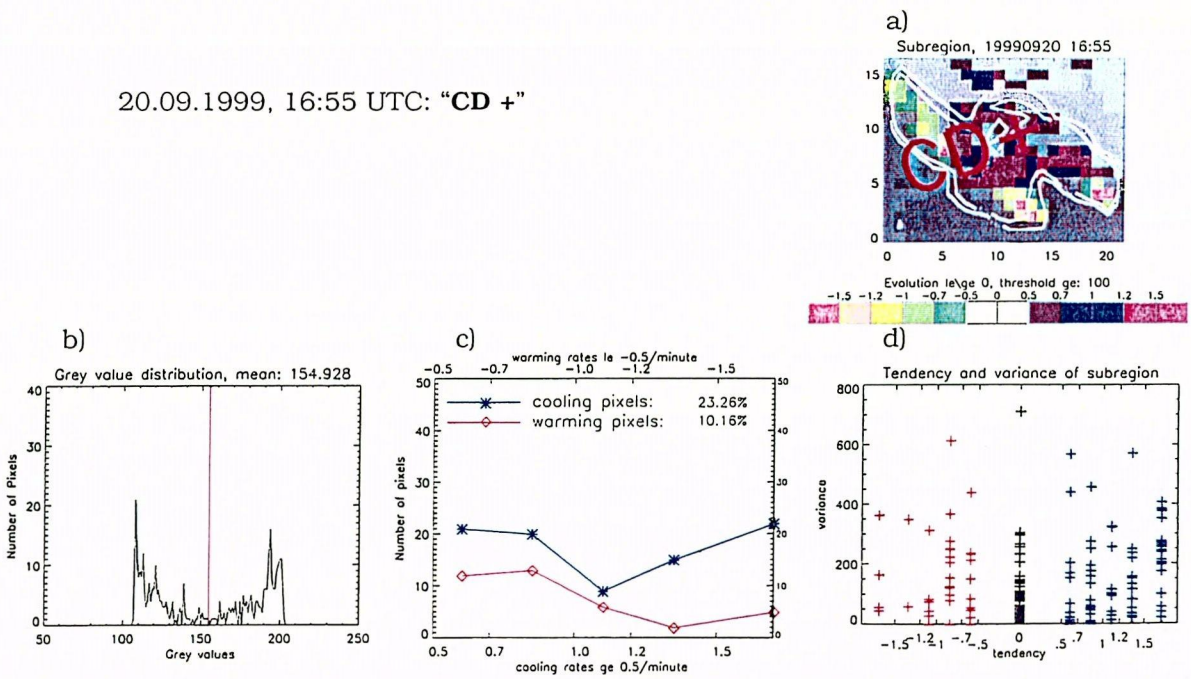

25.09.1999, 18:40 UTC: "**CD --**"

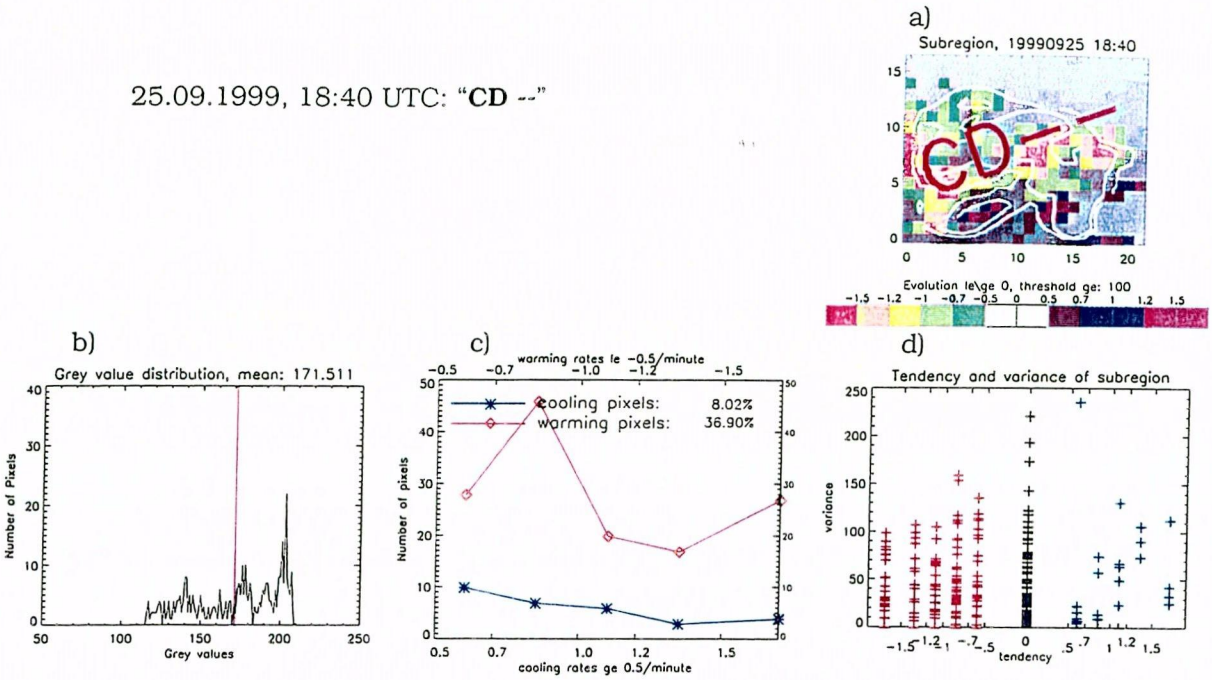

20.09.1999, 08:15 UTC: "**CD -**"

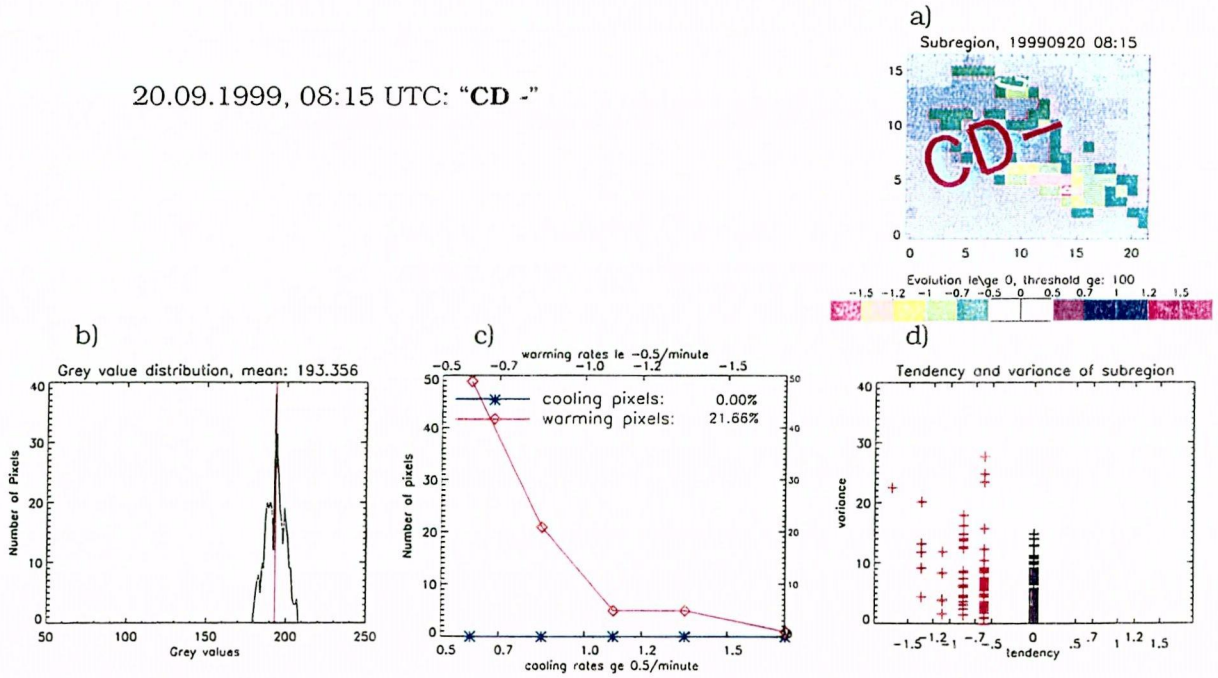

20.09.1999, 11:05 UTC: "**B**"

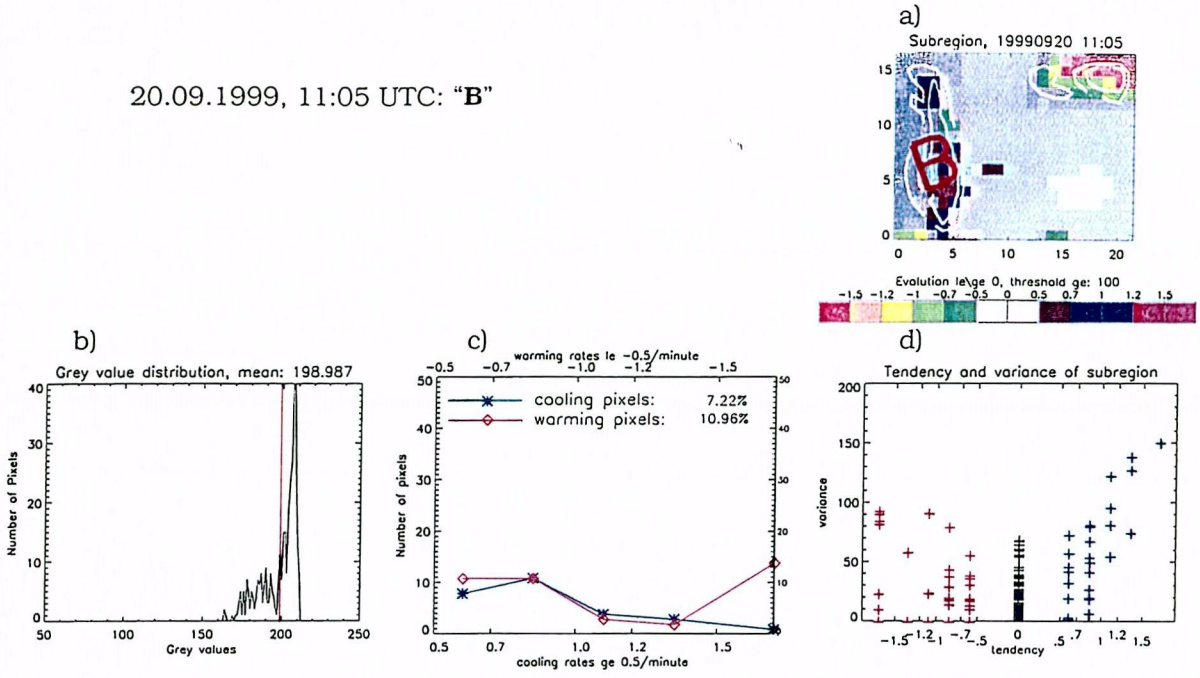

13.10.1999, 08:05 UTC: "**W**"

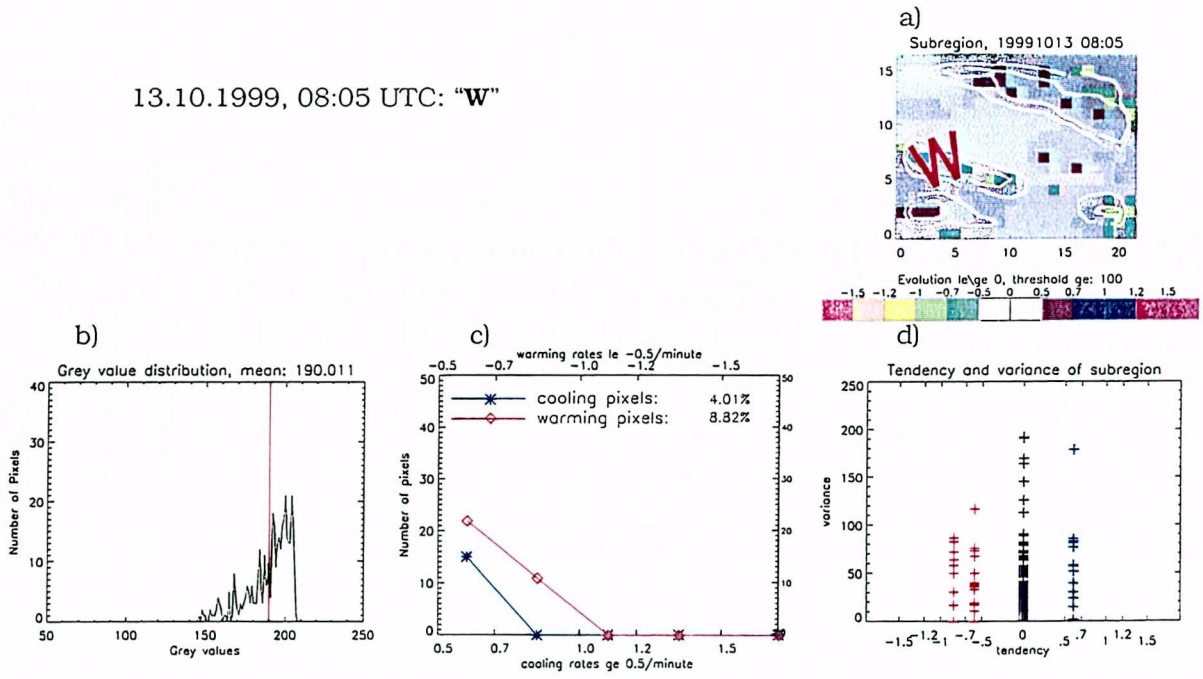

21.10.1999, 13:20 UTC: "**NE**"

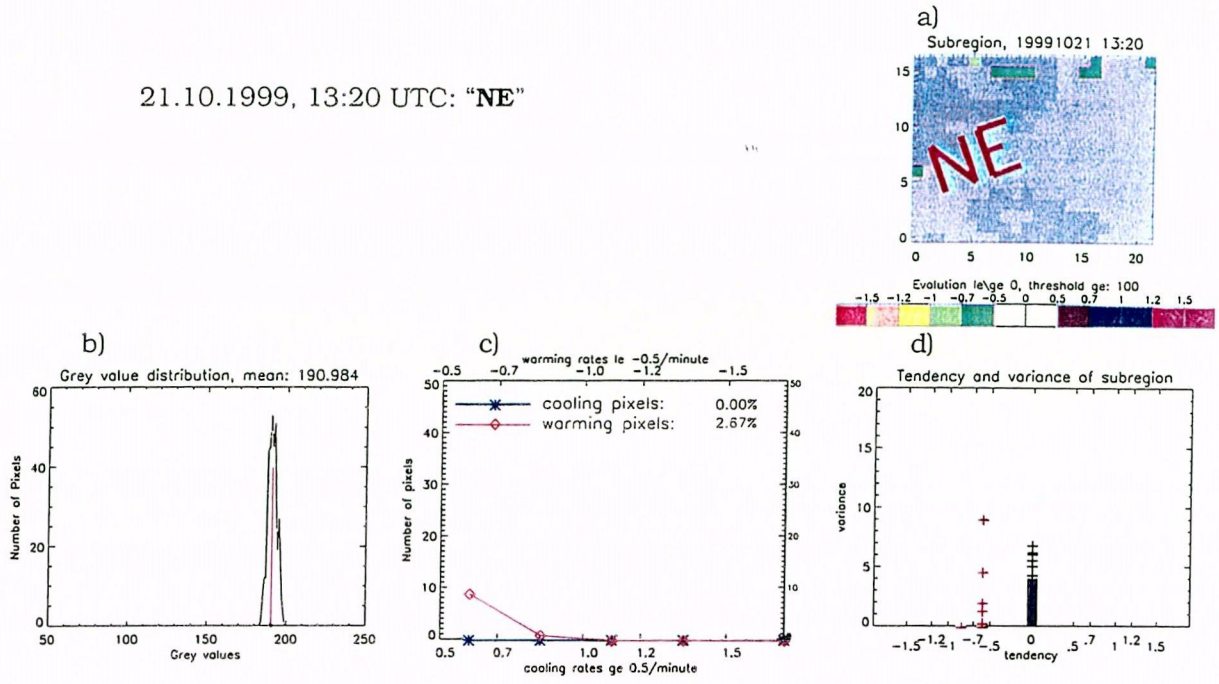

11.11.1999, 20:00 UTC: "**UC**"

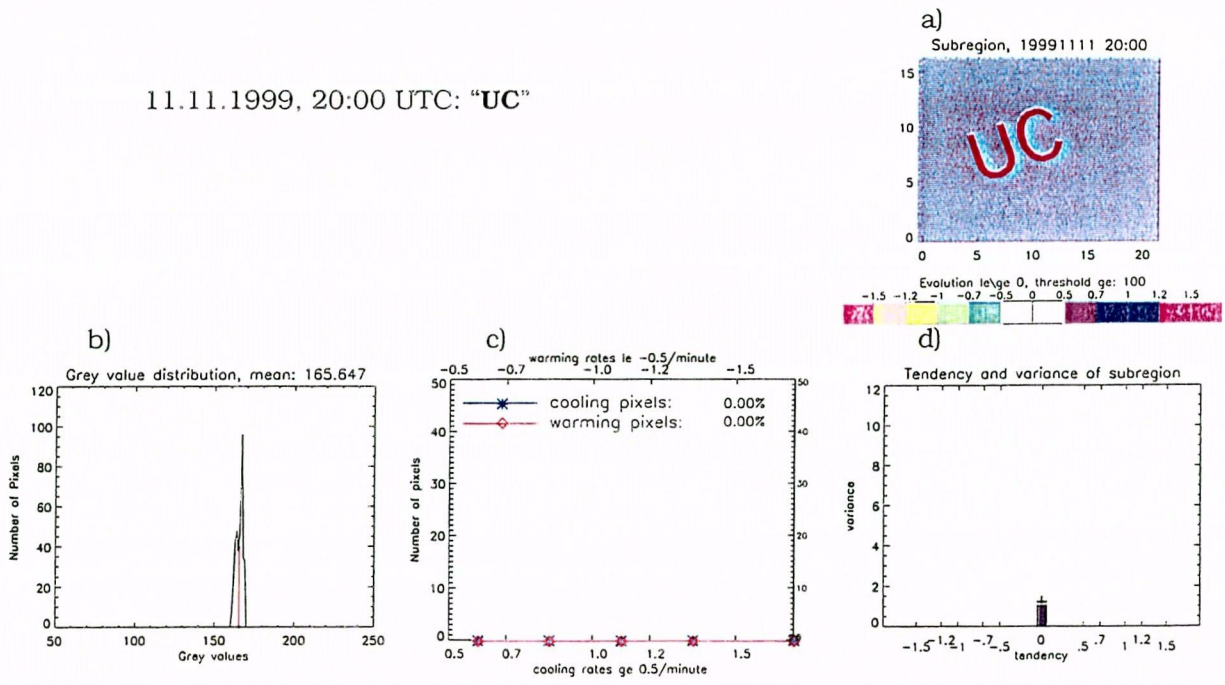

C. *IDL Programme code for the automated classification*

```
case 1 of
        Non-evolving: "NE"
        (diff_histo le 40) and (mean_histo ge 170) and $
        (percent_tot le 11) and (max(sub_var) lt 50): index_class = 'NE'

        Strong cooling cloud development: "CD ++"
        diff_histo gt 30) and (percent_tot gt 40) and $
        (percent_conv gt percent_warm) and $
        (cooling_class_points[3] gt warming_class_points[3]) and $
        (cooling_class_points[4] gt warming_class_points[4]): index_class = 'CD++'

        Moderate cooling cloud development: "CD +"
        (percent_tot gt 19) and (class_ovw_cool ge 3) and $
        (percent_conv ge percent_warm):index_class = 'CD+'

        Strong warming cloud development: "CD --"
        (diff_histo gt 30) and (percent_tot gt 40) and $
        (percent_warm gt percent_conv) and $
        (cooling_class_points[3] lt warming_class_points[3]) and $
        (cooling_class_points[4] lt warming_class_points[4]): index_class = 'CD--'

        Moderate warming cloud development: "CD -"
        (percent_tot gt 19) and $
        (class_ovw_warm ge 3) and $
        (percent_warm ge percent_conv): index_class = 'CD-'

        Balanced cloud development: "B"
        (percent_tot ge 15) and (percent_tot lt 60): index_class = 'B'

        Weak cloud development: "W"
        (percent_tot gt 0) and (percent_tot lt 15): index_class = 'W'

        Unclassified: "UC"
        else: index_class = 'UC'
endcase
```

Variable declaration

Legend

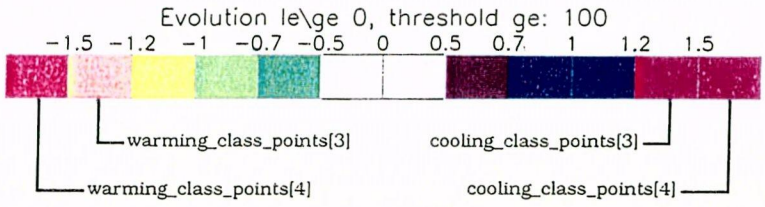

class_ovw_cool	number of classes represented by colors as predefined in the legend where the cooling pixels exceed the number of warming pixels
class_ovw_warm	number of classes represented by colors as predefined in the legend where the warming pixels exceed the number of cooling pixels
cooling_class_points[3]	number of cooling pixels within class interval 1.2 until 1.5 as predefined in the legend
cooling_class_points[4]	number of cooling pixels exceeding the magnitude of 1.5
diff_histo	width of histogram (maximum minus minimum greyvalue)
index_class	string array for classification result
max(sub_var)	maximum pixel variability
mean_histo	mean greyvalue of histogram
percent_tot	percentage of evolving warming and cooling pixels
percent_conv	percentage of evolving cooling pixels
percent_warm	percentage of evolving warming pixels
warming_class_points[3]	number of warming pixels within class interval -1.2 until -1.5 as predefined in the legend
warming_class_points[4]	number of warming pixels exceeding the magnitude of -1.5

LIST OF ACRONYMS

DOW	U.S. Doppler Radar on Wheels
Dry-MAP	Part of MAP devoted to the research of phenomena related to dry atmospheric dynamics (e. g. Foehn)
EUMETNET	Network of the European Meteorological Services
EUMETSAT	European Organisation for the Exploitation of Meteorological Satellites
GOES	Geostationary Operational Environmental Satellite (U.S.)
IOP	Intensive Observing Period
IR	infrared
LMTA	Lago Maggiore Target Area
MAP	Mesoscale Alpine Programme
MCS	Mesoscale Convective System
MDC	MAP Data Center
METEOSAT	Geostationary Meteorological Satellite (Europe)
MOC	MAP Operation Center
MSG	METEOSAT Second Generation
NOAA	U.S. National Oceanic and Atmospheric Administration
NOAA AVHRR	polar orbiting satellite of NOAA with Advanced Very High Resolution Radiometer
POC	Project Operation Center
PV	Potential Vorticity
RONSARD	French Doppler radar
SAF	Satellite Application Facility
SOP	Special Observing Period
SSM/I	Special Sensor Microwave Imager
VIS	visible
Wet-MAP	Part of MAP devoted to the research of phenomena related to precipitation
WV	water vapor
WWRP	World Weather Research Programme of the World Meteorological Organization
ZAMG	Zentralanstalt für Meteorologie und Geodynamik, Austria

REFERENCES

Adler, R. F., M. J. Markus, D. D. Fenn, G. Szejwach, and W. Shenk, 1983: Thunderstorm top structure observed by aircraft overflights with an infrared radiometer. J. Climat. Appl. Meteor., 22, 579-593.

Adler, R. F., M. J. Markus, and D. D. Fenn, 1985: Detection of severe mid-west thunderstorms using geosynchronous satellite data. Mon. Wea. Rev., 113, 769-781.

Adler, R. F. and A. J. Negri, 1988: A satellite infrared technique to estimate tropical convective and stratiform rainfall. J. Appl. Meteor., 27, 30-51.

Anagnostou, E. N. and C. Kummerow, 1997: Stratiform and Convective Classification of Rainfall Using SSM/I 85-GHz Brightness Temperature Observations. J. Atmos. Ocean. Technol., 14, 3, 570-575.

Arena, N., R. Benoit, P. Binder, A. Buzzi, G. Contri, M. Corazza, R. Cresta, M. Damonte, S. Gallino, D. Sacchetti, N. Tescaro, and E. Trovatore, 2001: Verification and intercomparison of limited area models operating during the MAP-SOP: Some results. MAP newsletter, 15, 98-101. [Available from the MAP Programme Office, MeteoSwiss, CH-8044 Zurich, Switzerland]

Bader, M. J., G. S. Forbes, J. R. Grant, R. B. E. Lilley, and A. J. Waters, 1995: Images in weather forecasting: A practical guide for interpreting satellite and radar imagery. Cambridge University Press, 499 pp.

Bader, St. and P. Kunz, 2000: Climate risks: the challenge for Alpine regions. Final scientific report NRP 31. vdf Hochschulverlag AG, ETH Zurich, 291 pp.

Banta, R. M., 1990: The Role of Mountain Flows in Making Clouds. AMS Met. Monographs, 23, 45, 229-283.

Benech, B., H. Brunet, V. Jacq, M. Payen, J. C. Rivrain, and P. Santurette, 1993: La catastrophe de Vaison-la-Romaine et les violentes précipitations de Septembre 1992: Aspects météorologiques. La Météorologie, 72-90.

Benoit, R. and M. Desgagné, 1996: Further non-hydrostatic modelling of the Brig 1993 flash flood event. MAP newsletter, 5, 36-37. [Available from the MAP Programme Office, MeteoSwiss, CH-8044 Zurich, Switzerland]

Benoit, R., M. K. Yau, A. Tremblay, F. Gayard, and S. Chamberland, 1997: Sensitivity of selected MAP episode(s) to the modelling of the cold phase precipitation. MAP newsletter, 7, 36-37. [Available from the MAP Programme Office, MeteoSwiss, CH-8044 Zurich, Switzerland]

Binder, P., 1989: A normalization procedure for Meteosat visible channel data. J. Atmos. Ocean. Technol., 6, 67-75.

Binder, P. and A. Rossa, 1995: The Piedmont Flood: Operational Prediction by the Swiss Model. MAP Newsletter, 2, 12-16. [Available from the MAP Programme Office, MeteoSwiss, CH-8044 Zurich, Switzerland]

Binder, P. and C. Schär, Eds., 1996: MAP Design Proposal. MeteoSwiss, 75 pp. [Available from the MAP Programme Office, MeteoSwiss, CH-8044 Zurich, Switzerland]

Binder, P. and Coauthors, 1999: MAP Implementation Plan. MeteoSwiss, 230 pp. [Available from the MAP Programme Office, MeteoSwiss, CH-8044 Zurich, Switzerland]

Boscacci, P., 1999: On the Dynamics of Thunderstorms in the Southern Swiss Alps: A Climatological Study using Surface and Radar Data. Diploma thesis MCR Lab, University of Basel, 88 pp.

Bougeault, P., P. Binder, and J. Kuettner, Eds., 1998: MAP Science Plan. MeteoSwiss, 64 pp. [Available from the MAP Programme Office, MeteoSwiss, CH-8044 Zurich, Switzerland]

Bougeault, P., P. Binder, A. Buzzi, R. Dirks, R. A. Houze Jr., J. Kuettner, R. B. Smith, R. Steinacker, H. Volkert, and all MAP scientists, 2001: The MAP Special Observing Period. Bull. Amer. Meteor. Soc., 82, 3, 433-462.

Browning, K. A. and C. W. Pardoe, 1973: Structure of low-level jet streams ahead of midlatitude cold fronts. Q. J. R. Meteorol. Soc., 99, 619-638.

Browning, K. A. and F. F. Hill, 1981: Orographic rain. Weather, 36, 326-329.

Browning, K. A., 1985: Conceptual models of precipitation systems. The Meteorological Magazine, 114, 293-319.

Buzzi, A., N. Tartaglione, C. Cacciamani, T. Paccagnella, and P. Patruno, 1995: The Piedmont flood in November 1994. MAP newsletter, 2, 2-6. [Available from the MAP Programme Office, MeteoSwiss, CH-8044 Zurich, Switzerland]

Buzzi, A., N. Tartaglione, and P. Malguzzi, 1998: Numerical Simulations of the 1994 Piedmont Flood: Role of Orography and Moist Processes. Mon. Wea. Rev., 126, 9, 2369-2383.

Buzzi, A. and L. Foschini, 2000: Mesoscale meteorological features associated with heavy precipitation in the Southern Alpine region. Meteor. Atmos. Phys., 72, 131-146.

Buzzi, A. and S. Davolio, 2001: Effects of orographic representation on simulations of cyclone development and mesoscale aspects of IOP 15. MAP newsletter, 15, 80-83. [Available from the MAP Programme Office, MeteoSwiss, CH-8044 Zurich, Switzerland]

Cacciamani, C., F. Battaglia, P. Patruno, L. Pomi, A. Selvini, and S. Tibaldi, 1995: A climatological study of thunderstorm activity in the Po Valley. Theor. Appl. Climat., 43, 185-203.

Carvalho, L. M. V. and C. Jones, 2001: A Satellite Method to Identify Structural Properties of Mesoscale Convective Systems Based on the Maximum Spatial Correlation Tracking Technique (MASCOTTE). J. Appl. Meteor., 40, 10, 1683-1701.

Collier, C. and R. B. Lilley, 1994: Forecasting thunderstorm initiation in north-west Europe using thermodynamic indices, satellite and radar data. Bull. Amer. Meteor. Soc., 78, 1411-1430.

Courvoisier, H. W., 1975: Katalog objektiv-statistischer Wetterprognosen für die Alpensüdseite und das Oberengadin. Veröffentlichung der SMA, Zürich, 32, 24 pp.

Courvoisier, H. W., 1981: Starkniederschläge in der Schweiz in Abhängigkeit vom Druck-, Temperatur- und Feuchtefeld. Veröffentlichung der SMA, Zürich, 42, 59 pp.

Courvoisier, H. W., 1998: Statistik der 24-stündigen Starkniederschläge in der Schweiz 1901-1996. Arbeitsbericht der SMA, Zürich, 194, 20 pp.

Csekits, C., A. Jann, and V. Zwatz-Meise, 1999: Automatic Detection of convective cells - a nowcast module at the Austrian Meteorological Service. In: Proceedings of the Meteorological Data User's Conference, Bologna, Italy, 715-721.

Endlich, R. M. and D. Wolf, 1981: Automatic cloud tracking applied to GOES and Meteosat observations. J. Appl. Meteor., 20, 309-319.

EUMETSAT, 1999: The Meteosat System. EUMETSAT TD05, 66 pp. [Available under http://www.eumetsat.de]

Ferraro, R. R., S. J. Kusselson, and M. Colton, 1998: An introduction to passive microwave remote sensing and its applications to meteorological analysis and forecasting. National Weather Digest, 22, 12-23.

Fliri, F., 1984: Synoptische Klimatographie der Alpen zwischen Mont Blanc und Hohen Tauern. Wissenschaftliche Alpenvereinshefte, 29, 686 pp.

Frei, C. and C. Schär, 1998: A precipitation climatology of the Alps from high-resolution raingauge observations. Int. J. Climatol., 18, 873-900.

Frei, C. and C. Schär, 2001: Detection probability of trends in rare events: theory and application to heavy precipitation in the Alpine region. J. Climate, 14, 1568-1584.

Frei, C. and E. Häller, 2001: Mesoscale precipitation analysis from MAP SOP rain-gauge data. MAP Newsletter, 15, 257-260. [Available from the MAP Programme Office, MeteoSwiss, CH-8044 Zurich, Switzerland]

Frontero, P., P. Binder, S. Pugnaghi, L. Lombroso, R. Santangelo, A. Buzzi, T. Paccagnella, and A. Selvini, 1997: Versilia flood: A pre-frontal supercell system embedded in weak flow impinging on a near-coastal mountain range. INM/WMO International Symposium on Cyclones and hazardous Weather in the Mediterranean, Palma de Mallorca, Spain, 159-167.

Germann, U., 2000: Spatial continuity of precipitation, profiles of radar reflectivity and precipitation measurements in the Alps. Ph.D. thesis, ETH Zürich, No. 13932, 104 pp.

Gheusi, F. and J. Stein, 2001: Semi-idealized modelling of heavy rain events over the MAP area. MAP Newsletter, 15, 51-53. [Available from the MAP Programme Office, MeteoSwiss, CH-8044 Zurich, Switzerland]

Goldenberg, S. B., R. A. Houze Jr., and D. D. Churchill, 1990: Convective and stratiform components of a winter monsoon cloud cluster determined from geosynchronous infrared satellite data. J. Meteor. Soc. Japan, 68, 37-63.

Grebner, D., 1993: Synoptische Zirkulationen während Extremniederschlägen in der nordalpinen Schweiz. In: Aktuelle Aspekte in der Hydrologie, Zürcher Geogr. Schriften, 53, 39-48.

Grebner, D., 1994: Meteorologische Analyse des Unwetters Brig und Saas Almagell vom 24. September 1993. Wasser, Energie, Luft, 86. Jg., Heft 1/2. 41-44.

Grebner, D., 1996: Starkniederschläge in der Schweiz: Signale einer Klimaänderung? Klima Seminar 6./7. Mai 1996, Swissre, 9 pp.

Grebner, D., 1997: Meteorologische Verhältnisse und Starkniederschläge im Alpenraum. In: Forschung auf dem Gebiet der Talsperren, Fachtagung ETH Lausanne.

Grebner, D. and T. Roesch, 1998: Flächen-Mengen-Dauer-Beziehungen von Starkniederschlägen und möglichen Niederschlagsgrenzwerten in der Schweiz. Schlussbericht NFP 31. vdf Hochschulverlag AG, ETH Zürich, 190 pp.

Hand, W. H. and S. Sénési, 1998: COST-78 Project 1.3: Climatology of convective systems. COST-78: Development of Nowcasting Techniques. Selbstverlag des Deutschen Wetterdienstes, 25-29.

Hanson, C. G., 1999: High temporal resolution Meteosat imagery of the Alps in support of the Mesoscale Alpine Programme. In: Proceedings of the Meteorological Satellite Data Users' Conference, Copenhagen, Denmark, 495-499.

Hanson, C. G., M. Williams and L. C. J. van de Berg, 2000: 5-minute Meteosat imagery of the Alps in support of the Mesoscale Alpine Programme. In: Proceedings of the Meteorological Satellite Data Users' Conference, Bologna, Italy, 789-795.

Hanson, C., personal communication

Held, E., 1995: Radarmessung im Niederschlag und Einfluss der Orographie. Arbeitsbericht der SMA, 185, 98 pp.

Heymsfield, G. M. and R. Fulton, 1988: Comparison of high-altitude remote aircraft measurements with the radar structure of an Oklahoma thunderstorm: implications for precipitation estimation from space. Mon. Wea. Rev., 116, 1157-1174.

Hilgendorf, E. R. and R. H. Johnson, 1998: A Study of the Evolution of Mesoscale Convective Systems Using WSR-88D Data. Weather and Forecasting, 13, 2, 437-452.

Hodges, K. I., 1998: Feature-point detection using distance transforms: application to tracking tropical convective complexes. Mon. Wea. Rev., 126, 785-795.

Hoinka, K. P., 1985: On cold fronts in Central Europe. Beitr. Phys. Atm., 58, 560-571.

Hong, Y., C. D. Kummerow, and W. S. Olson, 1999: Separation of Convective and Stratiform Precipitation Using Microwave Brightness Temperature. J. Appl. Meteor., 38, 8, 1195-1213.

Houze, R. A., B. F. Smull, and P. Dodge, 1990: Mesoscale organization of springtime rainstorms in Oklahoma. Mon. Wea. Rev., 118, 613-654.

Houze, R. A., Jr., 1993: Cloud Dynamics, Academic Press, 573 pp.

Houze, R. A., Jr., 1997: Stratiform Precipitation in Regions of Convection: A Meteorological Paradox? Bull. Amer. Meteor. Soc., 78, 10, 2179-2196.

Houze, R. A., Jr., J. Kuettner, and R. Smith, Eds., 1998: MAP U.S. overview document and experiment design. 101 pp.

Houze, R. A., Jr., C. N. James, and S. Medina, 2001: Radar observations of precipitation and airflow on the Mediterranean side of the Alps: Autumn 1998 and 1999. Q. J. R. Meteorol. Soc., 12, 2537-2558.

Houze, R. A., Jr., 2001: Orographic control of precipitation: what are we learning from MAP? MAP newsletter, 14, 3-6. [Available from the MAP Programme Office, MeteoSwiss, CH-8044 Zurich, Switzerland]

Image, 2001. EUMETSAT publication, Darmstadt, No. 15, 4-5.

Jansa, A., A. Genovés, J. Campins, and M. A. Picornell, 1995: Mediterranean cyclones and Alpine heavy-rainflood events. MAP Newsletter, 3, 35-37. [Available from the MAP Programme Office, MeteoSwiss, CH-8044 Zurich, Switzerland]

Jansa, A., R. Riosalido, and O. Carretero, 1996: Mesoscale Cyclones vs Heavy Rain and MCS in the Western Mediterranean. MAP Newsletter, 5, 24-25. [Available from the MAP Programme Office, MeteoSwiss, CH-8044 Zurich, Switzerland]

Johnson, D. B., P. Flament, and R. L. Bernstein, 1994: High-resolution satellite imagery for mesoscale meteorological studies. Bull. Amer. Meteor. Soc., 75, 5-33.

Joss, J., B. Schädler, G. Galli, R. Cavalli, M. Boscacci, E. Held, G. della Bruna, G. Kappenberger, V. Nespor, and R. Spiess, 1998: Operational use of radar for precipitation measurements in Switzerland. Final scientific report NRP 31. vdf Hochschulverlag AG, ETH Zurich, 108 pp.

Kappenberger, G. and J. Kerkmann, 1997: Tempi in montagna. Zanichelli Editore, Bologna, Italy, 255 pp.

Kidder, S. Q. and T. H. Vonder Haar, 1995: Satellite Meteorology an Introduction. Academic Press, 466 pp.

Kuettner, J. and B. Meitin, 2000: MAP: preliminary summary report on the field phase by the US MAP Project Office. UCAR/NCAR, Boulder, Colorado, 45 pp.

Lagouvardos, L., E. Liljas, B. Conway, and J. Sunde, Eds., 2001: Improvement of nowcasting techniques. COST 78 final report, EUR 19544, 368 pp.

Leese, J., C. S. Novak, and B. B. Clark, 1971: An automated technique for obtaining cloud motion from geosynchronous satellite data using cross correlation. J. Appl. Meteor., 10, 118-132.

Levizzani, V., 1998: Convective rain from a satellite perspective: achievements and challenges. SAF Training Workshop Nowcasting and Very Short Range Forecasting, Madrid, Spain, 75-84.

Levizzani, V., H. J. Lutz, J. Kerkmann, P. Alberoni, M. Cervino, and F. J. Turk, 1999: Precipitation estimates using Meteosat Second Generation (MSG): new perspectives from geostationary orbit. In: Proceedings of the Meteorological Satellite Data Users' Conference, Copenhagen, Denmark, 121-128.

Levizzani, V., 2000: Satellite rainfall estimates: a look back and a perspective. In: Proceedings of the Meteorological Satellite Data Users' Conference, Bologna, Italy, 344-353.

Lin, Y. L., J. Thurman, and S. Chiao, 2001: Influence of synoptic and mesoscale environments on heavy orographic rainfall associated with MAP IOP 2b and IOP 8. MAP newsletter, 15, 72-75. [Available from the MAP Programme Office, MeteoSwiss, CH-8044 Zurich, Switzerland]

Machado, L. A. T., W. B. Rossow, R. L. Guedes, and A. W. Walker, 1998: Life Cycle Variations of Mesoscale Convective Systems over the Americas. Mon. Wea. Rev., 126, 1630-1654.

MAP Field Catalogue, 2000. [Available at the MDC: http://www.map.ethz.ch]

Massacand, A. C., H. Wernli, and H. C. Davies, 1998: Heavy precipitation on the Alpine southside: An upper-level precursor. Geophys. Res. Lett., 25, 9,1435-1438.

Mecklenburg, S., 2000: Nowcasting precipitation in an Alpine region with a radar echo tracking algorithm. Ph.D. thesis ETH Zürich, No. 13608, 118 pp.

Menzel, P. W., 2001: Cloud Tracking with Satellite Imagery: From the Pioneering Work of Ted Fujita to the Present. Bull. Amer. Meteor. Soc., 82, 1, 33-48.

Monk, G. A., 1987: Topographically related convection over the British Isles. In: Preprints for a Workshop in Reading, EUMETSAT, 305-324.

Morel, C., F. Orain, and S. Sénési, 1997: Automated detection and characterization of MCS using the Meteosat infrared channel. In: Proceedings of the Meteorological Satellite Data Users' Conference, Brussels, Belgium, 213-220.

Morel, C. and S. Sénési, 1998: A fully automated detection and tracking of Mesoscale Convective Systems based on the Meteosat infrared channel. In Proceedings of the 9th Conference on Satellite Meteorology and Oceanography, AMS, Paris, France, 377-380.

Morel, C. and S. Sénési, 1999: The Rapid Developing Thunderstorms Product of the Nowcasting SAF. Involvement of Météo-France. In Proceedings of the Meteorological Satellite Data Users' Conference, Copenhagen, Denmark, 349-353.

Morel, C., S. Sénési, F. Autones, and L. Labatut, 2000: The Rapid Developing Thunderstorms (RDT) Product of the Nowcasting SAF. Prototyping activities and quality assessment using GOES images. In: Proceedings of the Meteorological Satellite Data Users' Conference, Bologna, Italy, 698-705.

Morel, C., S. Sénési, and co-workers, 2001: Climatology of mesoscale convective systems over Europe. In: Improvement of nowcasting techniques, COST Final report, EUR 19544, 82-85.

Morgenstern, O., 1998: Alpine-Southside Precipitation Events: Model Studies and Physical Concepts. Ph.D. thesis, ETH Zürich, No. 1242, 131 pp.

Nagle, R. E. and S. M. Serebreny, 1962: Radar precipitation echo and satellite cloud observations of a maritime cyclone. J. Appl. Meteor, 1, 279-295.

Negri, A. J., R. F. Adler, 1981: Relationship of satellite-based thunderstorm intensity to radar-estimated rainfall. J. Appl. Meteor., 20, 288-300.

Pankiewicz, G. S., 1995: Pattern recognition techniques for the identification of cloud and cloud systems. Meteorological Applications, 2, 257-271.

Pankiewicz, G. S., 1996a: Neural network classification of convective airmasses for a flood forecasting system. Forecasting Research Division Scientific Paper, U.K. Metoffice, England, 45, 15 pp.

Pankiewicz, G. S., 1996b: New Meteosat Pattern Recognition Productions for Use in Weather Forecasting. Forecasting Research Division Scientific Paper, U.K. Metoffice, England, 46, 7 pp.

Purdom, J. F. W., 1996: Advanced atmospheric studies using GOES-8/9 multichannel imagery. In: Proceedings to the Meteorological Satellite Data Users' Conference, Vienna, Austria, 77-86.

Quadri, C., R. Fehlmann, and H. C. Davies, 2000: An Alpine Rainstorm: Sensitivity to the Mesoscale Upper-Level Structure. Weather and Forecasting, 15, 1, 4-28.

Reudenbach, C. and J. Bendix, 1999: Investigation of summer convective rainfall in Western Europe based on a synergy of remote sensed data and numerical models. In: Proceedings of the Meteorological Satellite Data Users' Conference, Copenhagen, Denmark, 153-158.

Riosalido, R., 1996: Current status and principal challenges in strong convection nowcasting in COST-78 frame. COST-78 Int. Workshop on improvement of nowcasting techniques, Bologna, EUR 16996, 37-47.

Rosci, P., A. Balzamo, L. De Leonibus, and F. Zauli, 2000: Improvement of automatic detection and extrapolation of convective phenomena using MAP rapid scan Meteosat images. In: Proceedings of the EUMETSAT Meteorological Satellite Data Users' Conference, Bologna, Italy, 797-805.

Rosenfeld, D. and I. M. Lensky, 1998: Satellite-Based Insights into Precipitation Formation Processes in Continental and Maritime Convective Clouds. Bull. Amer. Meteor. Soc., 79, 11, 2457-2476.

Rossa, A., 1995: The Impact of Latent Heat Release on the Dynamics of Extratropical Cyclogenesis. Ph.D. thesis, ETH Zurich, No. 11039, 127 pp.

Rossa, A. and P. Binder, 1997: Towards a more comprehensive verification of high-resolution NWP precipitation fields using radar data. MAP newsletter, 7, 20-21. [Available from the MAP Programme Office, MeteoSwiss, CH-8044 Zurich, Switzerland]

Rossa, A. and J. Quiby, 1997: The operational forecasts produced by a meso-scale NWP model for two flash flooding events on the Mediterranean coast. INM/WMO International Symposium on Cyclones and hazardous Weather in the Mediterranean, Palma de Mallorca, Spain, 805-811.

Rotunno, R., 2001: Editorial of the MAP newsletter, MAP newsletter, 15, 1-2. [Available from the MAP Programme Office, MeteoSwiss, CH-8044 Zurich, Switzerland]

Rotunno, R. and R. Ferretti, 2001: Mechanism of intense Alpine rainfall. Journal of the Atmospheric Sciences, 58, 13, 1732-1749.

Schaaf, C. B., J. Wurman, and R. M. Banta, 1988: Thunderstorm-producing terrain features. Bull. Amer. Meteor. Soc., 69. 272-277.

Schiesser, H. H., R. A. Houze Jr., and H. Huntrieser, 1995: The mesoscale structure of severe precipitation systems in Switzerland. Mon. Wea. Rev., 123, 2070-2097.

Schmetz, J. and M. Nuret, 1987: Automatic tracking of high-level clouds in Meteosat infrared images with a radiance windowing technique. ESA Journal, 11, 275-286.

Schmetz, J., K. Holmlund, J. Hoffmann, B. Mason, V. Gaertner, A. Koch, and L. van de Berg, 1993: Operational cloud-motion winds from Meteosat images. J. Appl. Meteor., 32, 1206-1225.

Schmutz, C., 2000: Low frequency climate and precipitation variability in the Alpine region. Ph.D. thesis, Institute of Geography, University of Berne, 121 pp.

Schneidereit, M. and C. Schär, 2000: Idealised numerical experiments of Alpine flow regimes and southside precipitation events. Meteor. and Atmos. Phys., 72, 2-4, 233-250.

Smull, B., O. Bousquet, and D. Lüthi, 2001: Evaluation of surface precipitation and radar data during some MAP IOPs in Western Slovenia. MAP Newsletter, 15, 84-88. [Available from the MAP Programme Office, MeteoSwiss, CH-8044 Zurich, Switzerland]

Smyth, T. J. and A. J. Illingworth, 1998: Radar estimates of rainfall rates at the ground in bright band and non-bright band events. Q. J. R. Meteorol. Soc., 124, 2417-2434.

Spinedi, F., 1992: Synoptical analysis of the events of heavy precipitation on the southern slope of the Swiss Alps, 1961-1990. ICS/ICTP/WMO International Workshop in Mediterranean Cyclones Studies, Trieste, Italy, 44 pp.

Spinedi, F., G. Kappenberger, S. Sartori, P. Ambrosetti, and E. Zala, 1995: Le alluvione del 1993 sul versante sudalpino. Arbeitsbericht der SMA, Zürich, 21pp.

Spinedi, F., 1998: The Rovio case. Interner Arbeitsbericht SMA, unveröffentlicht, 3 pp.

Spinedi, F., 2001: La tempesta del Festival, 4 agosto 2001. Witterungsbericht der MeteoSchweiz, August 2001, MeteoSvizzera, Locarno-Monti, 2 pp.

Sprayd, L. E., and R. A. Scofield, 1984: An experimental Satellite-derived heavy convective rainfall short-range forecasting technique. In: Proceedings of the 10th Conference on weather forecasting and analysis, Clearwater Beach, USA, 400-408.

Steiner, M., R. A. Houze Jr., and S. Yuter, 1995: Climatological Characterization of three-Dimensional storm structure from operational radar and rain gauge data. J. Appl. Meteor., 34, 9, 1987-2007.

Steiner, M., J. A. Smith, M. L. Baeck, Y. Zhang, and R. A. Houze Jr., 2000a: Space-time analysis of rainfall in relation to topography for heavy precipitation events observed during MAP. In: Proceedings of the ICAM, Innsbruck, Austria, CD Rom, session 1, presentation 1.10.

Steiner, M., J. A. Smith, B. Smull, and R. A. Houze Jr., 2000b: Airflow within major river valleys on the south side of the Alps as observed during the MAP special observing period. In: Proceedings of the ICAM, Innsbruck, Austria, CD Rom, session 1, poster presentations.

Steiner, M., O. Bousquet, R. A. Houze Jr., B. F. Smull, and M. Mancini, 2002: Airflow within major Alpine river valleys under heavy rainfall. Submitted to Q. J. R. Meterol. Soc., 27 pp.

Vicente, G. A., R. A. Scofield, and W. P. Menzel, 1998: The Operational GOES Infrared Rainfall Estimation Technique. Bull. Amer. Meteor. Soc., 79, 9, 1883-1898.

Vicente, Gilberto A., J. C. Davenport, and R. A. Scofield, 1999: Impact of GOES-10 rapid scan data for estimating convective rainfall. Reprinted from the Reprint Volume of the third Symposium on integrated observing Systems, Dallas, USA, 227.

Wanner, H., R. Rickli, E. Salvisberg, C. Schmutz, and M. Schüepp, 1997: Global climate change and variability and its influence on Alpine Climate-concepts and observations. Theor. Appl. Climat., 58, 221-243.

Wanner, H., D. Gyalistras, J. Luterbacher, R. Rickli, E. Salvisberg, and C. Schmutz, 2000: Klimawandel im Schweizer Alpenraum. vdf Hochschulverlag AG, ETH Zürich, 285 pp.

Wanner, H., S. Brönnimann, C. Casty, L. Dretvik, L. Gomez, D. Gyalistras, J. Luterbach, C. Schmutz, N. Schneider, and E. Xoplaki, 2001: The North Atlantic Oscillation - Concepts and Studies. Surv. Geophys., 22, 4, 321-382.

Wexler, R. and R. H. Blackmer, Jr., 1982: Radar reflectivities and satellite imagery of severe storms: 20 May 1977. Mon. Wea. Rev., 110, 719-729.

Wibig, J., 1999: Precipitation in Europe in relation to circulation patterns at the 500 hPa level. Int. J. Climatol., 19, 253-269.

Williams, M., personal communication

Wirth, A., A. Jann, and V. Zwatz-Meise, 2000: ASII: First results of the SAF NWC demonstrator experiment. In: Proceedings of the EUMETSAT Meteorological Satellite Data Users' Conference, Bologna, Italy, 779-786.

www.eumetsat.de (homepage of EUMETSAT)

www.map.ethz.ch (homepage of MAP)

Yuter, S. E. and R. A. Houze Jr., 1998: The natural variability of precipitating clouds over the western Pacific warm pool. Q. J. R. Meteor. Soc., 124, 53-99.

Zenone, E., 1979: Atmosphärische Bedingungen - wiedergegeben durch die Radiosondierung von Mailand - bei Starkniederschlägen auf der Alpensüdseite. Rapporto di studio di MeteoSvizzera, Locarno-Monti, non pubblicato, 26 pp.

Zwatz-Meise, V., 2000: Manual of synoptic satellite meteorology: conceptual models. Version 3.0, CD Rom available from ZAMG, Vienna.

ACKNOWLEDGMENT

I would like to express my gratitude to Heinz Wanner, head of the Division of Physical Geography at the University of Berne and Director of NCCR Climate (National Center of Competence in Research in Climate). He gave me the opportunity to spend three years of my life in research what I consider as a privilege. I most appreciated his enthusiasm for meteorology, his motivating comments and his friendly manner.

My particular gratitude goes to Peter Binder, head of research and development at MeteoSwiss for the organization of the funding of my Ph.D. and his guidance. He always provided helpful advice, followed the working progress with great interest and initiated many stimulating discussions. I am grateful that I was able to carry out my work under his excellent guidance.

I thank Hanspeter Roesli, satellite meteorology counceller at MeteoSwiss, for his essential and constant support, being technical (Laptop) or scientific. I can always count on him what is good to know.

Special thanks go to Urs Germann, who supported me with his great knowledge of radar meteorology and of IDL. He patiently answered all my computer questions and provided the software for the exploitation of the radar data. I appreciated the meetings in Intragna and Locarno-Monti which were always good fun.

Michael Williams and Chris Hanson from EUMETSAT are acknowledged for the their valuable advice regarding the rapid scans.

Thanks go to Jean Quiby (head of the numerical modelling section at MeteoSwiss) giving me the opportunity to do my work within the friendly atmosphere of his group. I thank all mates of this group, Marco Arpagaus, Jean-Marie Bettems, Pirmin Kaufmann, Daniel Leuenberger, Guy de Morsier, Andrea Rossa, Francis Schubiger, and Emanuele Zala for their support and sense of humour. I would also like to thank Christian Häberli who made the radiosounding data accessible.

Further thanks go to Veronika Zwatz-Meise, head of the satellite group of ZAMG, who offered me the unique possibility of an interesting research visit in Vienna.

The financial support of the Swiss National Science Foundation grant No. 21-55802.98 and MeteoSwiss are gratefully acknowledged.

Last but not least I would like to thank my parents, Ruth and Peter Bolliger-Schneider, Monika Wohlfender, my sister Janine, and Thomas Gutermann for their continuous support throughout my path of life.